UNIVERSIDADE FEDERAL DE MINAS GERAIS
PROGRAMA DE PÓS GRADUAÇÃO EM ENGENHARIA MECÂNICA

Thermodynamic modelling and simulation of a Pumped Hydro - Compressed Air Energy Storage System (PH-CAES)

Daniel Leon Ferreira Pottie

Brasil, September, 2019

Daniel Leon Ferreira Pottie

Thermodynamic modelling and simulation of a Pumped Hydro - Compressed Air Energy Storage System (PH-CAES)

Dissertação apresentada ao Programa de Pós-graduação em Engenharia Mecânica da Universidade Federal de Minas Gerais como requisito parcial à obtenção do título de Mestre em Engenharia Mecânica.

Supervisor: Prof. Dr. Matheus Pereira Porto

Co-supervisor: Prof. Dr. Thales Alexandre Carvalho Maia

Belo Horizonte
Escola de Engenharia da UFMG

September, 2019

Pottie, Daniel Leon Ferreira.
P871t Thermodynamic modelling and simulation of a Pumped Hydro - Compressed Air Energy Storage System (PH-CAES) [recurso eletrônico] / Daniel Leon Ferreira Pottie. - 2019.
1 recurso online (xviii, 113 f. : il., color.) : pdf.

Orientador: Matheus Pereira Porto.
Coorientador: Thales Alexandre Carvalho Maia.

Dissertação (mestrado) - Universidade Federal de Minas Gerais, Escola de Engenharia.

Apêndices e anexos: f. 97-113.

Bibliografia: f. 85-96.
Exigências do sistema: Adobe Acrobat Reader.

1. Engenharia mecânica - Teses. 2. Energia - Armazenamento - Teses. 3. Métodos de simulação - Teses. 4. Modelagem matemática - Teses. I. Porto, Matheus Pereira. II. Maia, Thales Alexandre Carvalho. III. Universidade Federal de Minas Gerais. Escola de Engenharia. IV. Título.

CDU: 621 (043)

Ficha catalográfica: Biblioteca Profº Mário Werneck, Escola de Engenharia da UFMG

UNIVERSIDADE FEDERAL DE MINAS GERAIS
PROGRAMA DE PÓS-GRADUAÇÃO EM
ENGENHARIA MECÂNICA
Av. Antônio Carlos, 6627 - Campus Universitário
31270-901 – Belo Horizonte – MG
Tel.:+55 31 3409.5145
E-mail: cpgmec@demec.ufmg.br

"PH-CAES"

DANIEL LEON FERREIRA POTTIE

Dissertação submetida à Banca Examinadora designada pelo Colegiado do Programa de Pós-Graduação em Engenharia Mecânica da Universidade Federal de Minas Gerais, como parte dos requisitos necessários à obtenção do título de **"Mestre em Engenharia Mecânica"**, na área de concentração de **"Energia e Sustentabilidade".**

Dissertação aprovada no dia 05 de setembro de 2019.

Por:

Prof. Matheus Pereira Porto
Orientador - Departamento de Engenharia Mecânica/UFMG

Prof. Thàles Alexandre Carvalho Maia
Coorientador - Departamento de Engenharia Elétrica/UFMG

Prof. Rafael Augusto Magalhaes Ferreira
Departamento de Engenharia Mecânica/UFMG

Prof. Paulo Vinicius Trevizoli
Departamento de Engenharia Mecânica/UFMG

Prof. Jorge Maia Alves
Faculdade de Ciências, Universidade de Lisboa

Acknowledgements

Firstly, I thank my family, for always supporting me during a rough journey. Through the difficult days, knowing a had support when I got back home made it all easier. My eternal gratitude and debt. Especially, I thank my mother, for the assistance and always believing in me. To my father, my ever lasting gratitude for always providing and advising.

Only one person lived and experienced all, and no matter what, stood by me. My greatest friend, love and companion, I thank my girlfriend Nayara for support, patience, advice, tears and laughs. Thanks for getting me started in the academic life. I love you.

To my supervisor, Prof. Matheus Porto, I thank for the patience, advice and a faultless guidance throughout these two and a half years.

I thank my co-supervisor, Prof. Thales Maia, for many long conversations on the most diverse subjects, many of which were not engineering related.

I am grateful to Prof. Márcio Fonte-Boa Cortez, for inspiring me wander into the unknown.

I am thankful to all my LabTerm colleagues, especially Leonardo, Ramon, Maury and Prof. Rafael. Thanks for laughing at all my bad and mostly inappropriate jokes, making tough days end faster, nearly losing a toe due to frostbite and never abandoning me.

I thank my psychiatrist Cláudia, who in the darkest times, shone like a crazy diamond. Thank you my second mother and friend.

To my oldest friend, João, I am thankful for the advice and friendship.

To the best drummer I know, André, thanks for keeping the beat steady.

I thank my Fight Club friends, Prof. Gustavo, Grug, Felipe, Fred, Douglas, Henrique(s), for making my Mondays one of the best days in the week.

"Politicians hide themselves away
They only started the war
Why should they go out to fight?
They leave that role for the poor"
T. M. J. Butler, A. F. Iommi, J. M. Osbourne, W. T. Ward.

"Big man, pig man, ha ha, charade you are
You well heeled big wheel, ha ha, charade you are
And when your hand is on your heart
You're nearly a good laugh"
G. R. Waters, D. J. Gilmour, R. W. Wright †, N. N. Mason.

"Sometimes I grow so tired
But I know about one thing I got to do
Ramble on"
R. A. Plant, J. P. Jones, J. H. Bonham †, J. P. Page.

Abstract

The fundamental role of electricity in modern society cannot be overstated. In a ever increasing energy consumption world, shifting from fossil fuels towards a more renewable generation system will incur in deep changes, not only in the electric system, but also on society itself. In this rapidly changing scenario, Energy Storage Systems (ESS) are seen as a powerful ally to assist the transition. In this research, a novel ESS named Pumped Hydraulic Compressed Air Energy Storage proposes replacing the air the compressor and turbine, utilized in conventional CAES system by hydraulic pumps and turbines. Directly compressing the air, as is done in CAES is a energy demanding process, in which the gas is confined to a small chamber and undergoes a rapid transformation. As a result, its temperature increases considerably, which in turn, require special materials and methods to be handled. Instead of, a hydraulic pump pushed water into a closed tank, slowly and indirectly compressing the air inside. This way, a great deal of simplicity is achieved, temperature increase and power requirement are diminished and the system operates as a hybrid between PHES (charging and discharging) and CAES (storage medium). An extensive literature review is performed, aiming to describe and explain the possible types and applications ESS on the energy generation and distribution market. Following, the new system operating sequence is completely described and modelled under the scope of the Laws of Thermodynamics, fluid mechanics and heat transfer concepts. The proposed methodology is then applied to a laboratory scale simulation, performed in Matlab. Several operating scenarios were simulated, in order to assess the system performance over a wide range of conditions. The results found proved that the new system is able to quickly respond, generating a stable power output. Also, replacing the compressor by hydraulic pumps, and indirectly compressing the air with water results in a considerable decrease in power consumption. This way, a round trip efficiency figure of 45% is achieved, and considering the proposed system size and simplicity, it is considered a promising. To test this, the system efficiency is compared to several CAES literature references, and its value is comparable to larger, more complex and potentially expensive systems, which usually depend on multiple heat exchangers, burning fuel or an external heat source, validating thus, the technical relevance of the proposed system.

Keywords: CAES; PH-CAES; Energy Storage Systems; Mathematical modelling; simulation.

Resumo

O papel fundamental que a eletricidade desempenha na atual sociedade não pode ser subestimado. A atual tendência mundial de crescimento de consumo energético, aliado à redução na utilização de combustíveis fósseis rumo a uma matriz energética sustentável incorrerá em profundas mudanças, não apenas no mercado de energia, mas bem como na sociedade em si. Nesse documento, propõe-se um Sistema de Armazenamento de Energia em que se substitui compressores e turbinas a ar, utilizados em sistemas CAES convencionais, por bombas e turbinas hidráulicas, chamado Pumped Hydraulic Compressed Air Energy Storage (PH-CAES). A compressão direta do ar, como é feito em CAES, demanda uma grande quantidade de energia, e o gás confinado a uma pequena câmara de compressão, é submetido à rápida pressurização. Dessa maneira, o aumento de pressão é acompanhado por aquecimento substancial, levando à necessidade de materiais e métodos especiais para manipular a massa gasosa a altas temperaturas. Ao invés de comprimir o ar diretamente, no sistema proposto água é bombeada para um reservatório fechado, e assim, por meio da redução do volume disponível, pressuriza o ar armazenado. Dessa maneira, além da simplicidade construtiva e operacional, a amplitude térmica e potência requerida para operação são reduzidos, e o sistema opera como um híbrido de PHES (durante carregamento e descarregamento) e CAES (meio de armazenamento). A partir de uma extensa revisão bibliográfica, os principais tipos de ESS e suas aplicações no mercado energético foram descritos. Em seguida, a operação do sistema proposto foi descrita, e seu funcionamento modelado a partir de conceitos fundamentais das Leis da Termodinâmica, mecânica dos fluidos e transferência de calor. Esse modelo matemático foi então aplicado, por meio de simulação em Matlab, em um sistema de pequena escala. Essa simulação se deu sob diferentes aspectos operacionais, de modo a compreender o comportamento do sistema em diversos cenários. Os resultados das simulações indicaram que o sistema possuía rápida resposta, sendo capaz de produzir energia de maneira estável. Além disso, a proposição de redução de consumo e diminuição da amplitude térmica foram comprovados. Dessa maneira, uma eficiência global de 45% foi atingida, o que considerando a reduzida escala e simplicidade do proposto, é considerada promissora. Para comprovar tal constatação, esse valor foi comparado com diversas referências sobre CAES disponíveis na literatura. O valor encontrado de eficiência é comparável a sistemas maiores, mais complexos e que em muitos casos dependem de uma fonte externa de energia térmica, ou combustão para atingir valores aceitáveis de eficiência, o que comprova, de maneira definitiva, a competitividade técnica do sistema proposto.

Palavras-chave: CAES, PH-CAES, Sistemas de armazenamento de energia, Modelagem matemática; Simulação.

List of Figures

List of Tables

Acronyms

A-CAES Adiabatic Compressed Air Energy Storage. 33, 36, 37

BES Battery Energy Storage. v, 4, 6, 9, 13

CAES Compressed Air Energy Storage. iii, iv, 1, 2, 5, 27–29, 33–37, 42, 57, 59, 62, 66–68, 78, 82–84

CES Cryogenic Energy Storage. 27

D-CAES Diabatic Compressed Air Energy Storage. 33, 34, 36

ELDC's Electric Double-Layer Capacitors. 24, 25

ESS Energy Storage Systems. iii, 1–5, 7–16, 28–32, 67, 78, 82

FB Flow Battery. 21, 22

FES Flywheel Energy Storage. v, 5, 30, 31

HPP Hydro Power Plants. 2, 32, 42

I-CAES Isothermal Compressed Air Energy Storage. 33, 37

LAES Liquid Air Energy Storage. 27, 28

LiPo Lithium Polymer. 20

MAB Metal-Air Battery. 20, 21

MGU Motor-Generator Unit. 30

NSR Non-Spinning Reserve. v, 10, 11, 25, 29, 32

PCM Phase-Change Materials. 29

PH-CAES Pumped Hydraulic Compressed Air Energy Storage. iii, iv, 2, 38, 39, 44, 54, 55, 57, 62–66, 68, 70, 73, 78, 82–84

PHES Pumped Hydroelectric Energy Storage. iii, 1–3, 5, 9, 27, 31–33, 37, 67, 82

PV Photovoltaic. 5

RES Renewable Energy Sources. 7

RNE Renewable Energy Sources. 3

RTE Round-Trip Efficiency. vii, ix, 54, 67, 68, 70, 78, 84

SMES Superconducting Magnetic Energy Storage. v, 4, 11, 23, 25–27

SR Spinning Reserve. v, 10, 11, 29, 32

TES Thermal Energy Storage. 4, 27–29, 33, 36, 59, 82, 83

VRFB Vanadium Redox Flow Battery. 3

List of symbols

A	area, m^2
B	magnetic field, Wb
c	specific heat, $J\ kg^{-1}\ K^{-1}$
C	capacitance, F
d	distance, m
E	energy, J, Wh
g	acceleration of gravity, $m\ s^{-2}$
h	specific enthalpy, $J\ kg^{-1}$
H	head, m
i	electrical current, A
I	moment of inertia, $kg\,m^2$
J	friction head losses, m
L	inductance, H
m	mass, kg
n	polytropic coefficient,
P	pressure, kPa
Q	energy transferred as heat, J
$\dot{Q}$	energy transfer rate as heat, W
R	electrical resistance, Ω
s	specific entropy, $J\ kg^{-1}\ K^{-1}$
t	time, s
T	temperature, K
T_C	critical temperature, K

u	specific internal energy, $J\ kg{-}1$
v	velocity, $m\ s^{-1}$
V	voltage, V
$\forall$	volume, m^3
$\dot{\forall}$	flow rate, $m^3\ s^{-1}$
W	energy transferred as work, J
$\dot{W}$	energy transfer rate as work, W
X	exergy, J
Z	height, m

Greek letters

ε	electromotive force, V
η	energy efficiency
ρ	density, $kg\ m^{-3}$
υ	specific volume, $m^3\ kg^{-1}$
χ	combined exergy, J
ψ	rational efficiency
ω	rotational speed, s^{-1}

Subscripts

$Air - to - H_2O$	air to water heat transfer
char	charging
cons	consumption
conv	convective
c.v.	across a control volume boundary

exp	expansion
fl	relative to the mass flow between tanks
g	gauge
gen	generator, generated
in	inlet
$M-02$	relative to pump P-01 motor
out	outlet
p	pump
$PCV-01$	relative to pressure control valve PCV-01
rad	radiative
RTE	Round Trip efficiency
$TK-01$	tank TK-01
$TK-02$	tank TK-02
tur	turbine
w	water
$wall$	tanks walls
0	dead state
1	initial state
2	final state

Superscripts

$\langle i \rangle$	relative to time iterative process
$\langle j \rangle$	relative to mass flow convergence iterative process

Contents

1 Introduction

Solar and wind are the worlds fastest growing renewable energy source (IEA, 2017). During the last decade, the world installed PV capacity skyrocketed from 6.4 GW in 2006 to 303 GW in 2016. Wind powered generation followed a similar trend, increasing its global capacity from 74 GW to 487 GW in the same period (REN21, 2017). However, these technologies are particularly sensible to environmental conditions, and, their widespread application is, to some extent, dependent on the development of accessible and efficient Energy Storage Systems (ESS).

Different ESS can be used in a wide range of operating necessities. From small button cell batteries to large Pumped Hydroelectric Energy Storage (PHES) and Compressed Air Energy Storage (CAES), ESS are used to accumulate and transfer energy through time (SNL, 2016; BLACK; STRBAC, 2007), damp fluctuations in production and in the supply-demand-cost balance, provide blackouts support, power quality *etc.* (BLACK; STRBAC, 2007; CRUISE; GIBBENS; ZACHARY, 2014; BATHURST; STRBAC, 2003).For instance, whilst batteries and super capacitors are recommended for smaller applications, in which the stored energy is limited and the required response time is short, large scale storage ESS are usually restricted to PHES and CAES systems (SNL, 2016).

Pumped Hydroelectric Energy Storage represents over 90% of the energy storage systems installed worldwide (REN21, 2017), with over 300 large scale (> 100 MW) installations globally, representing an installed capacity of over 150 GW (SNL, 2016; BOGENRIEDER, 2006; PUNYS et al., 2013). Its principle of operation its to use excess, cheap or intermittent energy to power pumps, to drive water from a lower to an upper reservoir, storing thus, energy in earth gravitational field (REHMAN; AL-HADHRAMI; ALAM, 2015). Despite the high efficiency, PHES systems require suitable geographical conditions which can impose difficulties to its widespread application. CAES systems utilizing the energy surplus it to power a set of compressors, pressurizing and storing atmospheric air. Later on, when energy is required, the air passes through an expansion process, driving turbines and generators (SNL, 2016; BUDT et al., 2016). There are two large scale CAES plants worldwide, Huntorf in Germany (CROTOGINO; MOHMEYER; SCHARF, 2001) and McIntosh in the USA (BIASI, 1998; POLLAK, 1994). CAES has not achieved the same representativeness as PHES due to the elevated initial and operational costs, requiring a particularly large cavern to store the air (or an artificial vessel, which also increases the costs), comparatively lower round trip efficiency, and in some cases, requiring an external heat source or even dependent of combustion process (BUDT et al., 2016).

So, aiming to assess these drawbacks, whilst maintaining CAES and PHES respective advantageous aspects, a hybrid solution was developed, in which a hydraulic pump drives water into a closed tank, increasing the pressure of the air inside it. This way, the energy surplus is stored as compressed air mechanical exergy. Then, when energy is required, the compressed air pushes back the water through the piping towards a hydraulic turbine, returning energy to the final user. The pressure exerted by the air acts similarly to the hydraulic head at Hydro Power Plants (HPP). This way, the proposed solution operates as CAES and PHES systems simultaneously, and it has been named Pumped Hydraulic Compressed Air Energy Storage (PH-CAES).

1.1 Objectives and document structure

The main objective of this work was the concept development of a new ESS, by combining advantages from PHES and CAES, named Pumped Hydraulic Compressed Air Energy Storage (PH-CAES). To do so, firstly it was necessary to understand applications and features of various ESS, so an comprehensive review on the subject was developed. Then, the system layout and operating principles were proposed, followed by complete thermodynamic modelling for the proposed system. Next, a laboratory scale prototype was simulated by applying the developed theoretical model. Finally, the results were compared to other CAES performance figures found in the literature to verify the PH-CAES technical competitiveness.

2 Energy Storage Systems

2.1 Context

Energy Storage Systems (ESS) come in many forms, sizes and capacities. In general terms, ESS is a device, mechanism, material or contraption capable or moving energy through time (SNL, 2016), making energy generated at one moment available later on. From small triple A batteries (electrochemical), large oil reservoirs (chemical), heat stored in the Earth mantle (thermal), radioactive compound (nuclear), water storage in dams (mechanical) or even fat reserves in animals (biochemical), ESS dictates our relationship with energy and nature.

In the electricity market context, Energy Storage Systems consume and stores energy surplus, making it available again in the future (DAS et al., 2018). Mainly, ESS can be used to compensate or mitigate costs, damp power and voltage fluctuations in the distribution network, match the supply and demand requirements, increasing the overall energy system reliability. Given the world tendency to reduce the grid dependency on conventional fossil fuels (REN21, 2017; FOLEY et al., 2015; FOLEY; OLABI, 2017), moving towards more environmentally sustainable alternatives. However, by increasing Renewable Energy Sources (RNE) share, notably wind and solar generation, the entire generation and distribution system becomes more susceptible to power oscillations, generation outages and load-demand imbalances (DAS et al., 2018).

In this sense, ESS are considered one solution to mitigate these operational problems and challenges. The integration of short-duration ($\leqslant 1\ day$) ESS to an intermittent wind generation plant was studied by (BARTON; INFIELD, 2004), and installing a 400 kW, 3 MWh Vanadium Redox Flow Battery (VRFB) system (enough for 24 h demand) would result in a 41000 € extra revenue and 25% more wind energy to be effectively used. Likewise, a long-term technical and economical analysis of integrating large scale PHES to the British isles wind generation, under different scenarios, prices conditions and technological development, representing saving of up to 31 million €, and substantially increasing the power reserve (FOLEY et al., 2015).

Energy Storage Systems can be labelled depending on their storage medium and usual application. There are several ways to categorize ESS, however, this document will follow the definitions presented by (SNL, 2016).

2.2 ESS categories

Firstly, it is possible to categorize an Energy Storage Systems depending on their storage technology. Whether the energy is stored as mechanical, thermal, chemical or electrical exergy dictated the group in which each ESS will fall into. At this point, types of ESS will be mentioned. However, they will be fully explained later on the document, after all basic concepts have been introduced and properly explained. Following, the main types of ESS are presented:

2.2.1 Electrochemical (Batteries)

Perhaps the most intuitive picture of Energy Storage Systems, batteries are an intrinsic part of our lives. In terms of size, this is the most varying ESS, ranging from small button cell batteries which hold less than 1 Wh (ENERGIZER, 2018) to the world largest Battery Energy Storage (BES) in the world, currently under construction in China and will store 800 MWh (ELECTREK, 2017). Electrochemical systems are quick to respond, usually within milliseconds, medium to high efficiency ($> 50\%$), but face a serious problem of degrading over time. However, the latest advances in battery technology have mitigated, to some extent, this problem (DIVYA; ØSTERGAARD, 2009).

2.2.2 Electrical

In electrical ESS, energy is stored in electric or magnetic fields. Generally speaking, these systems respond rapidly, within milliseconds upon demand, and have good efficiency figures ($> 60\%$ in normal conditions). However, these systems do not store large amounts of energy without greatly increasing their cost, restricting their application at some cases. Their installation costs are intermediate to elevated, reaching up to 72000 $USD\ kWh^{-1}$, and there are two main types of electrical ESS: Supercapacitors and Superconducting Magnetic Energy Storage (SMES) (DAS et al., 2018; LI et al., 2017; DöSOGLU; ARSOY, 2016; CORRAL-VEGA; FERNÁNDEZ-RAMÍREZ; GARCÍA-TRIVIÑO, 2019).

2.2.3 Thermal

Differently from the above listed ESS, Thermal Energy Storage (TES) can be used as auxiliary systems to other Energy Storage Systems, industrial process in general (KUMAR; KISHORE, 1999) or even civil structures heating (KAMAL et al., 2019; SCHMIDT; MANGOLD; MüLLER-STEINHAGEN, 2004), and not strictly focused in generating electricity as its final product. However, there are examples of TES being used to this end (LIU; SAMAN; BRUNO, 2012). When acting as an auxiliary system, it removes excess or undesirable heat from the main ESS, and stores it as sensible or latent heat. Later, the TES delivers this stored energy when required (ALVA; LIN; FANG, 2018). Thermal

Energy Storage is widely applied worldwide, with many different heat sources, objectives, storage materials and techniques.

2.2.4 Mechanical

While electrical ESS store energy in electromagnetic fields, mechanical systems accumulate the energy surplus as mechanical exergy, whether kinetic - Flywheel Energy Storage (FES) -, potential gravitational - Pumped Hydroelectric Energy Storage (PHES) - or as mechanical exergy - Compressed Air Energy Storage (CAES). These systems can operate over a wide range of efficiencies, store large amounts of energy, and hold the largest installed capacity of any other ESS. Pumped Hydroelectric Energy Storage installed capacity is over 18 GW in the US alone (FERC, 2019), and at least 150 GW worldwide, representing more than 90% of the global Energy Storage Systems capacity (REN21, 2017). While PHES and CAES systems are already well established in the energy market, FES is now beginning to show up as a promising contender.

2.3 ESS application

As presented by (SNL, 2016), there are five main categories in which Energy Storage Systems may be fitted. These are not excludent, which means that a certain technology can perform more than one type of role.

2.3.1 Bulk Energy Storage

Firstly, Bulk Energy Storage systems deals with storing and returning larger amounts of energy. Within this category, there are many types of system, which attend to different purposes. In this class, Electric Energy time-shift systems consists of storing relatively high quantities of energy during low-demand or lower prices, and latter retrieving it when necessary, focused on economical advantages or to avoid wasting excess power production. The storage period can vary greatly, from a few hours to months, when an ESS is applied to seasonal context (*e.g.*, PV generation during the summer is stored to be later used in the winter).

Here, two Electric Energy time-shift techniques are more commonly discussed and applied: (i) load levelling and (ii) peak shaving. In load levelling, power is stored during periods of smaller demand, usually by the distribution company, to reduce the stress during peak consumption (ABB, 2017). (SHIMADA; MUKAI, 2006) explored the beneficial effects of the PHES storage in Japan's grid network, transferring electrical power from low demand periods (between midnight and noon) to the afternoon, which required more energy, as can be seen in Fig. 2.1

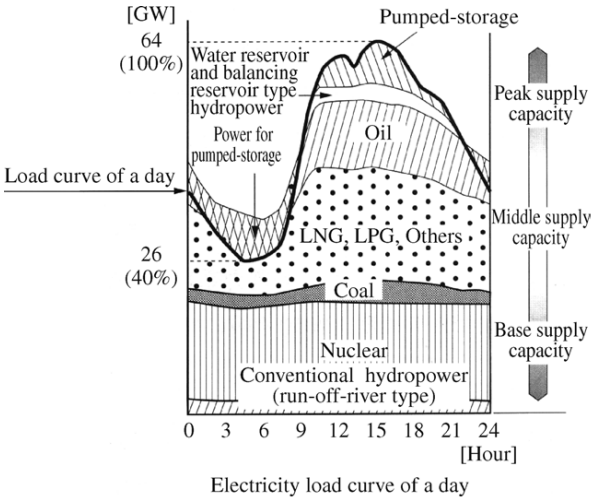

Figure 2.1 – Load levelling being applied to Japan, transferring energy from load to high demand periods (SHIMADA; MUKAI, 2006).

Load levelling consists of storing energy on lower consumption periods to reduce the stress on grid during higher demand, peak shaving aims to decrease the amount of energy bought by end consumers during high price periods (ABB, 2017). Effectively, it operates similarly to load leveling, however the goals are different. While peak shaving is intended to end users, load levelling is used by distribution companies. A generalized peak shaving technique is presented in Fig. 2.2

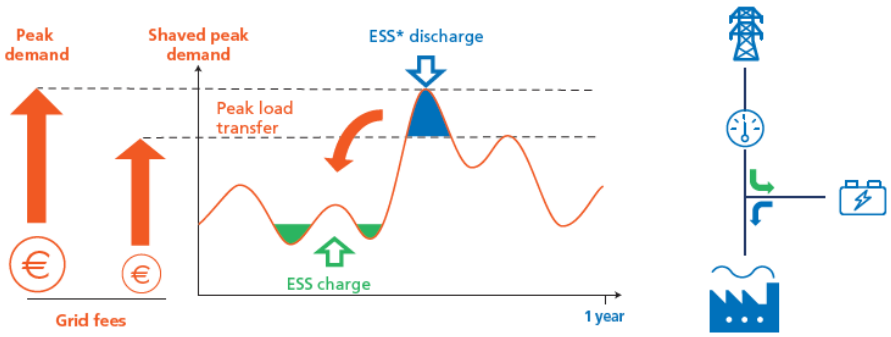

Figure 2.2 – Generalized peak shaving technique being applied. In this particular case, a Battery Energy Storage (BES) system is charged during lower price periods, and discharged during peak grid prices (EDF-RE, 2019).

In Fig. 2.2, a generalized peak shaving application is presented, in which energy is bought from the grid during lower prices periods, and stored. In this particular example, a Battery Energy Storage system is responsible for the energy storage. When the grid fees become more expensive, this stored energy is used to reduce the energy acquisition at higher prices, curtailing economical losses. These two Bulk Energy Storage techniques are applied to periods of at least one hour. For shorter periods, in which the operational goals

and purposes are not to transfer large amounts of energy through time, but to regulate, stabilize or back the grid up during outages, other techniques can be applied.

Additionally to Electric Energy time-shift services, Bulk Energy Storage can be used to reduce or avoid acquiring energy from the grid altogether, instead of being cost oriented. When this is the case, its called Electric Supply Capacity (SNL, 2016). This is perhaps one of the most generalized and intuitive usages of ESS, varying in size, type and location.

2.3.2 Power Quality and reliability

Whenever the main goal of an Energy Storage Systems is to mitigate any short-term disturbances in the grid from the consumer side, it can be labeled as a power quality system (SNL, 2016). When correctly installed, a power quality focused ESS can prevent problems as:

- Short term voltage surge, either positive or negative;
- Frequency deviation from the grid standard (50 or 60 Hz, depending on location);
- Low power factor (voltage and current excessively out of phase);
- Presence of harmonics (either in voltage or current);
- Short term outages.

So, in order to prevent these problems, a key requirement of a power quality ESS is the short response time, which generally restricts electrical, electrochemical or electronic systems to this applications (DAS et al., 2018). The amount of energy stored varies greatly, from the range of MWh (NICK; CHERKAOUI; PAOLONE, 2018; BABACAN; TORRE; KLEISSL, 2017; SEDGHI; AHMADIAN; ALIAKBAR-GOLKAR, 2016), applied to large active distribution grid balancing, to smaller plants, storing in the scale of a few kWh for smaller or decentralized systems highly dependent on Renewable Energy Sources (LEE et al., 2016).

Power reliability, on the other hand, focuses on providing a backup in case of power outages. For instance, if the wind suddenly stops blowing over a large on grid wind farm, there is the necessity of a quick response system to provide the energy deficit. In these cases, a power reliability ESS can be applied to fulfill the short spiked power requirements, until the distributing grid reroutes energy incoming from another generating source. Renewable Energy Sources are usually less reliable than conventional generation methods, and thus, when their share in the generation grid is increased, it is necessary to adapt the distributing system to mitigate variability and outages. For instance, (ČEPIN,

2019) investigated replacing a 696 MW nuclear power plant by three 1160 MW wind farms, resulting in a total capacity increase of nearly five times. However, even with this larger power figure, the system reliability decreased due to the variability of the wind generation, exposing the necessity of a efficient Energy Storage Systems to reduce the negative impacts. A didactic representation of power quality and reliability being applied to a generic 138 kV system is presented in Fig. 2.3.

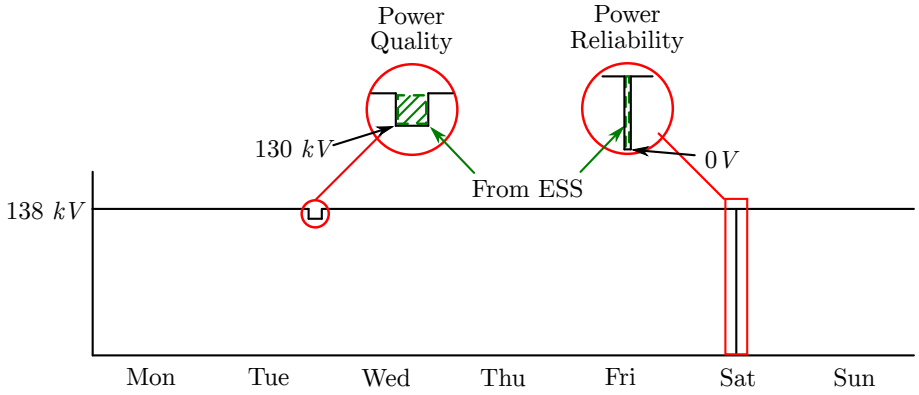

Figure 2.3 – Schematic depiction of power quality and reliability being used to a 138 kV electrical system over a week.

In Fig. 2.3, a generic 138 kV power line is presented over a week period. During this time, there were two instances in which the ESS resolved power quality and reliability issues. Firstly, between Tuesday and Wednesday a voltage drop can be seen, lasting from a few minutes to a couple of hours. To counter-act this deficit, the ESS acted until the generation returned to nominal levels. Then, on Saturday, a non-schedule rerouting would have caused a brief power interruption if the storage system did not fill the power gap, responding quickly until another generating source took place.

2.3.3 Ancillary services

Ancillary services are characterized by roles in which the ESS acts as supporting system to the grid. There are many applications that can be labeled as acillaty, and following, the main are presented and exemplified.

2.3.3.1 Regulatory services

Regulation services, sometimes called load-demand balancing are an important application of ESS (SNL, 2016). In this, the storage system is used to dampen instantaneous imbalances between supply and demand, absorbing any excess energy and returning it to the grid later on. A key aspect of this kind of application it is short time-span profile. A generalized usage of Energy Storage Systems as regulatory system is presented in Fig. 2.4.

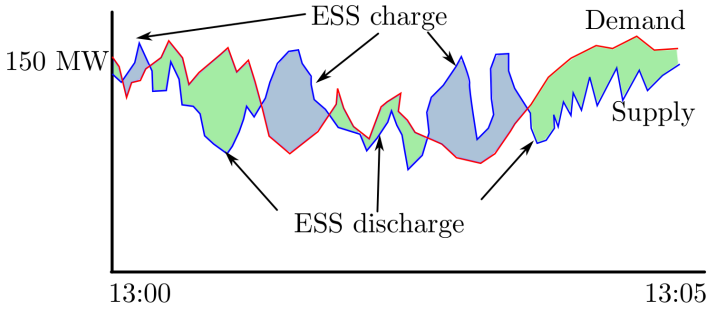

Figure 2.4 – Generalized ESS application as regulatory service, depicting the imbalance between demand (red) and supply (blue) in the grid.

In Fig. 2.4, a hypothetical behaviour of the grid demand and supply is presented between 13:00 and 13:05 is presented, exposing the fluctuating profile of the curves. When the supply is above the demand, the ESS absorbs the energy surplus, charging the storage system. This scenario is represented by the blue shaded areas. Conversely, when the demand is bigger than the instantaneous availability, the grid relies on the stored energy to compensate this deficit, discharging the Energy Storage Systems (SNL, 2016). A key feature of this kind of service is the rapid response time.

In this application, (JAIN; DAS; JAIN, 2019) proposed utilizing the increasing fleet of electric vehicles as the storage medium for a large grid regulatory service. In this study, the authors proposed utilizing the battery installed in these vehicles to absorb imbalances in the grid. Given the battery quick response time, and the fact that they are usually connected to the grid when stationary, either at home or in the workplace, they present as good candidates to fulfill this role. Simulations were performed utilizing grid and commercial battery data, with 1 *min* time resolution, and the results showed that even though the regulatory capacity depends on the sample specific driving habits, the implementation of electrical vehicles as BES regulatory services brings technical and economical advantages.

Similarly, (CHAZARRA et al., 2018) studied the economic viability of a variable speed Pumped Hydroelectric Energy Storage plant focused specifically to perform regulatory services. In this theoretical study, twelve different arrangements of fixed and variable speed pump-turbines are simulated, aiming to reduce economic penalties due to load unbalancing. The results show that the PHES systems are capable of returning the investment in most cases, even considering elevated initial expense necessary, especially if the pump turbine motor generating unit is capable of running in asynchronous speeds.

2.3.3.2 Contingency and supplemental reserves

Contingency and supplemental reserves are the electrical network back-up. When there is a major disruption on the distributing network, *e.g.,* a substation transformer blowing up, a large portion of the final consumer may be affected. So, there must be an energy reserve ready to step in and supply the required power. The ESS utilized for these purposes must be large, capable of delivering large amounts of energy and quick to respond, mitigating the immediate effects of the outage (USDE, 2011; SNL, 2016). Within this category, there are two sub-divions: (i) spinning and (ii) non-spinning reserves.

Spinning Reserve (SR) are the immediate response to an outage, first delivering energy within 10 seconds of the disruption event and being fully operational in less than 10 minutes. To achieve this, these systems must be always online, unloaded, synchronized and rated to the appropriate power and energy rates (HREINSSON; VRAKOPOULOU; ANDERSSON, 2014; SNL, 2016; USDE, 2011), allowing network operators to run with an suitable safety margin. The costs of installing and continuously operating a system must be compared to the expenses related to the grid uncertainty in disruptive events, and thus, defining the optimal quantity of stored energy is a crucial step. This was assessed in (ORTEGA-VAZQUEZ; KIRSCHEN, 2009), in which a stochastic analysis of load demand, wind generation and SR requirements was performed through the Monte-Carlo method, assuming a base load cost of 1000 $USD\ MWh^{-1}$ of disrupted energy. In this study, the authors did not study the ESS on itself, but the technical and economical impacts on the network. The results indicated that the spinning reserves are vital to reduce penalties, especially as the wind share on the market increases. Also, as the cost of energy disrupted increases, the SR must increase to match the production of the largest generation source likely to fail.

Differently from spinning, Non-Spinning Reserve (NSR) are not constantly online nor ready to be connected to the grid. Rather than, they ought to respond within 10 minutes of the disrupting event, and are responsible to assume when the SR are depleting, and hold the system operating until another generation source ramps up to the demand level. Since the response time does not require to be short, most of the large Energy Storage Systems are suitable as Non-Spinning Reserve (SNL, 2016; USDE, 2011). Similar to what has been done in the previous items, Fig. 2.5 depicts a general application of SR and NSR.

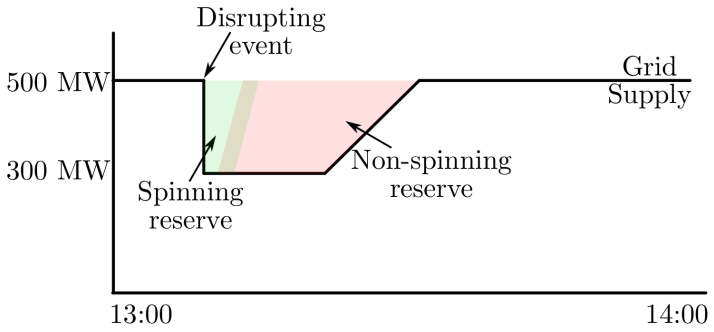

Figure 2.5 – General application of Spinning Reserve (SR) and Non-Spinning Reserve (NSR) to a generic 500 MW distributing system.

In Fig. 2.5, a general application of SR and NSR for a 500 MW distributing system is presented. Between 13:00 and 14:00, a disrupting event took place, which curtailed the power generation to 60% of the nominal level. Almost instantly, the Spinning Reserve was connected to the grid, compensating the power loss (green shaded area). When the SR reserves are close to an end, the Non-Spinning Reserve steps in (red shaded area), building up its energy output and matching the Spinning Reserve production, replacing it after its depletion. Later, as another generation source is brought online (for instance, a coal power backup power station) the Non-Spinning Reserve decreases its power delivery until it is no longer needed. It is worth highlighting that during the transitioning period, both spinning and non-spinning reserves overlap.

Furthermore, there is the supplemental reserves, which are safety redundancy to spinning and non-spinning reserves. They are only needed if the power outage is particularly large or long lasting, depleting the regular contingency reserves, and are similar to non-spinning reserves (SNL, 2016; USDE, 2011).

2.3.3.3 Black Start

In the event of total or partial failure of power generation and distributing system, an Energy Storage Systems can be used to perform a black start. Differently from most ESS previously presented, in the event of a black start the energy stored is used to start the generator/power plants, and not destined to the final consumers directly (SNL, 2016). It is desirable that the ESS chosen for black start support responds quickly, and can store and deliver enough power to start up a few generators. Once the generation starts to build up, the power delivery can be diverted to the final user, to activate substations or even ceased (VERMA et al., 2011). In a case study, (YANG; LIU; LIU, 2014) proposed applying two 30 MW Superconducting Magnetic Energy Storage (SMES) units to restore power after blackouts, powering a 30 MW gas turbine. The quick response of this ESS is vital to the process, starting the turbine in under 2 sec and restoring power in under 6 sec,

while also presenting good overvoltage control and dampening frequency oscillations.

2.3.3.4 Voltage support and Frequency response

Voltage support and frequency response are auxiliary services played by Energy Storage Systems, and are not usually intended to store active energy. In voltage support, the ESS adds capacitive or inductive loads to manage the grid reactance levels. So, instead of being defined by their stored energy, usually in kWh or MWh, these systems are labelled in terms of $kVAR$ or $MVAR$ (kilo or mega volt-ampere reactive) (SNL, 2016). Similarly, frequency response service aim at maintaining the grid operating frequency in case of disruptions. These systems operate in two phases: (i) in the first few seconds, a short duration high power system is utilized to prevent frequency oscillations, lasting up to 30 *sec*; (ii) in the mean time, a secondary, slower and larger system ramps up and steps in after the first stage depletion, maintaining the system frequency roughly stable around the nominal value (SNL, 2016)

2.3.4 Transmission Infrastructure Services

In the previous section ESS were applied focusing in storing energy to mitigate effects of blackouts, reduce costs, provide stability and reliability to the grid distributing system. Now, instead of these, Energy Storage Systems can be used as transmission infrastructure services, alleviating stresses in transmission line bottlenecks. Within this category, there are two main services: upgrade deferral and congestion relief.

2.3.4.1 Transmission upgrade deferral

Transmission upgrade deferral consists in delaying or avoiding structural infrastructure investment. If a key transmission line is running close to its maximum capacity during certain critical consumption periods, it may be convenient to install an Energy Storage Systems at the consumer end to be charged during lower demand periods, reducing the stress during the peak. This way, it is possible to avoid or postpone eventual upgrades in the distributing network, extending equipments expected lifetime (SNL, 2016). In Fig. 2.6 a generic application of ESS as transmission upgrade deferral is presented.

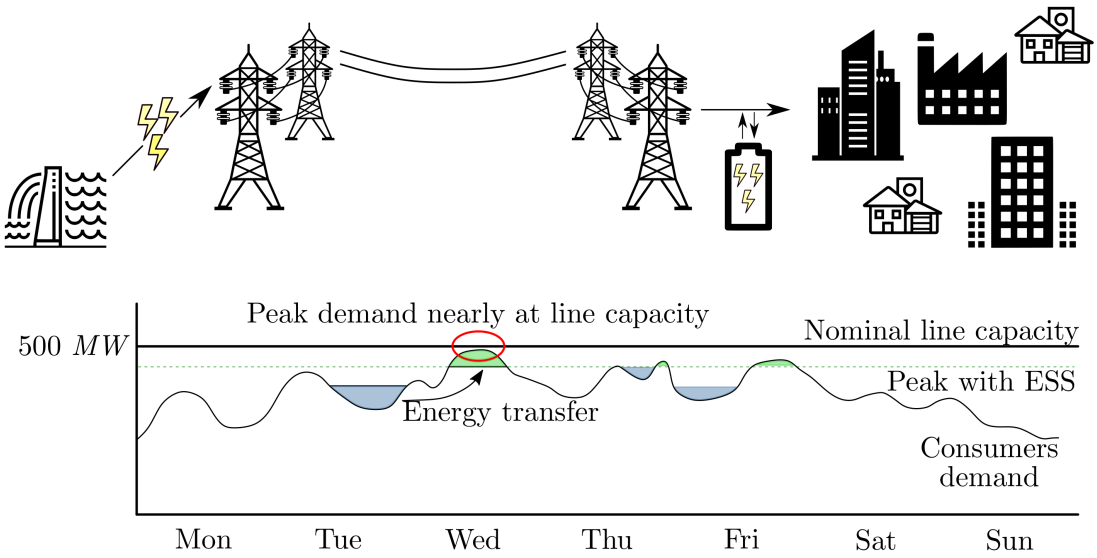

Figure 2.6 – Generic transmission upgrade deferral application.

In Fig. 2.6, a transmission line is running close to its nominal capacity in critical periods. This way, to avoid eventual problems, the distributing company could install a secondary transmission line so alleviate the stress on the main one. However, this solution would have heavy economical expenses, and would result on the new lines being underutilized for most of the time. So, a way around this problem would be to utilize a Energy Storage Systems that charges during lower demand (blue shaded areas), when the distributing network is operating well below its capacity, and discharge during these critical periods (green shaded areas). This way, the existing infrastructure can cope with a larger demand without requiring upgrades.

In their paper, (AGUADO; TORRE; TRIVIñO, 2017) studied introduction a Battery Energy Storage to a complex hypothetical distributing network, aiming to maintain the installed transmission capacity while increasing demand. In this paper, two main scenarios were simulated: (i) a 6-bus, 5 transmission lines, 3 generating sources and 5 demand points, coupled with 40 *MWh* of batteries installed and (ii) a 24-bus, 34 transmission line, 11 generating units and 17 demand nodes system was studied, with 30 *MWh* battery installed in each bus node. The results showed that even though the initial cost would be significant, the short and long term benefits of the BES would not only postpone upgrade necessity, but could also be used for economical benefits, and can be a potential solution to many real life transmission lines that are running close to their limits.

2.3.4.2 Transmission congestion relief

Transmission congestion relief is technically similar to transmission upgrade deferral application, in which an ESS is used to alleviate energy transmission during critical periods.

However, in congestion relief applications, the main focus is to reduce short term economical issues (SNL, 2016). Transmission congestion occurs when the consumers demand is greater than a line capacity, causing the distributing system to re-route the exceeding power through secondary or more distant lines, dispatching the energy from different source or denying it to consumers altogether (LESIEUTURE; ETO, 2003). In Fig. 2.7, the concept of transmission congestion is presented.

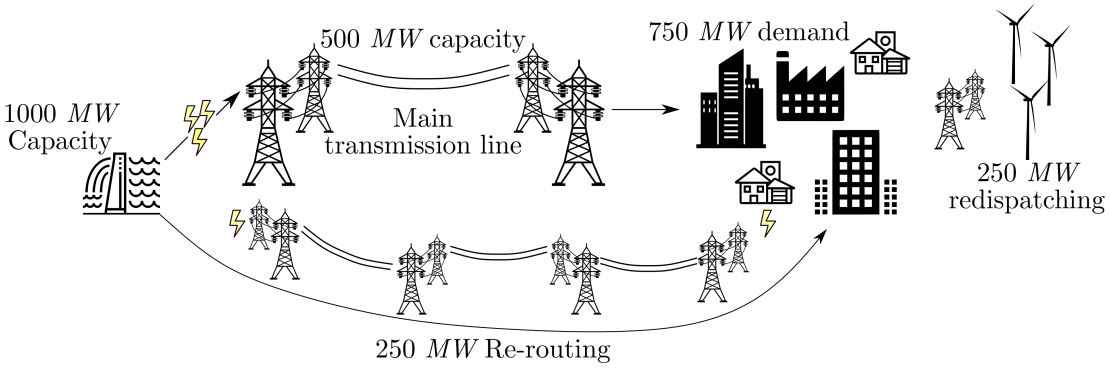

Figure 2.7 – Example on transmission congestion.

In Fig. 2.7, a hypothetical occurrence of transmission congestion is presented, in which a 750 MW consumer demand cannot be directly supplied by the hydro power plant, even though it is rated for 1000 MW. This is due to the 500 MW main transmission line being already at its maximum capacity. Two solutions were presented in the figure, either re-routing the remaining power through a secondary, longer and more expensive line or redispatching the generation to another source, in case, represented by a wind farm. In either way, there are significant economical losses. In the US, estimated costs of congestion figured at over 500 $Mi\ USD$ in the year of 2002 alone (LESIEUTURE; ETO, 2003). This is an escalating problem, given that in ten years, between 2006 and 2016 in the US, transmission costs jumped from $\approx 20\%$ to nearly 40% of the energy price (EIA, 2017).

Instead of re-routing or redispatching the energy, another way around this situation would consist on installing an Energy Storage Systems on the consumer end of the main transmission line. This way, during lower demand, the 500 MW line would simultaneously charge the ESS and supply the consumers demand. Then, during peak consumption over this 500 MW threshold, the extra required power would be provided by the nearly located ESS, mitigating economical losses and eliminating the requirement of re-routing and/or redispatching energy (SNL, 2016). In Fig. 2.8, a generic application of ESS operating to as transmission congestion relief is presented over a week.

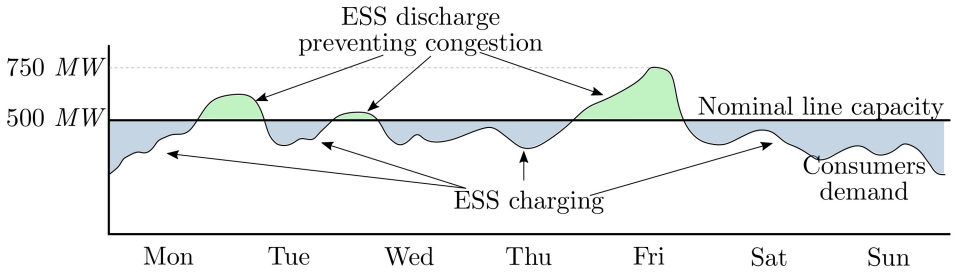

Figure 2.8 – Generic application of an ESS to eliminate transmission congestion.

2.3.5 Infrastructure upgrade deferral

Infrastructure upgrade deferral is similar to the previously explained transmission upgrade deferral, however being aimed not only at transmission lines, but also substations and generation sources. Additionally to power delivery, it can also apply to quality issues and voltage support (SNL, 2016). In this case, any technical upgrades in the distributing network can be postponed or avoided by applying ESS. A study published by the Sandia National Laboratories in 2009 estimated annual savings of up to $2000 USD\ kWh^{-1}$ of energy stored with infrastructure upgrade deferral purposes (SNL, 2009). In Fig. 2.9 a generalized application of ESS as infrastructure upgrade deferral is presented.

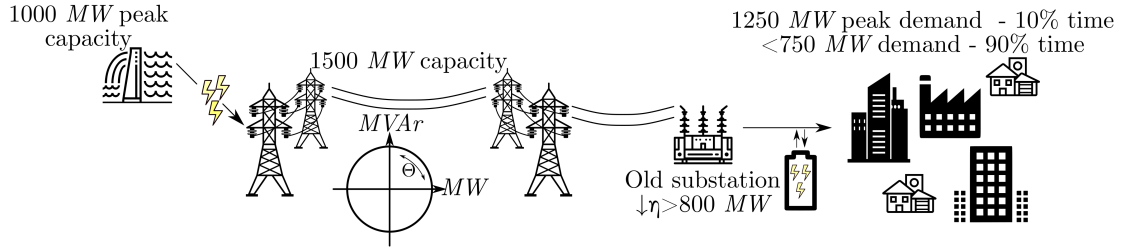

Figure 2.9 – Infrastructure upgrade deferral by utilizing ESS.

In the particular example presented in Fig. 2.9, the ESS was utilized to deal with three problems. Firstly, the final consumers demand peaks at 1250 MW for a short period of time ($\approx 10\%$), remaining under 750 MW for most of the period. However, the main generating source is only capable to output 1000 MWp, thus, not being able to directly supply the required peak power. If upgraded, the new generating capacity would not only represent economical impacts, but also be heavily underutilized for most of the time. For this reason, an Energy Storage Systems can be installed at the consumers end of the grid, charging during lower demand and providing the surplus during peak, avoiding generation upgrades.

Secondly, an old substation is installed next to the consumers. The equipment efficiency drops significantly over 800 MW, and a direct solution could be to replace the main transformer. However, if a Energy Storage Systems is installed downstream of this

bottleneck, it would be possible to mitigate the negative impact of running above the optimal point by managing the load-demand balance around this 800 MW threshold. Lastly, voltage support would be provided by the ESS, managing the power factor Θ. Instead of acquiring equipment specifically to modulate the power factor, the distributing company could use already installed ESS to control it.

These applications frequently overlap, with a single ESS performing many roles simultaneously. These definitions were based on (SNL, 2016), and are generally easily found in the available literature, however, there are different methods of classifying the various ESS. There are many other usages for ESS, but these are mostly case oriented and too numerous. Therefore, the applications hereby presented corresponds to the most commonly found in the literature and in practice worldwide. Furthermore, there are several *"grey-areas"* in the definitions, and categorizing a single application to a complex and interconnected system is certainly a non trivial task. Now, a review on the most relevant storage systems will be presented.

2.4 ESS types

Firstly, in Sec. 2.2, ESS categories were introduced, aiming to provide background information on their general features and application potential. The following section will now describe and assess specific details on the most commonly researched and applied ESS.

2.4.1 Electrochemical (Batteries)

For their widespread usage, batteries may be the most intuitive form of energy storage, powering mobile devices, vehicles and even houses. First proposed at late $1700's$ by Alessandro Volta, batteries are sets of stacked electrochemical cells generating DC electric potential. Even though a single cell may not provide enough power, they can be combined in different arrangements to create high voltage and current capability. Batteries work under the concept of chemical compounds being converted between two energy states. In batteries, this chemical reaction is divided into two electrodes, a positive and a negative one, immersed in a conductive electrolyte medium which allow charges to be exchanged between electrodes (KIEHNE, 2003). In Fig. 2.10, the basic working principle of a rechargable battery is schematically presented.

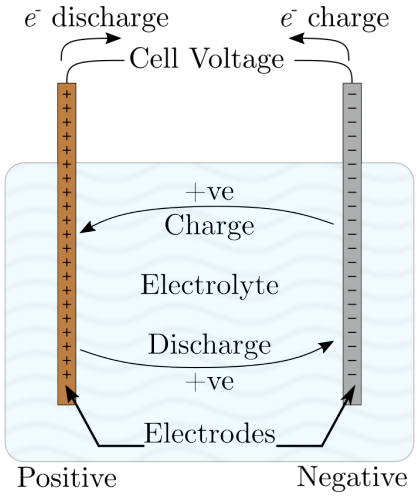

Figure 2.10 – Schematic representation of the working principle of a battery.

Two main types of battery are usually reported in the literature, primary and secondary (KIEHNE, 2003), which are essentially single use non-rechargeable and multiple cycle rechargeable batteries, respectively. The main focus of the following section will be secondary systems. According to (DIVYA; ØSTERGAARD, 2009), it is possible to categorize batteries by their working principle as follows.

2.4.1.1 Lead-Acid

In lead-acid batteries, the chemical reaction occurs between a negative lead sponge and a positive lead dioxide electrodes, submerged in a sulphuric acid solution working as electrolyte (DIVYA; ØSTERGAARD, 2009), described by the following chemical reaction

$$2PbSO_4 + 2H_2O \underset{Discharge}{\overset{Charge}{\rightleftharpoons}} Pb + PbO_2 + 2H_2SO_4$$

Lead-acid are popular choices due to their simplicity and low cost, making them the standard for car batteries and uninterrupted power supplies (UPS). Also, they can withstand elevated current surges, enabling them to be used for power quality, reliability and as sipping reserves (SKYLLAS-KAZACOS, 2010).

However, the lead-acid battery performance decreases severely under high charging or discharging rates, which hinders and limits its application (PINNANGUDI; KUYKENDAL; BHADRA, 2017). This is mainly due to gaseous accumulation in the electrodes, formed in the partial oxidation and reduction reaction. This gases, mainly O_2 and H_2 are not consumed quickly enough and decrease the system capacity (KIEHNE, 2003). Also, it is not recommended to maintain these batteries discharged for a long period, because lead sulfate crystals are formed in the electrodes, reducing their effective available area (SKYLLAS-KAZACOS, 2010).

Even though lead-acid batteries can be easily recycled, their incorrect disposal is harmful to the environment, and thus, must be properly handled. The self-discharge ratio

is relatively low under normal circumstances, figuring at $2 - 5\%$ per month (KIEHNE, 2003). Also, since lead is a high-density material, their practical specific energy is relatively low, figuring at only $20 - 50\ Wh\ kg^{-1}$.

Recently, the Australian Commonwealth Scientific and Industrial Research Organization developed a hybrid solution integrating lead-acid batteries to supercapacitors, named UltraBattery. The supercapacitor increases the capability under high power scenarios, with elevated charge and discharge ratios. For these reasons, UltraBatteries are being proposed to Electrical Vehicles, delivering high power rapidly and performing efficient regenerative breaking (LAM; FURUKAWA, 2009).

2.4.1.2 Sodium Sulphur NaS

In Sodium Sulphur batteries, differently from most batteries, the electrodes are liquid and the electrolyte is solid. The positive electrode is made of molten sulphur, whilst at the negative liquid sodium is used. They are separated by solid beta alumina ceramic electrolyte, which only allows positive sodium ions movement. The main reaction that describes the process is (KIEHNE, 2003; SKYLLAS-KAZACOS, 2010)

$$Na_2S_x \underset{Discharge}{\overset{Charge}{\rightleftharpoons}} 2Na + xS$$

In which x represents the sulphur oxidation state. NaS batteries have to be kept over $300°C$ at all times, otherwise the solidification processes can mechanically damage their interior structure. Furthermore, these type of battery have high efficiency rating (close to 90%) and are able to withstand power surges of up to 6 times its nominal capacity for small periods of time (PINNANGUDI; KUYKENDAL; BHADRA, 2017; KIEHNE, 2003; SKYLLAS-KAZACOS, 2010; DIVYA; ØSTERGAARD, 2009).

Sodium sulphur batteries can reach energy density figures up to $120\ Wh\ kg^{-1}$, however their higher price, requirement for special maintaining conditions and complicated construction are drawbacks of this technology. Figure 2.11 presents a schematic NaS battery.

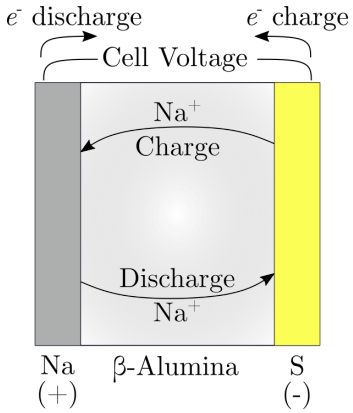

Figure 2.11 – Generic NaS battery.

In Fig. 2.11, during discharge, Na^+ ions leave the positive electrode towards the negative charged liquid sulphur in the right hand side. There, it forms Na_2S_x compounds, depending on the oxidation state. Then, when a back EMF force is applied during recharge, the Na_2S_x is converted back into metallic sodium and sulphur (KIEHNE, 2003).

2.4.1.3 Lithium-ion and Lithium-Polymer (LiPo)

Lithium-ion technology have had a major role in recent development of electronic mobile devices. Lithium-ion batteries offer excellent specific energy values while having low self discharge rate and extended life expectancy (QIAO; WEI, 2012). In these type of battery, the positive electrode (anode) is made out of activated carbon, usually some form of graphite. Conversely, the negative electrode (cathode) consists of a layered metallic lithium oxide, usually $LiCoO_2$ (lithium cobalt oxide). However, other options such as lithium iron phosphate $FeLi_O4P$ and lithium manganese oxide $LiMn_2O_4$ (QIAO; WEI, 2012; KIEHNE, 2003). The general chemical reaction dictating the process is

$$6C + LiCoO_2 \underset{Discharge}{\overset{Charge}{\rightleftharpoons}} Li_{1-x}CoO_2 + Li_xC_6$$

A major challenge in the development of lithium-ion batteries was discovering an appropriate electrolyte and containment structures. Lithium is a light, white-silvery and extremely reactive metallic element, which when exposes to air ignites spontaneously. These features make Li an attractive solution to electrochemical storage if properly handled, but also impose safety hazards in case of exposure, especially considering that lithium salts can be even more reactive than the metallic form (KIEHNE, 2003; PINNANGUDI; KUYKENDAL; BHADRA, 2017; QIAO; WEI, 2012; SKYLLAS-KAZACOS, 2010).

The electrolyte chosen to operate in Li-ion batteries are usually consisted of a solution of lithium salts (*e.g.,* $LiPF_6$) diluted in an organic solvent. In terms of specific energy, Li batteries return elevated values, ranging from $90 - 190\ Wh\ kg^{-1}$ (KIEHNE, 2003), with some sources reporting up to 400 $Wh\ kg^{-1}$, and close to 100% efficiency

with long life cycles (SKYLLAS-KAZACOS, 2010). However, the hazardous nature of lithium imposes technical complexity, which results in elevated costs. Nevertheless, recent developments towards high-energy batteries made Li batteries cheaper and smaller while holding more energy. This way, it is commonly used in mobile devices, electric vehicles and households (TESLA, 2019).

More recently a new trend in the development of lithium batteries are Lithium Polymer (LiPo). Differently from conventional Li batteries, in LiPo the electrolyte is not based on a liquid solution of Lithium salts, but instead consist of a semi porous polymeric matrix, embedded with lithium compound responsible for transferring ions between electrodes. These polymeric electrolytes can be solid or in a form of gel (ALDALUR et al., 2019; YAO et al., 2019). Due to the higher stability of the polymeric base when compared to conventional lithium-ion liquid electrolyte, LiPo are less likely to explode. Furthermore, liquid electrolytes are more likely to result in uneven lithium deposit in the electrodes, leading to dendrite formation (ZHU et al., 2019). A couple examples of polymers and lithium compounds used as the electrolyte matrix are:

- Polyacrylonitrile (PAN), Ethylene Carbonate (EC) and Propylene Carbonate (PC) embedded with lithium trifluoromethanesulfonate ($LiCF_3SO_3$), resulting in a specific energy of 155 $Wh\ kg^{-1}$ and electrolyte electrical conductivity of $1.2 \cdot 10^{-3}\ S\ cm^{-1}$ (PERERA et al., 2008);
- Alternating layers of electrically deposited poly(vinyl difluoride) (PDVF) and poly(methyl methacrylate) (PMMA). In the study, only the polymeric electrolyte was analyzed, and a electrical conductivity of $1.93 \cdot 10^{-3}\ S\ cm^{-1}$ was found (XIAO et al., 2009);

2.4.1.4 Metal-air

Unlike the previously presented system, in which both electrodes consisted on liquid or solid materials, in Metal-Air Battery (MAB) the cathode consists of a porous matrix which allows O_2 from the air to diffuse and react with ions coming from the metallic anode (LI; LU, 2017). The general operation of Lithium MAB is presented in Fig. 2.12.

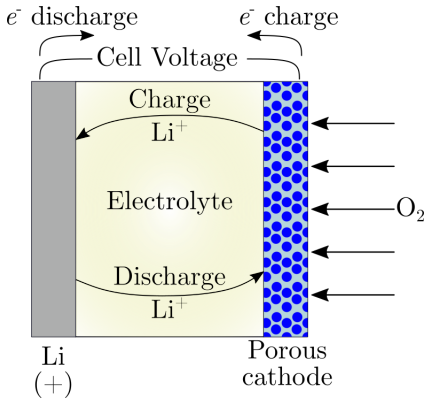

Figure 2.12 – Lithium-air battery operation.

During the battery discharge, electrons flow from the lithium anode through the load to the cathode, and start to build up and attract free positive lithium ions, which move through the electrolyte and combine with oxygen and the electrons to form LiO_2. Additionally, the reaction can continue further with another reduction forming LI_2O_2 (LI; LU, 2017; LEE et al., 2011; PARK et al., 2015). During recharge, the back EMF forces the opposite reaction, as follows

$$Li^+ + e^- + O_2 \underset{Discharge}{\overset{Charge}{\rightleftharpoons}} LiO_2$$

$$LiO_2 + Li^+ + e^- \underset{Discharge}{\overset{Charge}{\rightleftharpoons}} Li_2O_2$$

In Metal-Air Battery the electrolyte can be liquid or solid capable of transferring the lithium ions. MAB possess elevated specific energy figures, between 350 and 500 $Wh\ kg^{-1}$ (GIRISHKUMAR et al., 2010; KIEHNE, 2003). However, MAB present lower efficiency levels, or around 60% and have smaller life cycle expectancy (PARK et al., 2015; LI; LU, 2017). Another issue in Metal-Air Battery is found during the recharge process, in which an overvoltage of around 1 V is required to drive the chemical reaction. This leads to smaller efficiencies and faster electrode degradation.

2.4.1.5 Flow batteries

Flow Battery (FB) operates under the ionic exchange principle, like the previously presented examples. However, in FB the electrolyte and electrodes are combined in liquid solutions, catholyte and anolyte, which are stored in separated tanks. These solutions are then pumped into a third tank, divided by a ionic membrane which allows charge exchange (SKYLLAS-KAZACOS, 2010). A general representation of a single cell Zinc-Cerium flow battery is presented in Fig. 2.13.

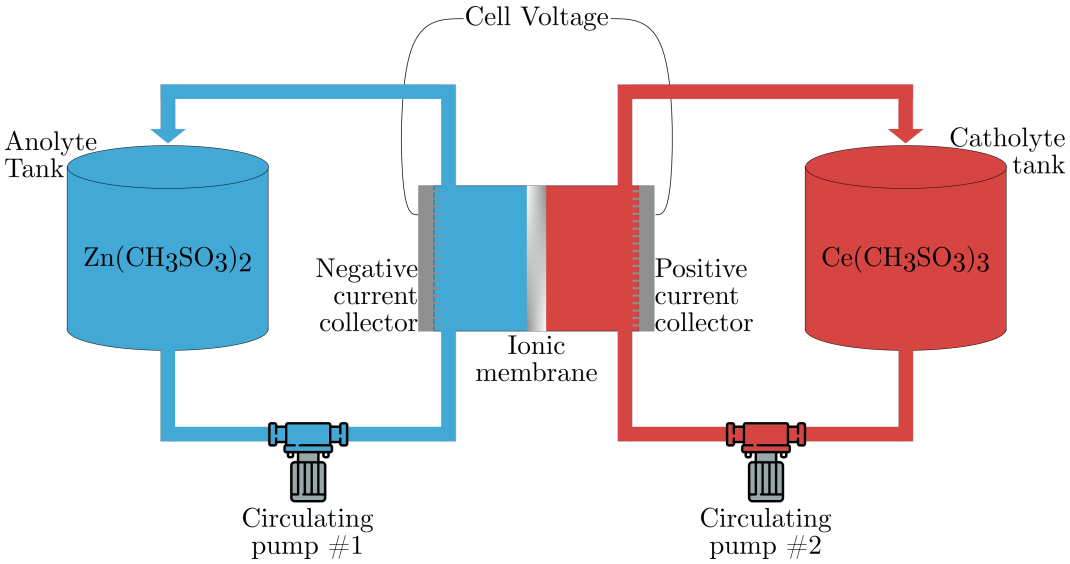

Figure 2.13 – Operating principles of a Zinc-Cerium flow battery.

Zinc-Cerium flow batteries, as presented in Fig. 2.13, operate by flowing Zn and Ce solutions to a divided tank, with an ionic membrane separating the liquid solutions. The electrolytic base of this type of battery is usually methanesulfonic acid (CH_3SO_3) due to the elevated solubility of both components, high electric conductivity and low corrosive potential (LEUNG et al., 2011b; NIKIFORIDIS et al., 2013; LEUNG et al., 2011a). During the system charge, in the negative side of the intermediate tank, zinc chemically bounded to the acid in a 2^+ oxidation state receives two electrons given by the Cerium oxidation. The main chemical reactions are

$$Zn^{2+}(CH_3SO_3)_2^- + 2e^- \underset{Discharge}{\overset{Charge}{\rightleftharpoons}} Zn + 2CH_3SO_3 \qquad (anode)$$

$$2Ce^{3-}(CH_3SO_3)_3^+ + 2(CH_3SO_3) \underset{Discharge}{\overset{Charge}{\rightleftharpoons}} 2Ce^{4-}(CH_3SO_3)_4^+ + 2e^- \qquad (cathode)$$

Then, yielding the the global chemical reaction

$$2Ce^{3-}(CH_3SO_3)_3^+ + Zn^{2+}(CH_3SO_3)_2^- \underset{Discharge}{\overset{Charge}{\rightleftharpoons}} Zn + 2Ce^{4-}(CH_3SO_3)_4^+$$

The reaction sometimes creates H_2 and O_2 as undesirable side products, which decreases durability and performance (LEUNG et al., 2011b). Flow Battery are unique in the sense that they require external energy to power the pumps during recharge. However, a positive aspect of the this singular operation is that since the charged electrolytes are stored in independent tanks, the self discharge ratio is practically negligible. Also, power output can be regulated by the pumps volumetric flow rate (DIVYA; ØSTERGAARD, 2009). Furthermore, FB have elevated efficiency, especially at higher temperatures (due to

diffusion effects) and reasonable to good life expectancy, and can reach high specific energy levels ($\approx 600\ Wh\ kg^{-1}$) (DIVYA; ØSTERGAARD, 2009; KIEHNE, 2003; LEUNG et al., 2011b; NIKIFORIDIS et al., 2013; LEUNG et al., 2011a; SKYLLAS-KAZACOS, 2010).

2.4.2 Electrical

Electrical storage differs from electrochemical in the sense of instead of depending on energy released or absorbed from chemical reactions, the energy is directly stored in electric (Capacitors and Supercapacitors) or magnetic fields (Superconducting Magnetic Energy Storage).

2.4.2.1 Capacitor and Supercapacitor

A capacitor is a simple and well-established passive electrical components, with its roots as old as the Leiden Jar, proposed in 1745 by Dutch researcher Pieter Van Musschenbroek (HEILBRON, 1979). It consists of two conductive electrodes (plates) separated by a dielectric material. When exposed to a external electromotive force, the electric field generated by this EMF creates a charge separation on the capacitor plates, storing energy. A generalized construction of a parallel plate capacitor is presented in Fig. 2.14.

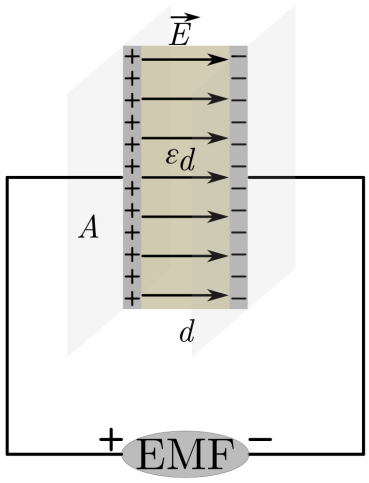

Figure 2.14 – General depiction of a flat place capacitor.

From figure 2.14 there are three main variables to the amount of charge a capacitor can hold: (i) the distance d between the electrodes, (ii) the plates area (A) in contact with the dielectric and (iii) the dielectric constant of the insulating material ε_d (HALLIDAY; RESNICK; WALKER, 2010). Then, the capacitance C, defined as the amount of electric

charge a capacitor can hold when exposed to a external V EMF is defined as

$$C = \frac{\varepsilon_d A}{d} \tag{2.1}$$

in which the capacitance C is given in farad F. Then for a given V EMF applied to the capacitor, its stored energy (E) can be given as (HALLIDAY; RESNICK; WALKER, 2010)

$$E = \frac{1}{2} C V^2 \tag{2.2}$$

From Eq. 2.2 it is easily noticeable that larger capacitance, for a given nominal voltage, result on more stored energy. However, conventional capacitors have capacitance in the order of μF, meaning that by themselves, are unable to store large amounts of energy. To make the matter worse, by combining capacitors in series to increase their overall voltage capacity, the resulting capacitance is decreased while its Equivalent Series Resistance (ESR) increases. Hence, conventional capacitors are most often used to store small amounts of energy, filtering, phase shifting and power factor control.

An evolution of the capacitor has emerged in the last decades. The Electric Double-Layer Capacitors (ELDC's), more commonly known as Supercapacitor (or Supercap) is constructed to optimize the parameters that define the capacitance, presented in Eq. 2.1. Firstly, however, it is necessary to present a general ELDC's constructive layout to improve understanding of its operation.

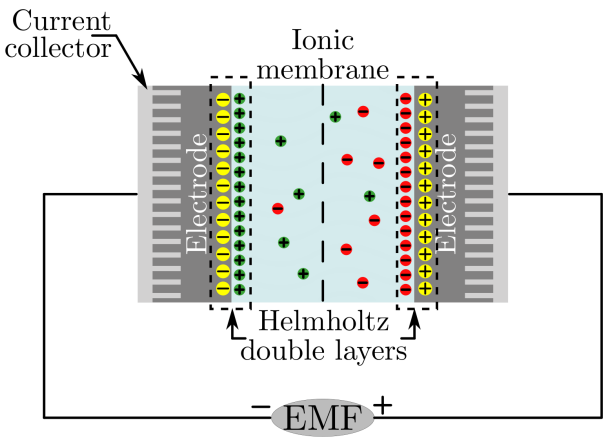

Figure 2.15 – Electric Double-Layer Capacitor constructive scheme.

The Electric Double-layer is an effect which greatly increases overall capacitance by its own. The Double-Layer effect occurs in the interface between the solid electrode and the liquid (or semi-liquid) electrolyte, and it consists on the charges accumulated in the electrode polarizing the electrolyte, attracting opposite charges towards it. In this

border, the opposing layers will not be able to cancel each other, remaining separated by atomic-scale distances and build up a capacitive behaviour (ZHANG; ZHAO, 2009). Conversely, on the opposite end of the supercap, the same effect occurs (CONWAY; BOCKRIS; AMMAR, 1951).

A second technique utilized to increase overall capacitance in Electric Double-Layer Capacitors is increasing the electrode areas. In conventional electrolytic capacitors, sheets of metal foil and insulating material are rolled into a cylindrical shape. Albeit increasing the capacitance, this technique can only increase the contact area to a certain limit, whilst also inducing considerable parasitic inductance. So, for supercapacitors another technique is implemented. Instead of utilizing a metal sheet for electrode, in ELDC's carbon based nanostructures are utilized (ZHANG; ZHAO, 2009; WANG; STRAUSS; KANER, 2019). These structure presents pores and protrusions which greatly increases the contact area, which reaches values up to 1700 $m^2\ g^{-1}$ (WANG; STRAUSS; KANER, 2019).

Lastly, advances have been made to increase the performance of the electrolyte. Ideally, the electrolyte should present elevated ionic conductivity whilst retaining its electrical insulating properties. In recent publications, it is possible to notice a tends to utilize polymeric gels embedded with ionic components, responsible for creating the Double-Layer effect (CHAE et al., 2018; YANG et al., 2019; PENG et al., 2019).

These three effect combined results in considerably large capacitances. While conventional electrolytic capacitors range from a few nF to a a few hundred mF (INTERTECHNOLOGY, 2015; TOKIN, 2017), supercaps can easily surpass 200 F, reaching nearly 1 kF in a single component (MOUSER, 2017).

A key aspect of ELDC's which differs from electrochemical storage is the quick response, capable of delivering high power nearly instantaneously. Electric Double-Layer Capacitors have high power density, whilst presenting low specific energy. For this reason, supercaps are often applied as first response to any power fluctuation or outage, being more often used for power quality and reliability issues as well as frequency and voltage support. However, due to their limited storage capacity, they cannot be applied to bulk energy storage, congestion relief, Non-Spinning Reserve to name a few (DAS et al., 2018; USDE, 2013).

2.4.2.2 Superconducting Magnetic Energy Storage (SMES)

Whilst Electric Double-Layer Capacitors systems store energy in electric fields, Superconducting Magnetic Energy Storage (SMES) utilizes magnetic fields in superconductors cooled to nearly absolute zero. SMES are usually constructed in toroidal shapes cores, wound by special copper alloys. When cooled below the critical temperature T_C, the core electrical resistance drops to zero, acting like a superconductor (BARDEEN; COOPER; SCHRIEFFER, 1957).

The operating principle of a Superconducting Magnetic Energy Storage is based on Maxwell-Faraday induction law, which states

$$\varepsilon = \frac{-\partial \phi_B}{\partial t} \tag{2.3}$$

From Faraday's law, it is possible to infer that the electromotive force ε is related to the change in magnetic flux (ϕ_B) in time. However, for a single resistive load, it is possible to establish

$$i = \frac{\varepsilon}{R} \tag{2.4}$$

in which the electrical current (i) is equal to the ratio between the applied EMF (ε) by the electrical resistance (R). If, in a superconducting material, the resistance $R \to 0$, then the electromotive force must also approach zero to avoid creating infinite amount of current, and consequently power. So, if the EMF $\varepsilon \approx 0$, from Maxwell-Faraday law, the rate of magnetic flux change in time must also be null. Consequently, if the SMES is kept below the critical temperature, T_C a large amount of current will flow without power losses, storing energy in the magnetic field B.

The storage operating procedure of Superconducting Magnetic Energy Storage consist on converting the AC power surplus into DC, and though a PWM operation, send short duration, high frequency current pulses at the primary winding cables. The current flowing in the primary winding cables induces the magnetic field in the secondary superconducting core, charging it (BHUNIA et al., 2014; SHI et al., 2019). When discharging, the opposite happens, decreasing the core current over time. This operation is schematically presented in Fig. 2.16

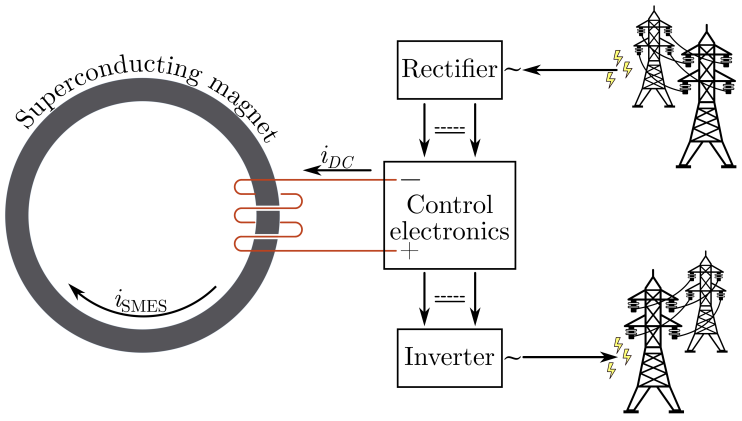

Figure 2.16 – SMES operating principle.

The energy stored in the superconducting core's magnetic field can be expressed by

$$E = \frac{1}{2}Li^2 \tag{2.5}$$

in which L is the inductance and i the current magnitude. The major drawbacks of SMES are the elevated costs, both in construction and operation, and the complexity in operation (JOHNSON et al., 2019). Superconducting materials are expensive to produce and obtain, and must be kept at extremely low temperatures, and preferably, under vacuum conditions during operation. Even the so-called High-Temperature Superconducting materials are required to be kept around 20 K (MUKHERJEE; RAO, 2019; USDE, 2013).

2.4.3 Thermal

Thermal systems have two main variants. Cryogenic Energy Storage (CES) stands on the verge of mechanical and purely thermal categories, while Thermal Energy Storage (TES) can be used for primary and secondary purposes. These technologies will now be explained.

2.4.3.1 Cryogenic Energy Storage (CES)

Cryogenic Energy Storage (CES), also known as Liquid Air Energy Storage (LAES), is a form of energy storage in which the energy surplus power an air liquefying plant. The liquid air is stored, usually at atmospheric pressure, in thermally insulated tanks until the energy is required. Then, it is heated and undergoes phase change, resulting in considerable pressure increase to be directed into air turbines (KIM; CHANG, 2019).

The main difference between CES and CAES systems, the liquefying stage and low pressure storage, significantly increases the storage specific energy, requiring considerably less space to store the same mass of air and simpler storage vessel construction. Also, geographical restriction are overcome (cave for CAES or water head for PHES) (PENG et al., 2019). These positive aspects, however, come for a high price. Air liquefying is a technically challenging, expensive, low efficiency process by its own (MAYTAL, 2006). A general LAES plant layout is presented in Fig. 2.17.

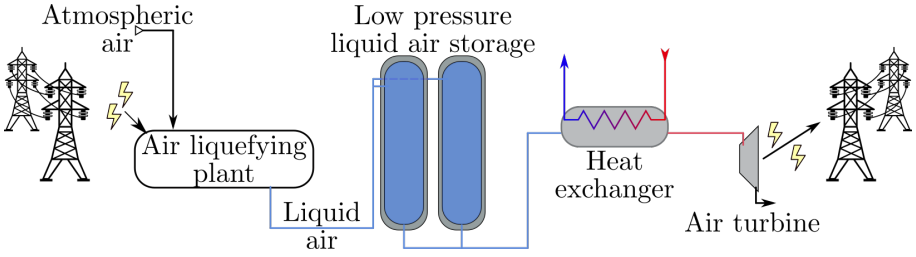

Figure 2.17 – Generalized LAES power plant.

For air at atmospheric pressure, the liquefying process reduces the specific volume from $0,2164$ to $0,00124$ $m^3\,kg^-1$, *i.e.*, a 175 times reduction. This way, the storage requirements are simpler, and cheaper. For instance, CAES Huntorf power plant air storage volume is around $300\,000$ m^3 at a maximum pressure of 70 *bar* (Air is stored close to ambient temperature due to cavern preservation issues) (CROTOGINO; MOHMEYER; SCHARF, 2001), meaning around $2,2 \cdot 10^7$ kg of air stored. The same mass of liquefied air, at atmospheric pressure would require nearly a tenth of the volume, figuring at ≈ 25000 m^3.

HighView Power is a novel project installed in the UK, consisting of the world first medium scale LAES plant. With an installed capacity of $2,5$ MWh, the plant installed at Birmingham University, claims to reach round trip efficiency around 60% (HIGHVIEWPOWER, 2019). Moreover, the available literature exploits changes in the conventional Liquid Air Energy Storage layout and operating principles to achieve higher efficiency figures.

(KIM; CHANG, 2019) proposes a mixture of LAES and CAES systems, in which the liquefied air is stored at pressurized tanks. Even though the liquid air is an incompressible fluid, by starting at a higher pressure already, after experiencing phase change and expansion, even higher output pressure levels are achieved, which in turn, increases the turbines power output and overall efficiency. The study claims that for two similar plants, the pressurized system efficiency would reach 65%, whilst a conventional LAES figured at $55,7$%. (PENG et al., 2019) proposes integrating a conventional LAES plant to a natural gas liquefying station. With this, the authors hope to increase both processes efficiency, by intertwining their thermal requirements. By simulating this proposed solution, the authors were able to increase the round trip efficiency from 53% (conventional LAES) to 76%, whilst also increasing liquid air production.

Anyhow, Liquid Air Energy Storage systems are usually considered for slow response applications, bulk energy storage and infrastructure upgrade deferral. This is mainly due to the high thermal inertia (DAS et al., 2018). Even though LAES presents large similarities to CAES, it is not considered a mechanical ESS because the energy storage is not due to pressure, but in the form of potential internal energy.

2.4.3.2 Thermal Energy Storage (TES)

Thermal Energy Storage (TES) is unique from all Energy Storage Systems presented in this document. Whilst all other solutions aim to directly convert electricity into some kind of storable energy, to later be directly converted back and returned to the grid or final user, TES usually acts as auxiliary storage. It takes heat that would otherwise be wasted, and reintroduces it later on when required (primary), or diverts it completely to another process that would otherwise require heat (secondary) (ALVA; LIN; FANG, 2018), as presented in Fig. 2.18

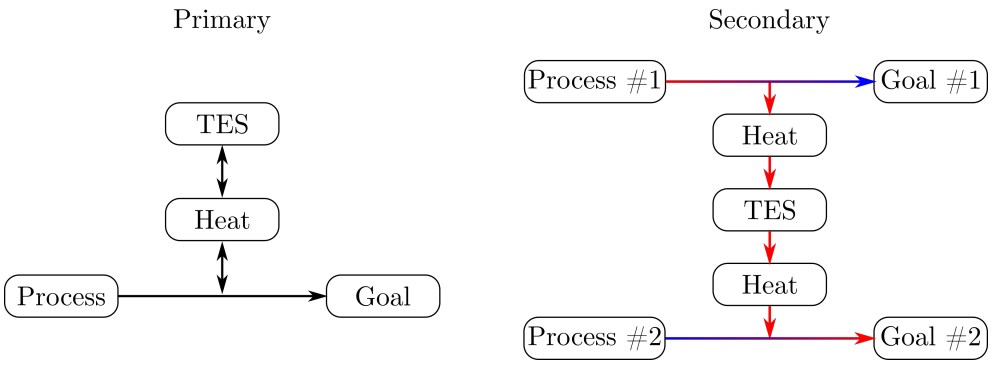

Figure 2.18 – Primary and Secondary TES applications.

Thermal Energy Storage systems operates under two main conceptual principles: (i) sensible and (ii) latent heat storage. In the first type, the heat flow reflects in temperature changes in the storage medium. These are the simpler and cheaper methods, being are widely implemented in industry and domestic context. In many northern countries, in which the winter temperatures are considerably low, maintaining constructions in comfortable temperatures requires large amounts of energy. In 2010 alone, Europe consumed $3,6\ EJ$ specifically for domestic heating, 17% of all electricity supply in that year (PERSSON; WENER, 2008). So, several publications study implementing heat storage in buildings concrete structures, heating during the day and releasing the stored thermal energy at night (ÖZRAHAT; ÜNALAN, 2017; LIANG et al., 2017; NIU et al., 2019).

Sensible heat TES also are applied as auxiliary to other ESS. Namely, in conventional CAES systems, air experiences a significant temperature increase during compression. Then, heat exchangers can be utilized in between compression stages to cool the air, and store the heat in a TES system. This topic is a main research subject as a efficient TES can significantly increase CAES performance (GRAZZINI; MILAZZO, 2008; GUO et al., 2019; WOLF; BUDT, 2014).

Conversely, latent heat TES operate at nearly constant temperature, operating with Phase-Change Materials (PCM). The advantage of latent heat systems is higher energy density. For instance, heating 1 kg of water from 95 to 100°C, 21 kJ of heat energy are required, however, vaporizing the same mass requires 2257 kJ. This way, a number of publication focuses on developing PCM with high latent heat values and low melting points (to decrease losses and complexity) (OUALI et al., 2019; YAN et al., 2019; ZHANG et al., 2013).

2.4.4 Mechanical

Mechanical Energy Storage Systems are usually deemed fit for large scale slow response operations. Peak shaving, load levelling, Spinning Reserve and Non-Spinning Reserve (NSR), upgrade deferral are applications in which mechanical systems were

historically recommended (DAS et al., 2018). However, in the last few years, there has been a new arising interest faster and smaller applications. Mechanical systems have elevated lifetime cycles, with the first PHES being reported in the late 19^{th} century (IHA, 2018). Following, the three main mechanical ESS are presented.

2.4.4.1 Flywheel Energy Storage (FES)

Flywheel Energy Storage (FES) consists on kinetic energy storage devices, with masses rotating around their own axis. Flywheels have long been used by humans to add kinetic inertia and reduce to rotational ripples in different scales, from small devices fitted in analog wrist watches to large wheels attached to hydraulic turbines, vehicles power transmission and steam engines. (AMIRYAR; PULLEN, 2017); The governing equation that describes the kinetic energy for a rotating mass (BUDYNAS; NISBETT, 2011):

$$E = \frac{1}{2} I \omega^2 \tag{2.6}$$

in which I is the rotational moment of inertia and ω is the rotational speed. So, from Eq. 2.6, there are two ways to increase the stored energy: (i) increasing the speed or (ii) the moment of inertia. Increasing the rotational speed produces expressive results because of the quadratic behaviour described in the equation, however there are practical limitations to the extense in which ω can be increased (bearings, stresses, power transmission etc.). So, the moment of inertia must be increased to achieve higher storage capacity. From (BUDYNAS; NISBETT, 2011), a solid cylindrical flywheel moment of inertia can be written as

$$I = mr^2 \tag{2.7}$$

From Eq. 2.7, there are two manners of increasing an object the moment of inertia: (i) making it more massive or (ii) distributing the mass farther away from the rotating axis, *i.e.*, increasing the radius. Once again, the first option has practical limits, so most designs aim to optimize the mass distribution on the flywheel. For instance, Velkess developed a flexible flywheel for energy storage, which would deform at higher rotational speeds, moving the mass further away from the rotation center, increasing the moment of inertia and storage capacity (VELKESS, 2013). The company, however, filed bankruptcy in early 2016.

Flywheel Energy Storage operation is simple, with the excess energy powering an electric Motor-Generator Unit (MGU) during storage, increasing the wheel rotational speed. Later on, during recovery, the flywheel momentum keeps the MGU turning, generating electricity that is returned to the distributing system. Historically, flywheels were not considered for direct energy storage, being restricted to ripple management. However, in

the last few years, the development of magnetic bearings, control electronics, composite materials and advanced assembly techniques has lead to the return of high power and energy flywheels (DAS et al., 2018; AMIRYAR; PULLEN, 2017).

FES systems, given the correct maintenance, have nearly infinite life cycle, high round trip efficiency, low self-discharge rate, high power and energy density. For long-term storage, frictional losses due to the rotational are mitigated with fully magnetic floating bearings, and encapsulating the rotor in a vacuum chamber (BEACONPOWER, 2014). As recent as May 2018, the largest US flywheel plants were installed in Stephentown, Ny and Hazle Township, PA, each with 40 MW nominal capacity distributed over 400 steel-composite rotors, each weighing 5 *ton* (BEACONPOWER, 2018).

The current trend in Flywheel Energy Storage is modular installation, in which a standard model offered by the manufactures can be applied to a large range of scales. This way, costs are reduced, mass manufacturing ensures higher reliability and flexibility. An example of an actual FES, followed by a schematic representation are shown in Fig. 2.19.

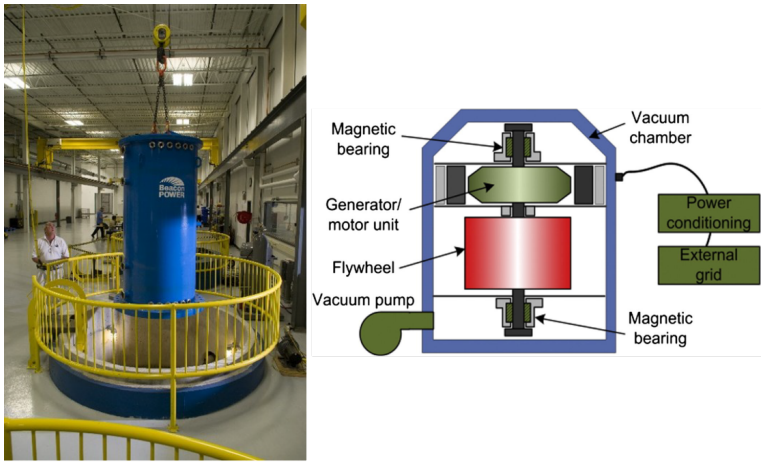

(a) (b)

Figure 2.19 – Flywheel Energy Storage (FES): (a) Beacon Power modular unit and (b) schematic representation of the components. Adapted from (BEACONPOWER, 2014) and (LUO et al., 2015).

FES application range is very wide, making it one of the most versatile ESS technology. Due to their quick response time, large charge and discharge rates, elevated power and energy density, with high rount-trip efficiency it is recommended for bulk energy storage, peak shaving and load levelling, ancillary services and upgrade deferral (AMIRYAR; PULLEN, 2017; LUO et al., 2015).

2.4.4.2 Pumped hydraulic Energy Storage (PHES)

Even though there are few purpose build installations, Pumped Hydroelectric Energy Storage (PHES) is the most utilized form of Energy Storage Systems in the world,

representing $<90\%$ of the global stored energy, with installed power and energy capacities of 150 GW and 9 TWh, respectively (REN21, 2017; IHA, 2018). Most PHES plants worldwide were commissioned for an existing Hydro Power Plants (HPP) (IHA, 2018). PHES operating principle is presented in Fig. 2.20

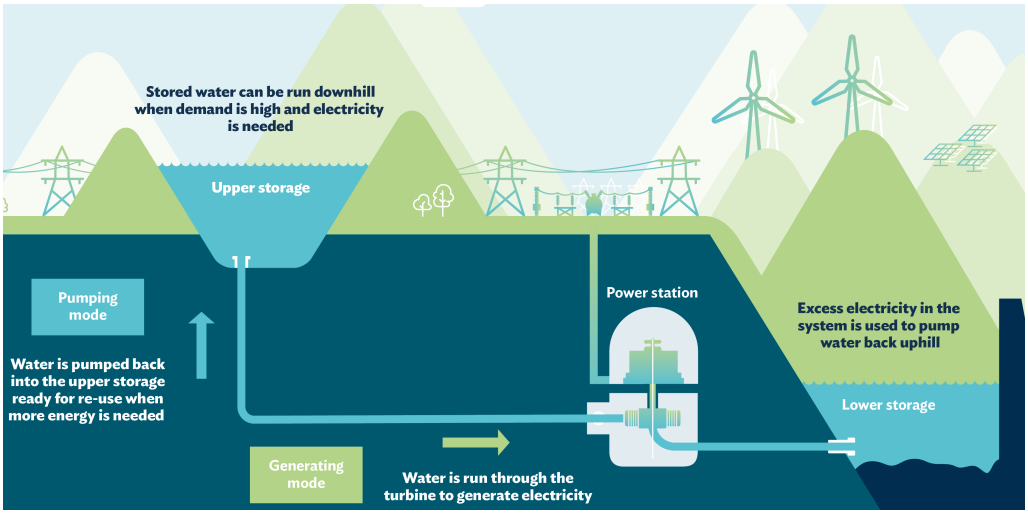

Figure 2.20 – PHES operating principles. Courtesy of Hydro-Tasmania.

Pumped Hydroelectric Energy Storage is one of the most positive ESS form, presenting excellent efficiency figures ,$\approx 75\%$ (LUO et al., 2015), little self discharging rate (evaporation and percolation only), large energy and power capacity. Also, is a versatile solution if incorporated to an already existing HPP, with little to no impact on the existing structure (REHMAN; AL-HADHRAMI; ALAM, 2015). However, the power density is relatively low, limited to the water density, figuring at 1 $Wh\ kg^{-1}$ (CHEN et al., 2009). This is a disadvantage, especially if a new PHES plant is to be constructed.

Another major challenge for new Pumped Hydroelectric Energy Storage (PHES) plants is finding a suitable geographical installation site. From the electrical point of view, it is desirable to locate the PHES near the center of the demands, reducing losses over long distribution lines. Socially, it is not adequate to have large water dams near populated cities, due to the elevated associated security reach in case a levee breaks. Geographically, the water basin chosen for installing the reservoirs and power strucutres must present adequate soil and elevation drop, and the social, environmental and economical impacts of flooding a large area must be considered when commissioning a new plant. For this reason, a number of recent publications deals with finding suitable locations for new PHES systems (LU et al., 2018; NZOTCHA; KENFACK; MANJIA, 2019; GHORBANI; MAKIAN; BREYER, 2019).

Pumped Hydroelectric Energy Storage systems usual applications are related to long term storage, peak shaving, load levelling as well as Spinning Reserve, Non-Spinning Reserve, black start applications, voltage and frequency support (DAS et al., 2018; LUO

et al., 2015; REN21, 2017).

2.4.4.3 Compressed Air Energy Storage (CAES)

The other major bulk energy storage system used worldwide is the Compressed Air Energy Storage (CAES). Similarly to PHES, CAES systems also mechanically store the surplus energy. However, instead of water, CAES utilizes atmospheric air as the working fluid. By utilizing compressors, air is pressurized and stored in artificial or natural pressure vessels. Later on, when energy is required, the air passes through an expansion process, driving turbines and generators (SNL, 2016; BUDT et al., 2016). A general depiction of an A-CAES system is presented in Fig. 2.21 There are two large scale CAES plants worldwide: (i) Huntorf in Germany, a originally 260 MW CAES plant (later revamped to 321 MW) (CROTOGINO; MOHMEYER; SCHARF, 2001) and (ii) McIntosh in the USA, with an installed capacity of 110 MW (BIASI, 1998; POLLAK, 1994).

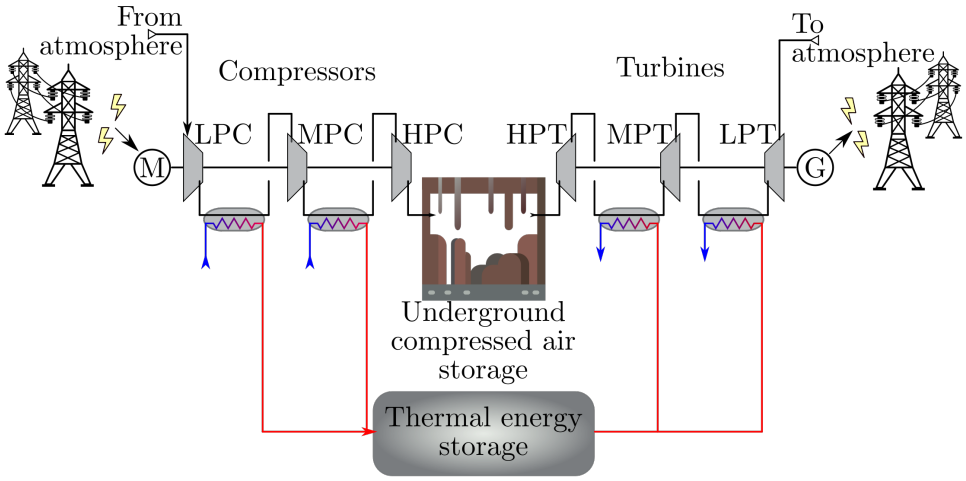

Figure 2.21 – General A-CAES system with three compressors and turbines in series. LPC, MPC, HPC, LPT, MPT and HPT are low, medium and high pressure compressors and turbines, respectively.

Conventional CAES systems, however, require a complex temperature management, as the air heats up considerably during the compression, and classic systems are divided into three main categories (BUDT et al., 2016): (1) adiabatic (A-CAES) in which the heat generated during the compression is stored, usually in a Thermal Energy Storage (TES), to later be reintroduced in the expansion stage (WOLF; BUDT, 2014; PENG et al., 2016; SCIACOVELLI et al., 2017; TOLA et al., 2017; GRAZZINI; MILAZZO, 2008); (2) diabatic (D-CAES) the heat is dissipated and lost to the surroundings, having as consequence the necessity of introducing an external source of energy during the expansion (BRIOLA et al., 2016; JIN; LIU; LI, 2017); and finally (3) isothermal (I-CAES) in which techniques such as extended surfaces installed on the compression chamber or turbine (HEIDARI; MORTAZAVI; RUFER, 2017), liquid pistons (VEN; LI, 2009), water droplets

(ZHANG et al., 2018; GUANWEI et al., 2018) or foam (MCBRIDE; BELL; KEPSHIRE, 2013) are used to prevent air temperature variation during compression and expansion. Both commercial CAES plants operate as D-CAES, and burn natural gas during expansion (CROTOGINO; MOHMEYER; SCHARF, 2001; POLLAK, 1994; BUDT et al., 2016). Additionally, many innovative solutions such as underwater U-CAES (LI; DECAROLIS, 2015; WANG et al., 2016; CHEUNG; CARRIVEAU; TING, 2014), aquifer (GUO et al., 2016; GUO et al., 2017), integration with floating photovoltaic plants (CAZZANIGA et al., 2017). Additionally, smaller systems are being studied as an option to increase the CAES share of the ESS market (MAIA et al., 2016; VOLLARO et al., 2015; SALVINI; MARIOTTI; GIOVANNELLI, 2017; ALAMI et al., 2017).

3 The PH-CAES System

3.1 Context

In section 2.4.4.3, the operating principles of CAES systems were presented. Besides the technical complexity of thermal management, conventional CAES system present other disadvantages that have hindered its economical success. Despite being a mature technology and literature regarding advances in the technology are abundant, the fact that only two large plants exist indicate that in the current state CAES is not viable. Following, a few main problems that the author credits as CAES major drawbacks will be presented: (i) compression and expansion method; (ii) variable pressure turbine inlet and (iii) geographical requirements.

- Compression and expansion method

  In conventional systems, compressors and turbines are used to impose pressures changes in the air. However, the operating principles of these devices result in technical and economical drawbacks. While small scale commercial compressors are not expensive, they are not constructed aiming high efficiency figures, as their usual applications do not require it. In a meeting with a global leading compressor manufacturer representative, it was explained that for smaller equipments the associated costs required to increase its efficiency are not economically worthy. In the opposite end, large air compressor can be highly efficient, however, are considerably expensive machines.

  For turbines, this problem is even worse. Small scale air turbines are not commercially manufactured, so, a one-off research built equipment would not be cheap. For this reason, most of the published literature are simulations (ENNIL, 2016), or adapt commercial solutions to CAES experimental applications (MAIA et al., 2016). Large turbines are also efficient, but suffer from expensive prices and a complex thermal management system.

  Another key aspect in this compression and expansion method is the necessity of multiple stages. Directly compressing atmospheric air to the high pressure levels in which CAES system operate would result in extremely low efficiency, impracticable discharge temperature and high power requirements. For this reason, several compression stages are required, with inter cooling in between, to achieve the desired output pressure. This not only increases operational complexity and costs, but also result in larger installation sites, associated maintenance costs and higher probability of breakdowns. To give an example of this effect, heating up 1 kg of air from ambient

conditions to Huntorf's 45 *bar* lower storage pressure limit in a single, near adiabatic compressor ($n \approx 1,3$) would result in discharge temperatures over $600°C$.

- Variable turbine inlet pressure

  In most CAES systems, storage occurs by varying the pressure of the compressed air in a fixed volume reservoir. For this reason, during the system discharge, the pressure at the turbine inlet would vary, reducing as time passes. However, turbines are designed to operate at specific conditions, and changes at inlet air properties have profound effects on the power output and efficiency (ÇENGEL; BOLES, 2011). So, for this reason, throttle valves are installed to limit and regulate the pressure downstream. dissipating the excess energy and incurring at losses (SCIACOVELLIA; LIA; DINGA, 2016). In Huntorf plant, for instance, the turbine operating pressure is 40 *bar*, while the storage pressure ranges from 43 to 70 *bar* (CROTOGINO; MOHMEYER; SCHARF, 2001). This way, it would be beneficial to maintain the turbine inlet pressure constant. If Huntorf's cave could be maintained at constant pressure, the same power and energy output could be achieved with 23% of the cavern volume (KIM; SHIN; FAVRAT, 2011).

- External energy source

  Many published papers on CAES, especially D-CAES, consider an energy input during the discharge. Since air was cooled between and after compression stages in the storage process, it leaves storage at an inappropriate temperature to drive the turbines. While on D-CAES the heat output in charging is wasted, in A-CAES the energy removed in charging is returned during generation. However, heat exchanges and the TES are not 100% efficient, so energy is lost. This leads to the necessity in both cases to add energy during discharge.

  In both CAES plants, Huntorf and McIntosh, this energy is provided by burning natural gas with the compressed air, greatly increasing the temperature and pressure levels. Taking Huntorf case as an example, $62,5\%$ of the output energy comes from the fuel combustion input (ZHANG et al., 2019). In many cases, the published articles consider this heat input from an undisclosed source, which is not priced nor limited in any means, and are frequently associated to waste heat by other components. So, minimizing or fully eliminating the external energy source issue would be of great value.

- Inertia

  Conventional CAES systems are not fast to respond. From black starts, they take several minutes to reach nominal output levels (SNL, 2016), around 15 *min* in Huntorf and McIntosh plants (BUDT et al., 2016). This elevated response time is mostly associated with thermal inertia. When ramping up or down a conventional

CAES plant, it is necessary to heat air to a minimum prior to allow it entering the turbine train. If air enters too cold, it is possible that during the expansion condensate droplets are formed, and damage the turbine internal structure. At the turbine inlet, air humidity is high due to combustion, and avoiding condensation is a major safety requirement. So, adapting the operating conditions to decrease the response time could expand CAES applications.

- Complexity

  Decreasing the complexity while maintaining efficiency is a major goal of any engineer problem. A simpler solution leads to cheaper and less sensitive equipment, broaden its application in smaller scales and enhances economical parameters. In general term, CAES systems are complex and expensive. For instance, a study utilized a complex three stage compression, two stage expansion, dual TES installation for generating less than 2 kW for a remote radio station. Even with all this complexity, the average yearly efficiency figured at $\approx 58\%$, and the associated installation costs would surely make the project impracticable (JANNELLI et al., 2014).

These are a few factors that contribute to the restricted CAES application. In recent years, a new interest in the subject has arised, with companies proposing innovative solutions in Adiabatic Compressed Air Energy Storage. Hydrostor and ALACAES are two large projects, in which new state of the art CAES systems are proposed, with promising payback rates and elevated efficiency figures. These are however, in early development, with few prototype plants installed. Another company which promised excellent results with CAES was *SustainX*, a start-up founded in 2007 which proposed an near Isothermal Compressed Air Energy Storage operation with outstanding efficiency. The company, however, went out of business without any installed plants. *Toronto hydro* is a pilot project which uses underwater flexible balloon-like storage bags to store compressed air. However, the lack of available data for this project unable further analysis.

Nevertheless, these projects expose the interest and necessity of new, efficient and simpler CAES solutions. Hence, this document will present a novel CAES technology, characterized by implementing aspects and features of conventional CAES and PHES systems, aiming to create a simple and efficient system, merging positive aspects of these technologies into a single solution.

3.2 Concept and description

The system concept was developed aiming a steady energy production, reducing the power consumption during the charging stage, while maintaining the simplicity in construction and operation. The key parameter focused in the conception process was the

round trip efficiency, which consists ultimately in quantifying how much energy is lost by the system.

The operational principles that guided the system concept are an evolution of the experimental setup developed in (CAMARGOS et al., 2018) and literature references for similar PH-CAES systems. These can be summarized in the following guidelines

- A compressor will only be used to introduce the required air mass to the system;
- During regular storage operation, a hydraulic pump will perform the compressor role in conventional systems;
- Water driven by the pump will act as a piston, compressing the entire air mass;
- The pressurized air will store energy as mechanical exergy;
- When energy is required, the compressed air will act upon the water, driving it towards a hydraulic turbine;
- In order to produce a constant energy output, the air pressurizing the water must be kept isobaric;
- Rather than discarding the air mass, as it happens in conventional systems, the proposed solution will manage the constant air mass between tanks.

So, following these requirements, the PH-CAES was proposed, and a piping and instrumentation diagram (P&ID) representing its layout is presented in Fig. 3.1. In order to properly explain the proposed PH-CAES operation sequence, as well as the role of each component, the operation was divided into three consecutive phases (i) Start-up, (ii) charge and (iii) generation.

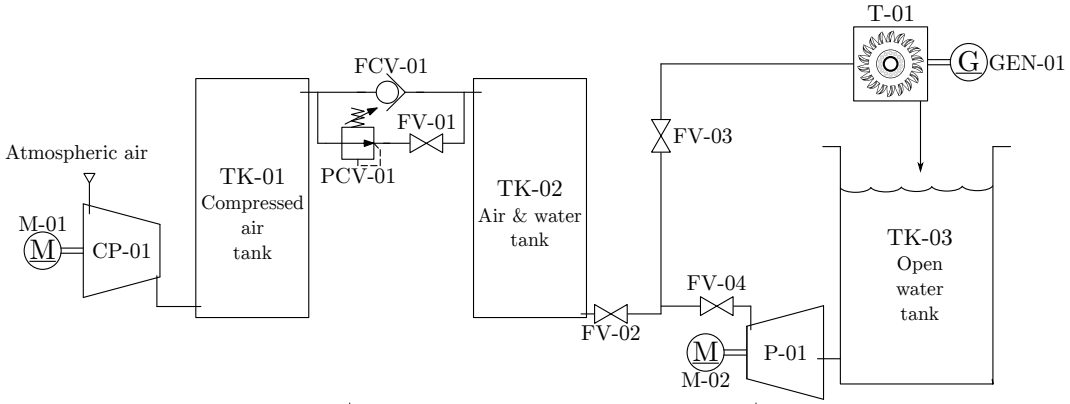

Figure 3.1 – General layout for the proposed PH-CAES system

3.2.1 System start-up

When a new PH-CAES is installed, or after maintenance operations in which the tanks had to be depressurized, a specific procedure need to be followed in order to properly start-up the system. For clarification purposes only, all the valves will be considered open, tanks TK-01 and 02 are depressurized and containing only air, while all the water is in tank TK-03. Firstly, valve FV-02 is closed and compressor CP-01 is turned on, introducing air to tanks TK-01 and 02, increasing their pressures.The system layout is depicted in Fig. 3.2, in which green components are active, red are inactive and blue corresponds to power consumption/generation. Also, open valves are indicated by *O* and closed ones by *C*.

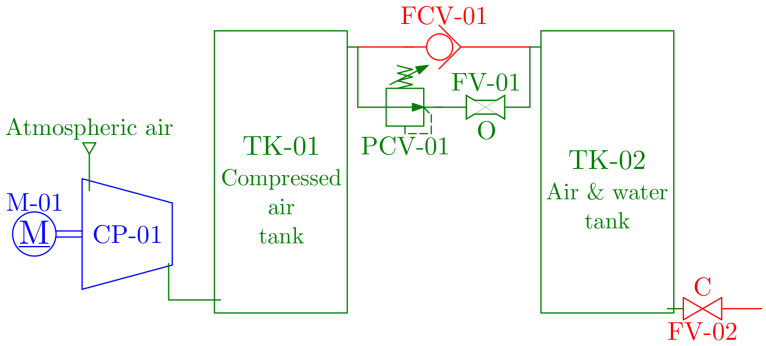

Figure 3.2 – System layout during stat up procedure.

The pressure control valve PCV-01 is a device that allows fluid flow while the pressure downstream is below a certain level. Since at first, tanks were depressurized, this valve is opened. For this reason, at first, both tanks increase their pressure simultaneously but when the pressure reaches a preset threshold, PCV-01 closes preventing air from leaving TK-01 towards 02.

From this moment onwards, the connection between tanks is ceased and only TK-01 experiences pressure increase. This stage will end when the mass of compressed air inside the system reaches its design value, which depends on very specific factors and it is unique to each application. The compressor is then turned off. At the end of the startup, the air pressure TK-02 will be equal to the preset value of PCV-01, while in TK-01 it will be higher, depending on a number of factors (*e.g.,* tank volume, energy storage capacity, power and energy requirements).

It is important to highlight that this is the only time in which the compressor is used, and disregarding any leaks, will not be necessary in routine operation. Energy consumption wise, this step is more demanding than the regular charging process, as compressing air directly requires a significant amount of energy. A didactic representation of the evolution of the pressures in each tank is represented in the Fig. 3.3.

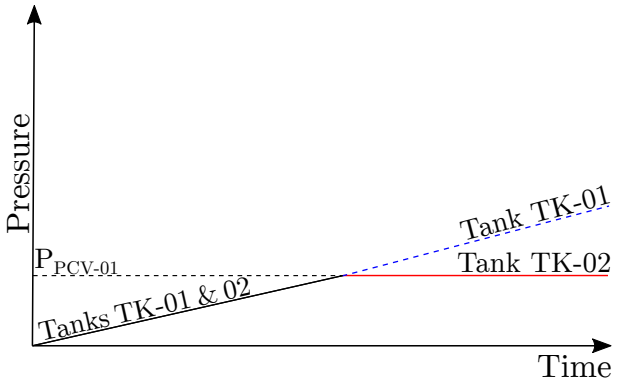

Figure 3.3 – Start-up stage pressures general behaviour. This graph indicates the pressure increasing together at the beginning, and when the limit defined by the PCV-01 is reached, only tank TK-01 experiences the pressure increase.

3.2.2 Energy storage (Charging)

The procedure now is similar regardless if it follows the start-up or during the routine operation. The following set of instructions is focused on the overall system operation, and specific procedures for equipment will not be addressed (*e.g.*, pumps or turbines). The first step is to adjust the valves positions, opening FV-02 while FV-01 and 03 are shut. Then, the pump P-01 is activated, and begins to transfer water from TK-03 to 02. The flowing water acts as a piston, compressing the air stored in TK-02 even further, above the precharge level after the start-up, or the remaining pressure from a previous operation cycle. The system layout is presented in Fig. 3.4. The same color coding used in Fig. 3.2 was used in the following figure.

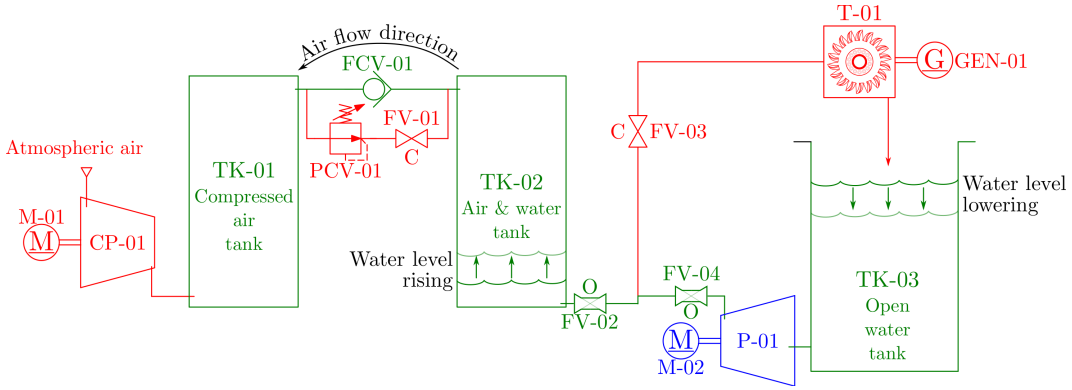

Figure 3.4 – PH-CAES layout during energy storage procedure.

While the pressure inside TK-02 is lower than in TK-01, the check valve FCV-01 will remain closed, and only TK-02 will experience pressure increase. When the tanks pressures equalize, FCV-01 will automatically open, establishing a connection between the tanks. From this moment onwards, both reservoirs will be charged simultaneously. The energy storage stage will terminate when TK-02 is filled with the appropriate volume

of water. Then, valve FV-04 closed, pump P-01 is turned off and the system is ready to generate energy.

This stage represents the *de facto* energy storage, in which the excess, cheaper or altogether unused energy is reserved for later use. The charging method is the one of the key differences from conventional CAES systems, which uses compressors. When air is pressurized in compressors, a small mass is compressed extremely fast (under 1 *sec*), confined to a compression chamber, resulting in a significant temperature increase, associated to negative consequences such as: (i) potentially useful compressing work is wasted on heating the air; (ii) this may impose the necessity of multiple compression stages with coolers in between; (iii) likely a Thermal Energy Storage (TES) system might have to be installed to increase the overall efficiency; (iv) may require especial or more expensive materials that are able to withstand higher temperatures; and (v) the equipments themselves heat, and secondary heat exchangers/sinks might be required to cool them down. By using the water to compress the air, the increase in pressure occurs considerably slower and throughout the tanks, resulting in smaller temperature increase and larger available heat transfer area, mitigating the rising temperature negative effects.

Furthermore, since water can be assumed as an incompressible fluid, the specific energy required to increase its pressure is much smaller than for air. In addition, larger pumps have excellent efficiency levels of over 85% (FOX; MCDONALD, 1985), are simpler and cheaper than compressors. In Fig 3.5, the general pressure behaviour in tanks is presented.

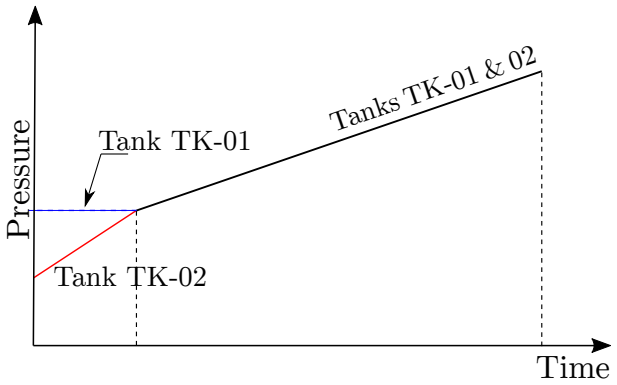

Figure 3.5 – Schematic pressure evolution in tanks TK-01 and 02 during energy storage. Firstly, only P_{TK-02} increases, due to the valve FCV-01 being closed. However, when the pressure in tanks equalize, FCV-01 is opened, and both tanks charge simultaneously.

3.2.3 Energy generation

When the stored energy is required, the system can quickly start to deliver electricity. By opening both FV-01 and 03 valves, the water is pushed by the compressed air, leaves tank TK-02 and drives the hydraulic turbine T-01, which is connected to the electrical

generator GEN-01.

The water pressurized by the compressed air results in a virtual head difference, as found in actual Hydro Power Plants (HPP). For instance, a TK-02 operating pressure of 650 kPa_g is roughly equivalent to a 65 m inlet head. During the first few seconds of generation, a brief transient will occur, in which the pressure in tank TK-02 will rapidly decrease. From the ending of the charging stage, the TK-02 pressure is higher than the the limit set on the PCV-01 ($P_{TK-02} > P_{PCV-01}$), and air cannot flow from TK-01 to 02. This decreasing pressure in TK-02 results on a similar power generation behaviour. When enough water has left the tank TK-02 to decrease its pressure below the PCV-01 threshold, this control valve opens and establishes the connection between tanks. From this moment onwards, air will leave tank TK-01 for TK-02 in a controlled manner, keeping the pressure downstream constant, and equal to the PCV-01 setting, throughout the generation process. When all of the water is consumed or the energy demand ceases, valve FV-03 is closed and the generation ceases. The system setup is presented in Fig. 3.6

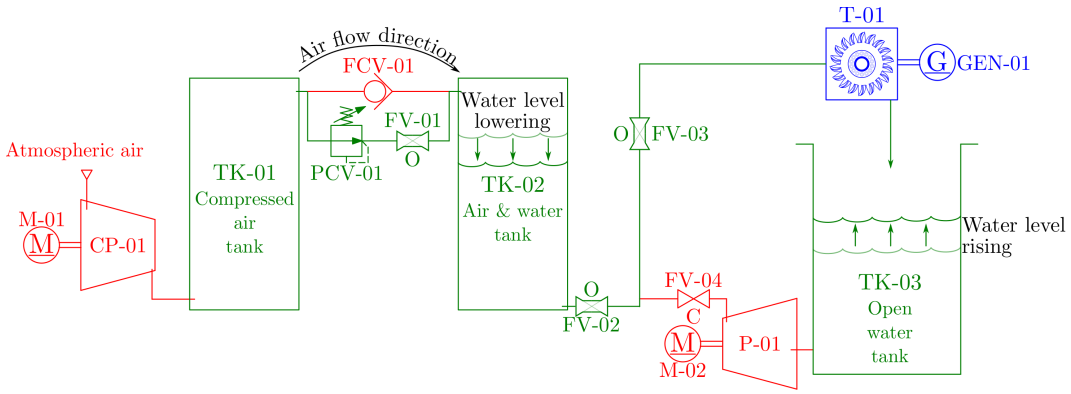

Figure 3.6 – PH-CAES layout during energy generation procedure. Once again, Green indicate active components, red inactive ones and blue represents energy consumption/generation.

By replacing the air turbine by a hydraulic one, a great deal of simplicity is achieved. Unlike in air turbines, a water operated device does not requires such fine level of control in temperature and pressure, besides eliminating the necessity of burning fuel to increase the total energy output, while being considerably cheaper than gas or superheated steam turbines. Another key feature of this design is that the air is not discarded after the generation. In conventional CAES power plants, after passing through the turbine, air is released to atmosphere, and when another operational cycle begins, the compressors have to replace this lost mass. In this design, the total mass of air inside the system remains constant, and it is simply managed rather than replaced.

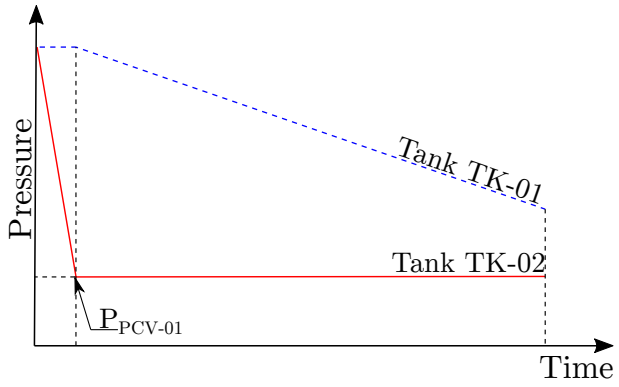

Figure 3.7 – Schematic pressure evolution in tanks TK-01 and 02 during generation. Firstly, only P_{TK-02} decreases, due to the valve PCV-01 being closed. However, when the $P_{TK-02} \leqslant P_{PCV-01}$, PCV-01 opens, and air flow from TK-01 to TK-02. Then, only the pressure in TK-01 decreases.

3.3 Mathematical description

The system mathematical model was based on three key engineering concepts: Thermodynamics, Heat Transfer and Fluid mechanics. The analysis was divided into the operating stages previously described, and it consists on analyzing successive coupled control volume, in which a *c.v.* output is used as input for a subsequent. An important aspect that must be mentioned in advance is that designing the equipment themselves is not the purpose of this research.

The system transient behaviour will be discretized into successive time steps (represented by the superscript $\langle i \rangle$), wherein all variables will be considered constant and the steady state equations are valid. The overall model will be a succession of called *"quasi-steady"* states. The surrounding air will be considered as an ideal gas at $T_\infty = 298\ K$ and $P_0 = 101.325\ kPa$ at all times. Water will be considered isothermic throughout the process, due to being incompressible and having high specific heat combined with enough time and area to transfer any heat to the surroundings, ultimatelly acting as a heat sink. Pump P-01 and turbine T-01 will be treated as adiabatic. The compressed air properties will be taken for saturated humid air, and changes in its thermodynamic states will be defined through the Laws of Thermodynamics.

3.3.1 Air mass

At the beginning of the energy storage process, tank TK-02 will be nearly filled with air, with the exception of a small amount of leftover water that prevents air from reaching the hydraulic turbine and escaping the system, arbitrated as 2% of the total volume. Also, the pressure inside the tank TK-02 will be equal to the value set in the PCV-01 regulator and at 298 K. In the air tank TK-01, the temperature will also be

considered to be 298 K.

Given these conditions, and knowing the tanks volumes, it is possible to determine the specific volume of the air inside both tanks by using thermodynamics tables or an appropriate software. It is important to highlight that the properties should be taken for saturated humid air, rather than as a dry ideal gas.

After determining the specific volumes υ_{TK-01} and υ_{TK-02}, given in $m^3\ kg^{-1}$, the mass in each tank can be determined as follows:

$$m_{air,TK-01} = \frac{V_{TK-01}}{\upsilon_{TK-01}}, \tag{3.1}$$

$$m_{air,TK-02} = \frac{0.98V_{TK-02}}{\upsilon_{TK-02}}, \tag{3.2}$$

in which both masses $m_{air,TK-01}$ and $m_{air,TK-02}$ are given in kg, and each tank volume V_{TK-01} and V_{TK-02} in m^3. Once again, as stated before, 2% of the tank volume will be filled with water, hence the 0.98 multiplicative factor in Eq.3.2. Determining the masses is a major aspect in all of the design process, and now, it is possible to begin the study of the charging process. The start-up process does not happen in routine operation, and its simply a compressor filling tanks. For this reason, it was not studied nor modelled.

3.3.2 Charging stage

The charging process is divided into two stages. The first one happens while the pressure inside the TK-02 tank is smaller than in TK-01, and the compression is exclusively held inside the air/water tank. When the pressures in tanks TK-01 and 02 equalize, the check valve FCV-01 is automatically opened and the connection between them is established, beginning thus, the second stage. From this point onwards, as the water enters TK-02, air is forced out of it and into tank TK-01. This causes the pressure in both tanks to increase together.

To mathematically describe the charging stage, the PH-CAES system was divided into control volumes, depicted in Fig 3.8. The first, *c.v.* 1 is drawn around the pump, its inlet and outlet pipes and water in tanks TK-02 and 03. The second control volume, *c.v.* 2, encompasses the air inside tank TK-02. Lastly, *c.v.* 3 consists of the air in TK-01. As water leaves TK-03 and enters TK-02, the boundaries of *c.v.* 1 and 2 are updated and redrawn.

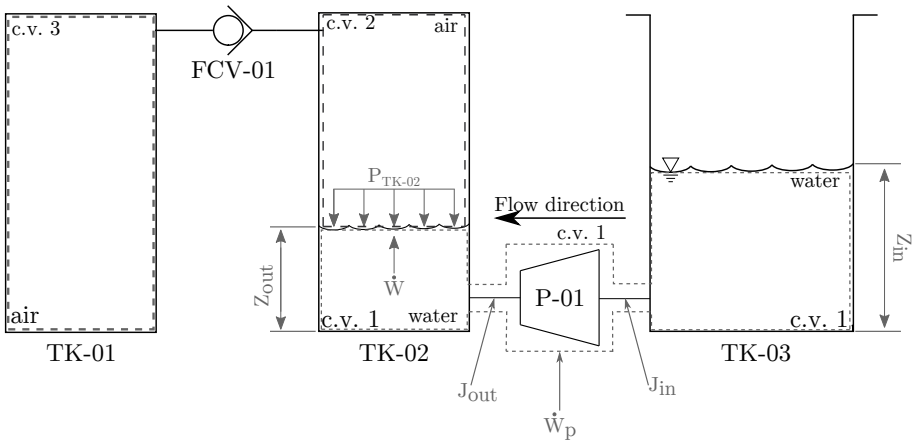

Figure 3.8 – Control volumes assumed for each stage of the charging process. For the first, *c.v.* 1 and *c.v.* 2 are considered. Then, after the pressures equalize, the final part considers all control volumes.

3.3.2.1 First stage: TK-02 only

During the first stage of charging process, water entering tank TK-02 compresses the air inside it. Since the connection between tanks is closed, only *c.v.* 1 and *c.v.* 2 are considered at this point.

For *c.v.* 1, at any given $\langle i \rangle$ time step, the instantaneous pump head (H_p) can be expressed as a function of the air pressures (P), water column heights (Z) in each tank added to the head losses due to friction (J) at pump inlet (in) and outlet (out) piping. In Eq. 3.3, the dominant term dictating the pump head is the pressure inside TK-02 (P_{TK-02}).

$$H_p^{\langle i \rangle} = \left[\frac{P_{TK-02}^{\langle i \rangle} - P_0}{\rho_w g}\right] 10^3 + \left[Z_{out}^{\langle i \rangle} - Z_{in}^{\langle i \rangle}\right] + \left[J_{out}^{\langle i \rangle}(\dot{V}^{\langle i \rangle}) + J_{in}^{\langle i \rangle}(\dot{V}^{\langle i \rangle})\right], \tag{3.3}$$

in Eq. 3.3, the air pressures P_{TK-02} and P_0 are given in kPa, water density ρ_w in $kg\,m^{-3}$, local gravitational acceleration g in $m\,s^{-2}$. Water column heights and head losses are given in m. The data used to determine the head losses must be based on a preliminary piping layout. Then, given that the pump is rotating at synchronous speeds, the instantaneous pump head is input to pump charts, provided by the manufactures, to return data on volumetric flow ($\dot{V}$, $m^3\,s^{-1}$), electric motor consumption ($\dot{W}_{M-01}$, $watt$) and efficiency (η_p).

Then, with this data, it is possible to compute the volume of water stored in tank TK-02, V_w in m^3, (and consequently, the remaining air volume) and the energy added to the water, as work W_p in J, by pump P-01, over a Δt time interval, representing

$\langle i \Rightarrow i+1 \rangle$.

$$V_w^{\langle i \rangle} = V_w^{\langle i-1 \rangle} + \dot{V}(H_p^{\langle i \rangle})\Delta t, \tag{3.4}$$

$$W_p^{\langle i \rangle} = \dot{W}_{M-02}(H_p^{\langle i \rangle})\eta_p(H_p^{\langle i \rangle})\Delta t. \tag{3.5}$$

Water entering TK-02 acts as a piston, compressing the air inside the tank. The compression work, W, can be expressed as the pump work (W_p) decreased by head losses in the piping. Since the tank diameter is considered large enough to neglect friction losses inside TK-02 (for reference, see Fig. 3.8). This way, the compression work is expressed in Eq. 3.6. Additionally, by considering that the air temperature inside tanks are uniformly distributed, the heat exchanged by the air (Q) can be expressed as the sum of heat transferred with the tank walls and the water, Eq. 3.7.

$$W^{\langle i \rangle} = W_p^{\langle i \rangle} - J_{out}^{\langle i \rangle}\rho_w g\dot{V}^{\langle i \rangle}\Delta t, \tag{3.6}$$

$$Q^{\langle i \rangle} = (\dot{Q}_{conv,air-to-H_2O} + \dot{Q}_{conv,in})^{\langle i \rangle}\Delta t. \tag{3.7}$$

Then, the heat and work figures were used as input for the First Law of Thermodynamics. The objective of this stage is to determine the thermodynamic properties after a single time step (P, T, υ). Since the thermodynamic state is completely defined at the beginning of the $\langle i \rangle$ time step, Equations 3.8 to 3.11 were applied.

$$u^{\langle i+1 \rangle} = \frac{[Q - W]^{\langle i \Rightarrow i+1 \rangle}}{m_{air}} + u^{\langle i \rangle}, \tag{3.8}$$

$$\upsilon^{\langle i+1 \rangle} = \upsilon^{\langle i \rangle} - \frac{\dot{V}_w^{\langle i \rangle}\Delta t}{m_{air}}, \tag{3.9}$$

$$T^{\langle i+1 \rangle} = f(u^{\langle i+1 \rangle}), \tag{3.10}$$

$$P^{\langle i+1 \rangle} = f(T^{\langle i+1 \rangle}, \upsilon^{\langle i+1 \rangle}). \tag{3.11}$$

in which u is the specific internal energy, in $J\ kg^{-1}$, the temperatures in K.

The tank walls temperature evolution is given considering temperature uniformity. Then, an energy balance can be written. A further assumption made is that only the area exposed to the air participates in the heat exchange process.

$$T_{wall}^{\langle i+1\rangle} = \frac{\left(\dot{Q}_{conv,in}^{\langle i\rangle} - \dot{Q}_{conv,out}^{\langle i\rangle} - \dot{Q}_{rad}^{\langle i\rangle}\right)\Delta t}{m_{wall}c} + T_{wall}^{\langle i\rangle}. \tag{3.12}$$

in Eq. 3.12, the net heat exchanged is defined by the difference between the inflowing and outflowing convective ($\dot{Q}_{conv}$) and radiative ($\dot{Q}_{rad}$) heat transfer rates, all given in W over a Δt time interval. This net value is then divided by the exposed tank mass and specific heat, and added to the previous temperature to update this variable value. Equations 3.3 to 3.12 are part of the computing algorithm detailed in Fig. 3.9

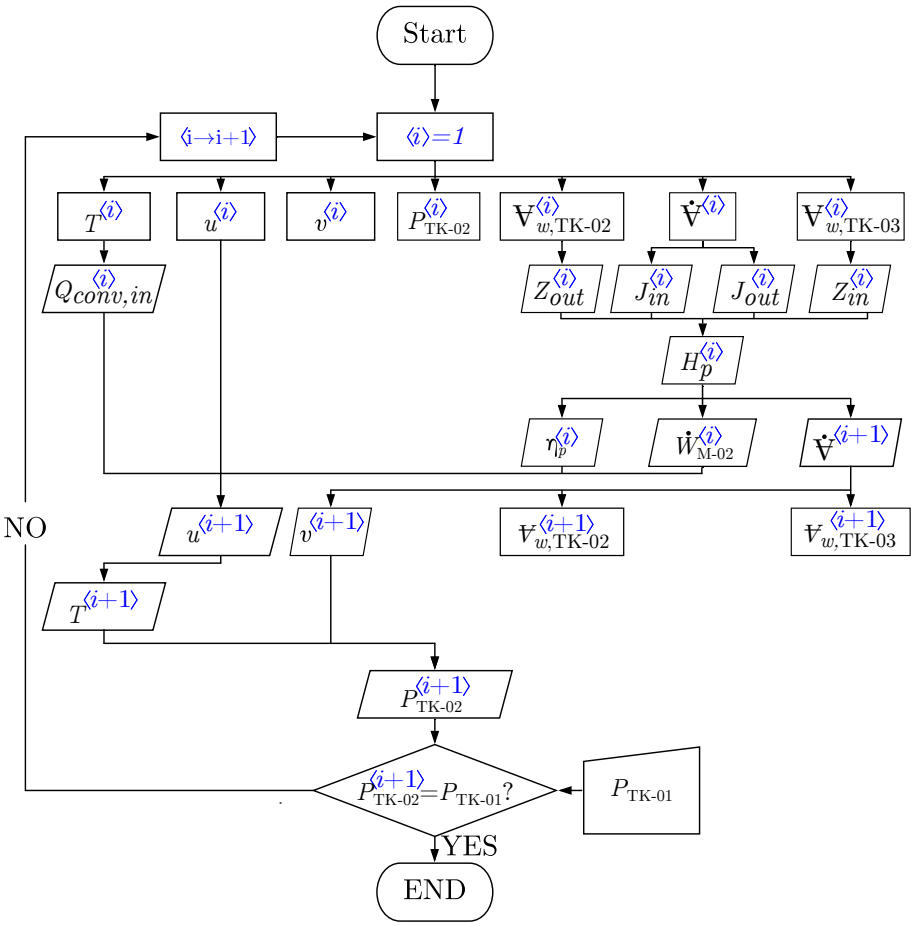

Figure 3.9 – First stage of the charging process as a flowchart. The initial conditions are represented by the superscript $\langle i\rangle$, while the final values of these parameters were given $\langle i+1\rangle$.

The iterative calculating procedure presented in Fig. 3.9 exit condition, $P_{TK-02} = PTK-01$, represents the end of the first stage of energy storage. For computational reasons, a residual convergence difference between these pressures will occur, and it was arbitrated $|P_{TK-02} - PTK-01| \leqslant 0,1\ kPa$. At this point, FCV-01 automatically opens, and the charging occurs on both tanks.

3.3.2.2 Second stage: Both tanks

Once the first stage of the energy storage process finishes, the second one promptly starts. As soon as the valve FCV-01 opens, the air is allowed to flow from tank TK-02 to 01, and thus, the pressure in both tanks increases simultaneously. Therefore, the control volume boundaries had to be updated to consider all three control volumes, as shown in Fig. 3.8.

This second stage is characterized by the air flow between tanks, ensuring this way, the pressure equilibrium. However, calculating this air mass flow between TK-02 and 01 is not trivial because even though the tanks must be at the same pressure, they are at different temperatures and consequently, air specific volumes. Also, despite the compression process acts upon the total combined mass of air, the effects on each tanks is different, and the air mass flow must be considered to define thermodynamic properties in each tank in a single time step $\langle i \Rightarrow i+1 \rangle$. In other words, the total increase in pressure in the tanks is a combination of several factors.

To solve this problem, the tanks were decoupled into two control volumes (*c.v.* 2 and *c.v.* 3), and a mass and energy balance was performed. The relationship that recouples them is the product between mass and enthalpy that leaves tank TK-02 (*c.v.* 2) must be the same that entering TK-01 (*c.v.* 3), disregarding any pressure losses in between. This scenario is depicted in Fig. 3.10.

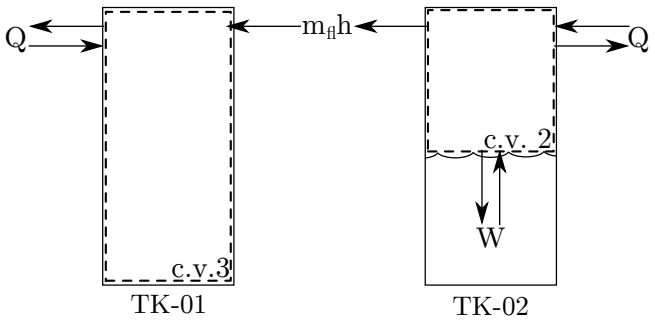

Figure 3.10 – Tanks decoupling process, in which each control volume (*c.v.* 2 & *c.v.* 3) was analyzed separately.

Each tank presented in Fig. 3.10 was analyzed through a transient analysis of the First Law of Thermodynamics (BORGNAKKE; SONNTAG, 2013)

$$\begin{aligned} Q_{c.v.}^{\langle i \rangle} + \sum m\left(h + \frac{v^2}{2} + gZ\right)\Big|_{in}^{\langle i \rangle} &= \sum m\left(h + \frac{v^2}{2} + gZ\right)\Big|_{out}^{\langle i \rangle} \\ + \left[m\left(u + \frac{v^2}{2} + gZ\right)\Big|^{\langle i+1 \rangle} - m\left(u + \frac{v^2}{2} + gZ\right)\Big|^{\langle i \rangle}\right] &+ W_{c.v.}^{\langle i \rangle}, \end{aligned} \tag{3.13}$$

which can be rearranged, and neglecting any effective changes in potential and kinetic

energy, can be simplified to tanks TK-02 (Eq. 3.14) and TK-01 (Eq. 3.15)

$$c.v.2^{\langle i \Rightarrow i+1 \rangle} \begin{cases} m^{\langle i+1 \rangle} u^{\langle i+1 \rangle} = Q_{c.v.}^{\langle i \rangle} - W_{c.v.}^{\langle i \rangle} + m^{\langle i \rangle} u^{\langle i \rangle} - m_{fl}^{\langle i \rangle} h^{\langle i \rangle} \\ m^{\langle i+1 \rangle} = m^{\langle i \rangle} - m_{fl}^{\langle i \rangle}, \end{cases} \tag{3.14}$$

$$c.v.3^{\langle i \Rightarrow i+1 \rangle} \begin{cases} m^{\langle i+1 \rangle} u^{\langle i+1 \rangle} = Q_{c.v.}^{\langle i \rangle} + m^{\langle i \rangle} u^{\langle i \rangle} + m_{fl}^{\langle i \rangle} h^{\langle i \rangle} \\ m^{\langle i+1 \rangle} = m^{\langle i \rangle} + m_{fl}^{\langle i \rangle}, \end{cases} \tag{3.15}$$

$$m_{in} h_{TK-02} \Big|_{TK-01}^{\langle i \rangle} = m_{out} h_{TK-02} \Big|_{TK-02}^{\langle i \rangle} = m_{fl}^{\langle i \rangle} h^{\langle i \rangle}. \tag{3.16}$$

In Eqs. 3.14 and 3.15, it was considered that the input work acts on *c.v. 2*, and it is transferred to *c.v. 1* through the energy associated with mass flow $m_{fl}^{\langle i \rangle} h^{\langle i \rangle}$.

In the energy balance presented in Equations 3.14 and 3.15 there are three unknown variables, $u^{\langle i+1 \rangle}$ for each *c.v.* and the mass flow $m_{fl}^{\langle i \rangle}$, which means that an iterative process is necessary, as described in Fig. 3.11. For this mass flow determination, a convergence iterative index $\langle j \rangle$ was defined, and within each time index $\langle i \rangle$, several $\langle j \rangle$ iterations take place. An initial $m_{fl}^{\langle j \rangle}$ was estimated and used to test the pressure equilibrium criterion ($P_{TK-02}^{\langle i+1 \rangle} = P_{TK-01}^{\langle i+1 \rangle}$). Then, the resultant pressure differential ratio was used as reference to update the mass flow estimation $\langle j \Rightarrow j+1 \rangle$, until a satisfactory converge was achieved ($|P_{TK-02} - PTK-01| \leqslant 0,1\ kPa$). Equation 3.16 presents the mass and energy balance coupling the two control volumes. It is worth noticing on Eq. 3.16 that the air enthalpy of the mass entering TK-01 must be taken for TK-02 thermodynamic state. The calculation of heat and work is performed similarly to the first part of the energy storage process, presented in Fig. 3.9.

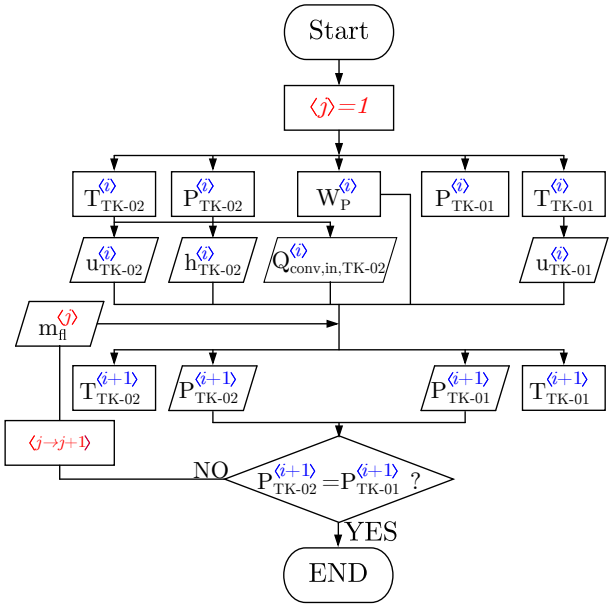

Figure 3.11 – Flowchart representing the iterative process used for determining the mass flow.

The energy storage process will continue until tank TK-02 is nearly filled with water, with the exception of a safety margin, and the air is stored in TK-01. Then, valve FV-04 is closed, pump P-01 is shut off and the system is ready to start generating energy.

3.3.3 Generation stage

The generation process may start just after the energy storage is over, or after some time interval. Differently from the charging stage, during generation the system operates with constant water volumetric flow (except for a brief initial transient) that depends on the power rating requirement.

The overall theoretical formulation for the generation process is similar to the one presented in the charging process. As previously shown, the generation process is divided in two stages, as it can be seen in Fig. 3.5. During the first part, the tank TK-02 pressure is above the threshold set in the pressure control valve PCV-01, and thus, no air is allowed to flow from TK-01 to 02. This results in an initial transient state in which the generation decreases. This transient is very short however, given that the tank TK-02 was nearly filled with water, and so, even a small increase in the available volume will result in a significant decrease in the pressure. When P_{TK-02} reaches the preset PCV-01 value, the generations reaches its nominal value, remaining constant throughout the entirety of the process. Similarly to what has been done in the previous section, the considered control volumes in each of the generation stages are shown in Fig. 3.12.

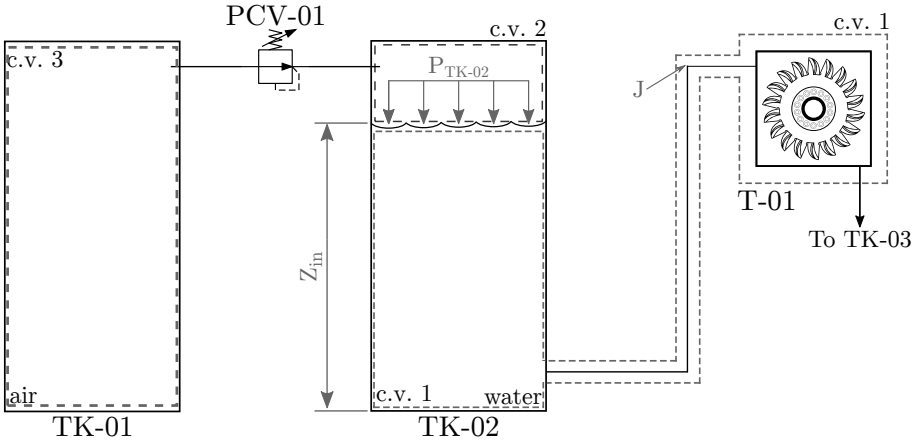

Figure 3.12 – Control volumes assumed for each stage of the generation process. For the first stage, control volumes *c.v.* 1 and *c.v.* 2 were considered, whilst in the last part, *c.v.* 1, *c.v.* 2 and *c.v.* 3 were taken into account.

During the generation process, Fig. 3.12, the compressed air pushes the water through the piping to turbine T-01, in which the hydraulic power is converted into shaft rotational kinetic energy, and later into electricity by the generator GEN-01.

3.3.3.1 First stage: Transient stage

For the first part of the generation process, control volumes *c.v.* 1 and *c.v.* 2 are considered. So, energy balance is applied to the constant air mass inside TK-02. The work W_{exp} done by the expanding air upon the water was calculated with Eq. 3.17.

$$W_{exp}^{\langle i \rangle} = 10^3 \dot{V}_w^{\langle i \rangle} P_{TK-02;g}^{\langle i \rangle} \Delta t, \tag{3.17}$$

in which the expansion work W_{exp} is given in J and $P_{TK-02;g}$ is the gauge pressure, in kPa.

Then, heat transfer are calculated for the air inside TK-02, and with the expanding work, are applied to the First Law of Thermodynamics (Eq. 3.8). In possession of the updated internal energy $u^{\langle i+1 \rangle}$, and the known volumetric flow rate $\dot{V}_w$, equations 3.9 to 3.11 are utilized to fully determine the air thermodynamic state. Simultaneously, air in TK-01 (*c.v.* 3) undergoes an isovolumetric transformation, transferring heat to the surrounding environment.

Then, at the turbine T-01 inlet the energy carried by the water, W_{hyd} in $joules$, is equal to the expansion work W_{exp} decreased from losses due to friction in the piping, and is calculated as in Eq. 3.18

$$W_{hyd}^{\langle i \rangle} = W_{exp}^{\langle i \rangle} - \dot{V}_w^{\langle i \rangle} \rho_w g J^{\langle i \rangle}(\dot{V}^{\langle i \rangle}) \Delta t. \tag{3.18}$$

The energy output at generator GEN-01 output can be calculated as

$$W_{gen}^{\langle i \rangle} = W_{hyd}^{\langle i \rangle} \eta_{tur}^{\langle i \rangle} \eta_{gen}^{\langle i \rangle}. \tag{3.19}$$

These steps are repeated for as long as the pressure inside TK-02 remains under the threshold set in PCV-01, within a $0,1\ kPa$ convergence limit. In the first stage, there is no air flow between tanks. The general algorithm describing the first stage of the generation process is presented in Fig. 3.13.

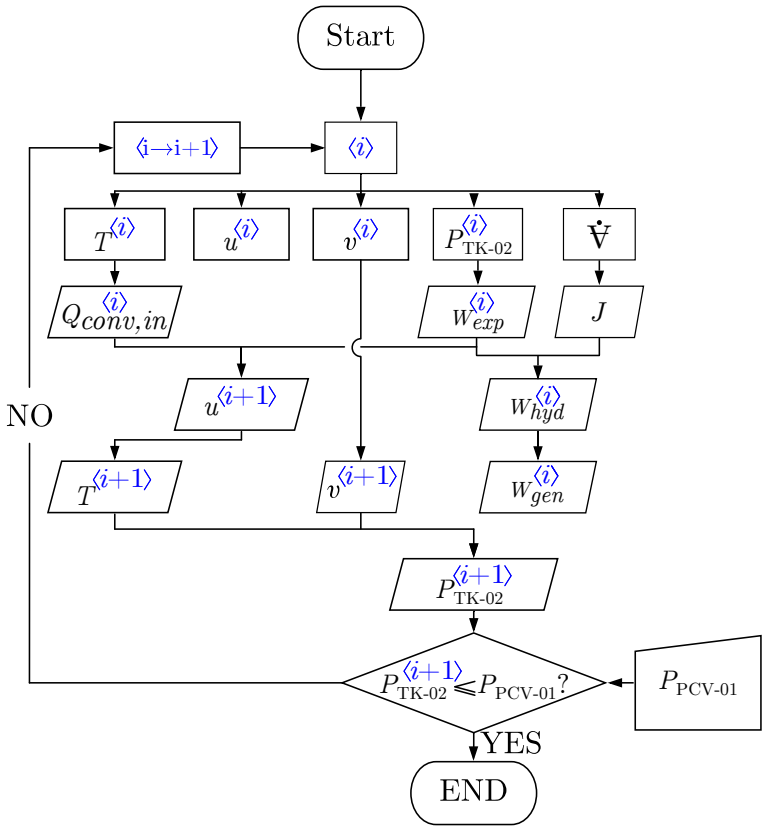

Figure 3.13 – Flowchart representing the iterative process applied to the first stage of the generation process.

When the pressure in tank TK-02 reaches the PCV-01 set point the connection between tanks is established, and from this point onwards, the second generation stage takes place.

3.3.3.2 Second stage: Constant power output

For the second part of the generation process, the control volumes considered are *c.v.* 1, *c.v.* 2 and *c.v.* 3 (see Fig. 3.12). As soon as the pressure inside TK-02 reaches the limit set on PCV-01, air leaves TK-01 in such manner to maintain TK-02 pressure constant. From this stable pressure, a constant power output is guaranteed (Eqs. 3.17 to 3.19). Once again, the First Law of Thermodynamics was applied to each control volume, and Eqs. 3.14 to 3.16 are rewritten as Eqs. 3.20 through 3.22 for *c.v.* 2 and *c.v.* 3, respectively, and the mass balance. In Eqs. 3.20 to 3.22, it was considered that valve PCV-01 is adiabatic and isenthalpic.

$$c.v.\ 2^{\langle i\Rightarrow i+1\rangle}\begin{cases} m^{\langle i+1\rangle}u^{\langle i+1\rangle} = Q^{\langle i\rangle}_{c.v.} - W^{\langle i\rangle}_{c.v.} + m^{\langle i\rangle}u^{\langle i\rangle} + m^{\langle i\rangle}_{fl}h^{\langle i\rangle} \\ m^{\langle i+1\rangle} = m^{\langle i\rangle} + m^{\langle i\rangle}_{fl}, \end{cases} \tag{3.20}$$

$$c.v.\ 3^{\langle i \Rightarrow i+1 \rangle} \begin{cases} m^{\langle i+1 \rangle} u^{\langle i+1 \rangle} = Q_{c.v.}^{\langle i \rangle} + m^{\langle i \rangle} u^{\langle i \rangle} - m_{fl}^{\langle i \rangle} h^{\langle i \rangle} \\ m^{\langle i+1 \rangle} = m^{\langle i \rangle} - m_{fl}^{\langle i \rangle}, \end{cases} \tag{3.21}$$

$$m_{in} h_{TK-01} \Big|_{TK-02}^{\langle i \rangle} = m_{out} h_{TK-01} \Big|_{TK-01}^{\langle i \rangle} = m_{fl}^{\langle i \rangle} h^{\langle i \rangle}. \tag{3.22}$$

The iterative process defined in the second stage of charging is now applied, with the necessary adaptations, to describe the second part of generation. This part of the operating cycle end when all the water (except the safety margin) has left tank TK-02, or when the energy demand ceases.

Now, in order to assess the performance of this proposed PH-CAES system design, a case study is presented. The mathematical model presented in section three is coded in Matlab assisted by CoolProp thermodynamic data package, with a time step $\Delta t = 1$ *sec.*

4 Case study: laboratory-scale PH-CAES system

4.1 Context

This chapter presents simulation results for the methodology previously presented. To assess the performance of the proposed PH-CAES system, a laboratory scale application is proposed. Designing and sizing individual components it is no the goal of this study, so, commercial data for equipment will be used to define layout particularities, equipment operation and overall performance. This leads to restriction in certain aspects (*e.g.*, pipes diameter), which had to be in accordance with standard commercial dimensions and common practices. However, for larger applications, this issue would be mitigated, if not eliminated.

This case study was in part based on the analysis performed by (CAMARGOS et al., 2018; CAMARGOS, 2018), in which a PH-CAES prototype was built and thoroughly tested. However, in the aforementioned research, it was possible to observe a few problems with its setup, mainly: (i) requiring to use the compressor after each cycle, (ii) the necessity to release the compressed air from tank TK-02 after the generation stage, (iii) elevated frictional losses due to insufficient piping diameter, (iv) small turbine and transmission efficiencies and (v) inappropriate electrical generator. These operational drawbacks combined resulted in poor Round-Trip Efficiency values, around 1%. However, as the prototype built for the study was used primarily as a proof of concept and all of the above stated drawbacks can be easily assessed, it was chosen as a comparative conceptual reference of the proposed design.

Furthermore, data for smaller equipments is more abundant, and easily accessible. Even though larger hydraulic components present higher efficiency values, their operational data is not readily available, and often, suppliers are reluctant to share technical information. For these reasons, even though the smaller laboratory scale application returns smaller efficiency figures, it was chosen over larger systems.

4.2 Simulation parameters

General conditions assumed in simulations can be found in Tab. 4.1. While the pump efficiency will be acquired from charts provided by manufacturers, the turbine and generator efficiencies will be considered constant and equal to $\eta_{tur} = 0,90$ and $\eta_{gen} = 0,90$. This is due to the fact that turbines are usually custom built and the commercial suppliers

are often reluctant to provide operational information without actually acquiring an equipment. Furthermore, hydraulic turbines are designed to operate at an optimal point, the constant efficiency assumption is justified. Also, it is important to highlight that the air properties were taken for saturated humid air, rather than as a dry ideal gas.

Table 4.1 – General assumptions and conditions used in the case study (at 3600 rpm).

Condition	Symbol	Value
Initial temperature	T	298 K
Water temperature	T_w	298 K
Ambient temperature	T_0	298 K
Atmospheric pressure	P_0	$101,3$ kPa
Turbine efficiency	η_{tur}	$0,90$
Generator efficiency	η_{gen}	$0,90$
Time step	Δt	1 sec
Assumption #1	Adiabatic pump P-01	
Assumption #2	Adiabatic Turbine T-01	
Assumption #3	Isothermal water	
Assumption #4	Isenthalpic PCV-01	

For the case study, six pumps were chosen,aiming to address the influence of this key equipment on the PH-CAES overall performance. All pumps chosen are manufactured by Schneider, because the data sheets and technical information quality is high and are easily found online. Full operating charts for the pumps are provided in Annex A. Nonetheless, in Tab. 4.2, a technical summary is presented. Due to the wide range of operating pressures during charging process, multiple stage centrifugal pumps were chosen. Then, on Fig. 4.1, a picture of each pump model is shown.

Table 4.2 – Pumps utilized in the simulation: technical summary (at 3600 rpm).

			Rotor diameter	Motor		Max. output head	Max. flow
#	Model	Stages	mm	kW	CV	m	$m^3\ h^{-1}$
1	BT4-2040E15	15	79	3	4	171	$6,9$ @ 40 m
2	BT4-2030E12	12	79	2,2	3	137	$6,9$ @ 30 m
3	BT4-2020E10	10	79	1,5	2	114	$6,8$ @ 30 m
4	BT4-2010E5	5	79	0,73	1	57	$6,4$ @ 20 m
5	WME-5840	10	97	3	4	130	$8,6$ @ 60 m
6	WME-5630	6	97	2,2	3	100	$8,8$ @ 50 m

An important aspect presented in Tab. 4.2 relates to the maximum flow. The information presented in the table was directly extracted from the manufacturer data sheet, and no values for lower pressure levels are provided. So, during simulations, whenever the pump had to operate below this minimum pressure, a numerical extrapolation had to

(a) (b)

Figure 4.1 – Picture of the chosen pump models. On **a** the BT4 series is presented and in **b** WME models is depicted.

be performed. Extrapolating data is dangerous, because there is no physical guarantee that the predicted behaviour will be reflected on reality. For this reason, a visual inspection on how the extrapolated data was placed in comparison to the actual pump curve had to be performed, and if the results were not satisfactory, the pump was deemed unsuitable for the application. A way to solve this problem would be to acquire the equipment, and perform an experimental characterization, covering the missing operating points. Additionally, Rateaux relations could be used to try and predict how the pumps would operate at different rotational speeds, and so, avoid the missing data. On the opposite end, when the output pressure was above the maximum output, a similar procedure was done. By extrapolating on the provided curves, missing data was estimated. Once again, the results on the extrapolation were manually checked to confirm the operation quality.

In Tab. 4.3, a description on the type, dimensions and materials chosen for the case study is presented.

Table 4.3 – Description of the equipment chosen for the case study PH-CAES system.

M-01	$3,75\ kW$
M-02	$1,5\ kW$
CP-01	Pressure ATG3
TK-01	$2\ m^3$
TK-02	$0,5\ m^3$
TK-03	$0,55\ m^3$
P-01	Various models (see Tab 4.2)
Water Pipes	CPVC $\varnothing 66\ mm$
Air Pipes	Aluminium $\varnothing 40\ mm$

Water volumetric flow rate during discharging was determined taking into account tank TK-02 volume, $0,5\ m^3$, and establishing that the system would need to provide

100 s of power generation, resulting in 5 ℓs^{-1}. In this way, the methodology presented was applied to simulate the system in operational pressures in TK-02 (during generation stage) varying from 300 to 800 kPa_g, in 50 kPa steps. This operating pressure will be used as a reference for each simulation.

The following topics will present and discuss results for one pump operating standalone, two pumps in series/parallel and a comparison to other CAES systems.

4.3 Single pump operation

Firstly, the PH-CAES simulation considered each pump operating alone in all 11 pressure levels. However, at higher pressure levels, the smaller pumps could not output water, and for this reason, were considered unfit to the application.

Firstly, it is necessary to determine if a given pump can operate at a certain operating pressure level. For reasons presented in the previous section, not all pumps were fit to function in all pressure ratings. So in, Tab 4.4, an indication on whether a pump is capable to operate in each scenario is presented.

Table 4.4 – Summary on whether each pump is able to operate in a certain operating pressure conditions.

Op. pressure (kPa_g)	Pump Model					
	BT4-2040E15 #1	BT4-2030E12 #2	BT4-2020E10 #3	BT4-2010E5 #4	WME-5840 #5	WME-5630 #6
300	✓	✓	✓	✓	✓	✓
350	✓	✓	✓	✓	✓	✓
400	✓	✓	✓	×	✓	✓
450	✓	✓	✓	×	✓	✓
500	✓	✓	✓	×	✓	✓
550	✓	✓	✓	×	✓	✓
600	✓	✓	✓	×	✓	✓
650	✓	✓	✓	×	✓	✓
700	✓	✓	✓	×	✓	×
750	✓	✓	✓	×	✓	×
800	✓	✓	×	×	✓	×

4.3.1 Pressure

The first aspect presented is the pressure evolution in tanks TK-01 and TK-02 over the operating cycle. Given the numerous combinations of pumps and pressures, the results will first be presented for a single pump, and different pressure levels, and then for a given pressure setting, for selected pumps. Firstly, for pump #2 (BT4-2030E12), the pressure behaviour in tanks TK-01 and 02 over the energy storage and generation processes are presented in Fig. 4.2. For clarity purposes, the author chose to omit a few intermediate results, which presented the same general behaviour.

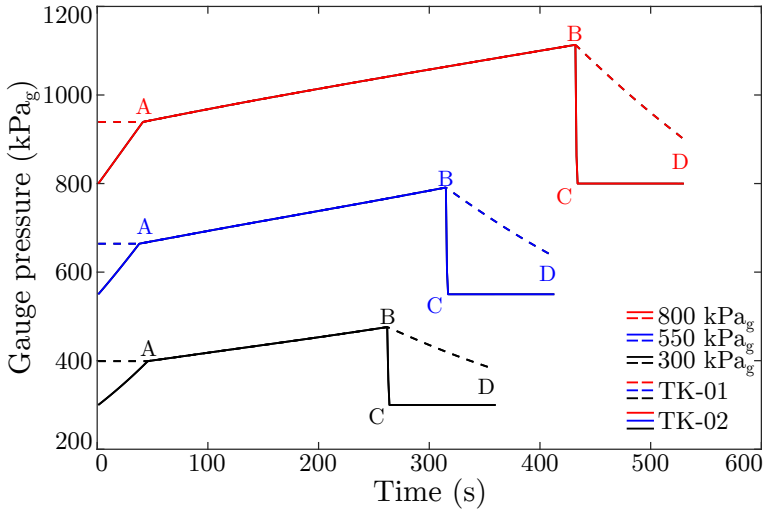

Figure 4.2 – Pressure evolution in tanks TK-01 (dashed line) and TK-02 (solid line) during both charging and generation stages, for pump #2 (BT4-2030E12). For clarity purposes, only three operating pressures were depicted: 300 (black); 550 (blue) and 800 kPa_g (red).

In Fig. 4.2, point **A** represents the end of the charging first stage, **B** the end of the energy storage process; **C** the beginning of generation process second stage, which ends at point **D**. The pressure behaviour closely resembles the prediction presented in Figs. 3.5 and 3.7. In the beginning, only tank TK-02 experiences pressure increase (first part of the storage stage), until the pressure equalizes (point **A**). Then, both tanks are charged simultaneously, (**A**→**B**), until the storage process is over. Point **B** represents the end of the charging stage, and the beginning of the generation.

During the energy generation, tank TK-01 experiences a nearly linear pressure decline, (**B**→**D**), resultant from the outflowing air mass towards tank TK-02. In tank TK-02, conversely, a severe pressure drop can be seen in the first few seconds of the generation stage (**B**→**C**), resultant of the considerable increase in the available volume. By the end of the charging stage, tank TK-02 will hold approximately 485ℓ of water, leaving 15 ℓ to air. Then, as the water volumetric flow rate was defined as 5 ℓs^{-1}, the initial expansion process happens considerably fast, lasting 3 *sec* on average. Finally, on TK-02, the pressure remains constant, maintained by the air flow regulated by PCV-01 (**C**→**D**). The values obtained for points **A** to **D**, for all 66 operating points simulated are presented in the Appendix A.1.1.

The influence of the operating pressure for a fixed point is straightforward, increasing the required time and power consumption as the operating pressure gets bigger (discussed later, in Fig. 4.6). Now, to address the influence different pump models have on the system, Fig. 4.3 depicts the results for an operating pressure of 350 kPa_g. Again, to increase the readability of the displayed information, data for three pumps are presented, with the omitted results standing in between the plotted curves.

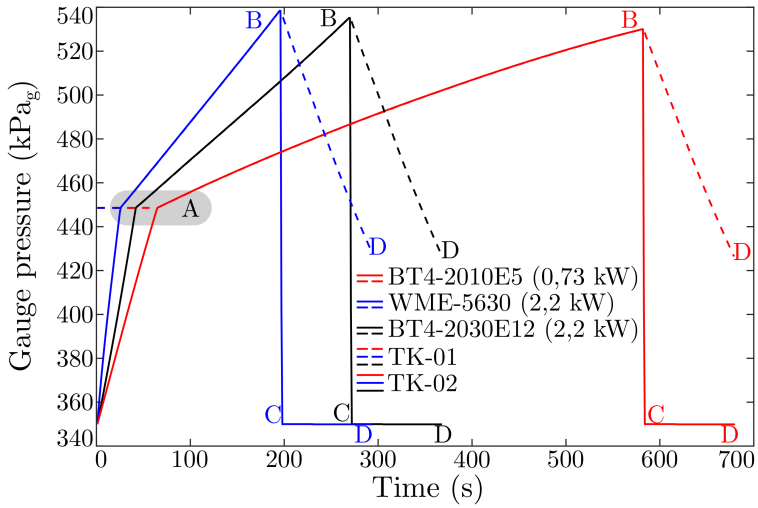

Figure 4.3 – Pressure evolution in tanks TK-01 (dashed line) and TK-02 (solid line) during both charging and generation stages, for an operating pressure of 350 kPa_g. For clarity purposes, only three pumps are presented: BT4-2010E5 #4 (red); WME-5630 #6 (blue) and BT4-2030E12 $2 (black).

From Fig. 4.3 it is clearly noticeable the deep influence the chosen pump has on the system operation, from the pressure point of view. When comparing two BT4 series pumps, the smaller pump resulted in longer charging times. While BT4-2010E5, pump #4 (red line), with an installed electric motor with $0,73\ kW$ takes nearly 10 min to pump 485 ℓ of water, the larger similar model BT4-2030E12 (black line) requires roughly 55% of the time. In Fig. 4.3, points **A** to **D** are kept for ease comparison and reference to Fig. 4.2.

Comparing different models, however, its not so simple as checking for the power. Even though pump #6 (WME-5630) installed motor power is equal to the BT4-2030E12 (#2), the first model is able to pump the water in less time. However, the constructing parameters of WME-5630 results in larger water flow rates within a narrower pressure range when compared to BT4-2030E12 (See pump charts in Annex A). To further evidence this fact, the pump BT4-2030E12 can operate on all 11 pressure levels, whilst WME-5630 is not suitable for applications with an operating pressure higher than 650 kPa_g (see Tab. 4.4)

Following, the temperature behaviour will be discussed. It is important to understand and describe its changes during operation to fully determine the thermodynamic state at any given time, and to assess the necessity of a Thermal Energy Storage (TES), special components or materials, heat exchangers to name a few. Also, avoiding severe temperature variation is desirable in CAES systems, as previously explained. Similarly to the manner in which pressure was presented, the temperature analysis will first be performed for a single pump over three pressure levels, and later on, for a given pressure setting and three pumps. Again, the full results are presented in Appendix.

4.3.2 Temperature

Considering that the air mass is in thermodynamic equilibrium, its temperature in each tank is presented in Fig. 4.4.

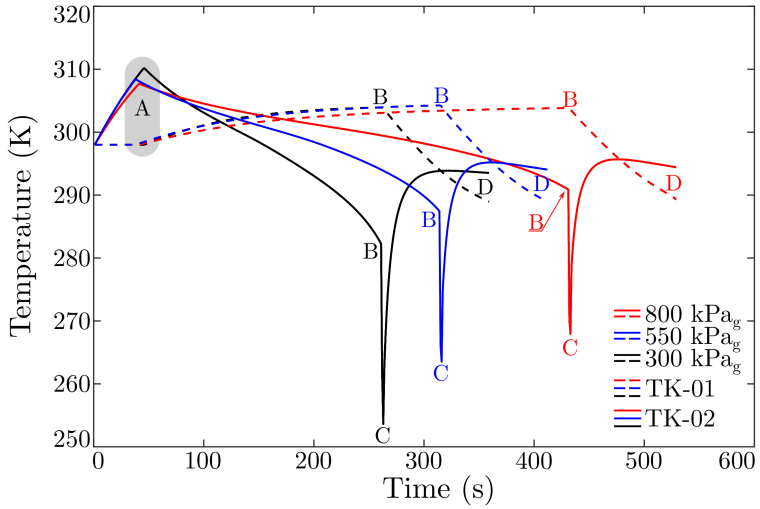

Figure 4.4 – Temperature evolution in tanks TK-01 (dashed line) and TK-02 (solid line), for three operating pressures. The results are relative to pump #2,BT4-2030E12.

Once again, for increased clarity, only three curves were presented in Fig. 4.4, for operating pressures of 300 (black), 550 (blue) and 800 kPa_g (red). Once again, point **A** represents the end of the charging first stage, **B** the end of the energy storage process; **C** the beginning of generation process second stage, which ends at point **D**. In this figure, points **A** for both tanks and three operating pressures are indicated by a single marking on the graph, highlighted by the gray area.

Figure 4.4 presents the instantaneous air temperature in each tank, along the storage and generation processes. For tank TK-01, represented by the dashed lines, the temperature evolution behaviour is fairly straightforward. It remains at room temperature until the end of the first stage of the energy storage process (point **A**), from which it begins to experience pressure increase (see Fig. 4.2). By analyzing it under the scope of the First Law of Thermodynamics, Eq. 3.15, it is clearly visible that the incoming energy as $m_{fl}^{\langle i \rangle} h^{\langle i \rangle}$ results in increasing the total internal energy, given by $m^{\langle i+1 \rangle} u^{\langle i+1 \rangle}$, which in turn, increases the air temperature.

Another important aspect presented in Fig. 4.4 is the temperature variation is minimal when compared to conventional systems. As explained previously, the slower and evenly distributed compression results in smaller increases in temperature, whilst reducing the required compression work, the exergy destruction rate and increasing the efficiency.

This behaviour continues along the **A**→**B** path, representing the entirety of the second part of the storage process. The generation process analysis is similar. By applying

Eq. 3.21, the outflowing energy $m_{fl}^{\langle i \rangle} h^{\langle i \rangle}$ reduces the internal energy over time, decreasing thus, the temperature (process **B** $\rightarrow$ **D**).

For tank TK-02, the results are not intuitive at first sight, however, the same analysis can be performed. In the beginning of the charging stage, only tank TK-02 experiences increase in pressure and there is no connection between tanks. So, the First Law of Thermodynamics (Eq. 3.8) indicates that the work entering the control volume *c.v.* 2 tends to increase the total internal energy $u^{\langle i+1 \rangle}$ after a single time step $\langle i \Rightarrow i+1 \rangle$. Also, since during the first stage of the charging process, the absolute figures of work $W^{\langle i \rangle}$ are always greater than the heat exchanged $Q^{\langle i \rangle}$, the internal energy increases, elevating the temperature until point **A**.

When the connection between the control volumes *c.v.* 2 and *c.v.* 3 is established, Eq. 3.14 is used to describe the variation in internal energy over a time step. In this equation, there are three components of energy flowing through the control volume boundary, $W_{c.v.}^{\langle i \rangle}$ which always tends to increase the total energy, $m_{fl}^{\langle i \rangle} h^{\langle i \rangle}$ that contributes to reduce $u^{\langle i+1 \rangle}$ and the heat flow $Q_{v.c.}^{\langle i \rangle}$ that firstly removes energy from the system, while $T_{air} > T_0$ and than later shift to add energy to the control volume (while $T_{air} < T_0$). In absolute terms, the value of $m_{fh}^{\langle i \rangle} h^{\langle i \rangle}$ is always greater than the work entering the control volume $W_{c.v.}^{\langle i \rangle}$ and the heat exchanged $Q_{c.v.}^{\langle i \rangle}$, resulting in decreasing internal energy $u^{\langle i+1 \rangle}$ and consequently temperature.

The second stage of the charging process ends at point **B**. Then between points **B** and **C** a severe decrease in temperature can be observed, which corresponds to the first part of the generation stage, in which a rapid expansion takes place. From Eq. 3.20, it can be clearly seen that the expansion work tends to decrease the internal energy. Simultaneously, the heat is unable to counteract this effect for two reasons (i) the thermal inertia of the system, which decreases the responsivity of the heat flow and (ii) the small available area to exchange heat, as most of the tank is filled with water and the air is restricted to a small portion of the tank. So, these effects coupled with the small air mass currently in the tank causes the expressive temperature drop.

Then during the last portion of the generation stage, **C**$\rightarrow$**D** the temperature quickly rises in the first few instant, and then stabilizes at a plateau. This initial increase in temperature is resultant of the incoming air mass flow from TK-01, which is hotter. Then Eq. 3.21 is used to calculate the resultant internal energy and temperature.

Another interesting aspect presented in Fig. 4.4 is the fact that smaller operating pressures result in larger temperature differences. Two factors contribute to this fact: (i) even though the pressure values are different, their absolute changes during the entire operating cycle are similar, around $250 - 300\ kPa_g$. So, the relative pressure changes are more significant to lower operating pressures, and thus, the temperature increase in larger. (ii) Simultaneously, when the system is operating at a lower pressure setting, the required

time to perform the charging procedure is smaller, resulting in less time to exchange heat. Also, whenever the air transformation happens faster, the temperature variations are more expressive. Now, to study the influence of the pump on the temperature behaviour, a similar procedure was done, evaluating the changes for three pumps at a fixed operating pressure.

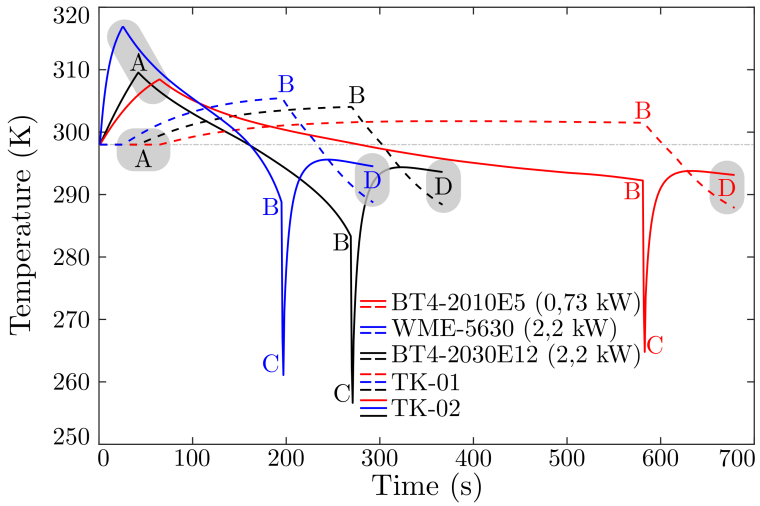

Figure 4.5 – Temperature evolution in tanks TK-01 (dashed line) and TK-02 (solid line) during both charging and generation stages, for an operating pressure of 350 kPa_g. For clarity purposes, only three pumps are presented: BT4-2010E5 (red); WME-5630 (blue) and BT4-2030E12 (black).

In Fig. 4.5 it is possible to notice the temperature behaviour to all pumps is similar. Again, slower compression rates result in smaller temperature variations, as expected (comparing red and blue curves). Points **A** to **D** have been kept, indicating the same operating moments as before. Given the system thermal behaviour, in which the temperature variations is considerably smaller than conventional CAES (BUDT et al., 2016), it is possible to conclude that, excluding extremely fast or slow compression, the pump model choice does not greatly influence the temperature behaviour.

4.3.3 Power and energy

Now that the thermodynamic behaviour of the PH-CAES is fully described, the power and energy consumption will be addressed. The power consumption during energy storage process is presented in Fig. 4.6. The convention dictates that the work entering a control volume is less than zero, hence the negative values.

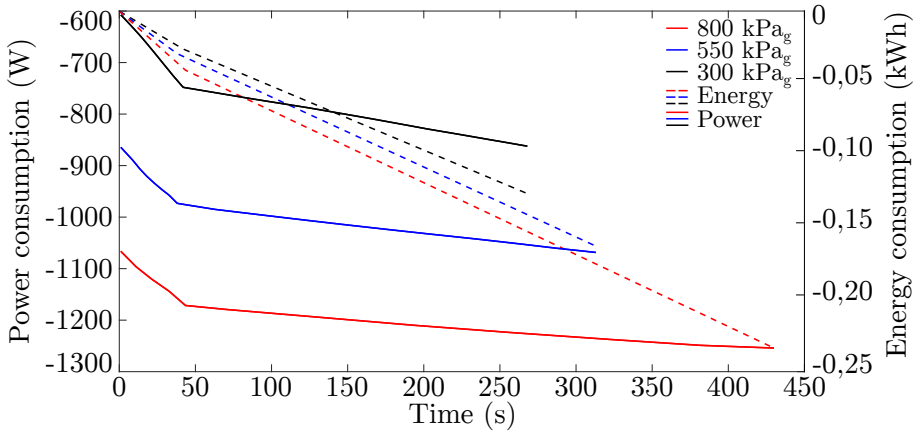

Figure 4.6 – Power (solid) and energy (dashed) consumption during charging, for pump #2 (BT4-2030E12). For clarity purposes, only three operating pressures were depicted: 300 (black); 550 (blue) and 800 kPa_g (red).

As expected, a higher pressure setting requires power from the pump over a longer period. Also, a noticeable difference in power consumption can be seen from the first to second storage stages. In the energy consumption, although not so visible, the same behaviour occurs. Also, even though the energy consumption over time seems to be linear, it is actually a parabola. However, the second degree curvature is extremely attenuated in the conversion between J to kWh. The energy saving of using a pump to compress the air, instead of a compressor can now be briefly addressed. In the previous PH-CAES study (CAMARGOS et al., 2018), a compressor was used to pressurize $0,2\ m^3$ of air, from approximately 600 to 900 kPa_g in a single stage, consuming $\approx 0,10\ kWh$, over 120 s. By utilizing a pump, between similar pressure levels (black lines in Fig. 4.6) air contained in $2,5\ m^3$ is compressed utilizing a similar amount of energy ($0,13\ kWh$). The benefits of managing the air, instead of replacing it, and not utilizing a direct, fast and restricted to a small chamber compression method are evident.

Now, different pumps will be addressed. As explained previously in the pressure section, two pumps with equal electric motors can present distinct power and energy consumption, depending on mechanical and constructive characteristics.

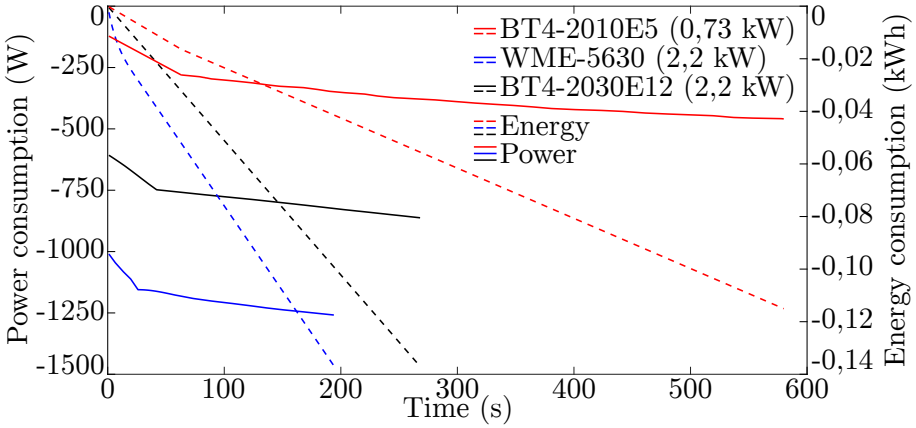

Figure 4.7 – Power (solid) and energy (dashed) consumption during charging, for an operating pressure of 350 kPa_g. For clarity purposes, only three pumps are presented: BT4-2010E5 (red); WME-5630 (blue) and BT4-2030E12 (black).

Once again, the pump's influence on the PH-CAES final performance is evident. In Fig. 4.7, for two similarly constructed pumps, BT4-2010E5 (#4) and BT4-2030E12 (#2), the corresponding shapes and results are expected, and follow the intuitive behaviour of the larger pump requiring less time and consuming more power and energy. Between distinctly constructed models, however, the power consumption behaviour differs. As explained before, in Fig. 4.3, WME-5630 (#6) is constructed in such fashion that the pressure *vs.* flow rate curve is flatter, outputting more water in a narrower pressure range. This leads to a higher power consumption during less time than BT4-2030E12. Nevertheless, since both pumps ultimately have similar efficiency values in the studied pressure range, their energy consumption ends nearly at the same value, around $0,13$ kWh.

As an example of the importance of analyzing the quality of eventually extrapolated data, in Fig. 4.8, the power behaviour of pump #3 (BT4-2020E10), considered unable to operate at the highest pressure setting, is presented.

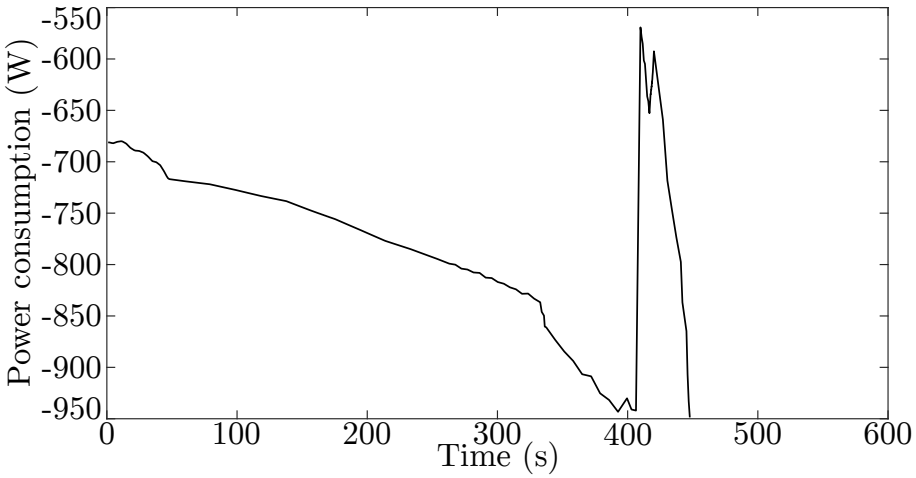

Figure 4.8 – Failed extrapolation reflected on the power consumption. This case corresponds to pump #3, BT4-2020E10 on the highest pressure setting.

In Fig. 4.8 the importance of carefully analyzing the extrapolated data is clear. The presented behaviour is an extreme case of extrapolation failure. Under normal conditions, the Matlab routine would have been stopped around 320 *sec*, but for demonstrations purposes, the break conditions were bypassed, and the process forced to continue. After around 400 *sec*, however, the results quickly and severely diverged, causing an error and stopping the program. Also, it is worth noticing that a failed extrapolation occurs on extrapolation the data from the manufacturer chart, and the misinterpreted data results on all depended variables failing to meet any representative meaning.

Differently from the energy storage process, during generation a steady power output is desired. The quality of the generated energy is as important as its quantity, so, a key preliminary aspect of the design is to produce energy steadily. From the previous studied with the technology (CAMARGOS et al., 2018; CAMARGOS, 2018), the PH-CAES system proved to be able to output power in a constant fashion, and rapidly respond to transient scenarios, quickly settling to a stable value. Furthermore, aiming to increase the overall efficiency of the PH-CAES, it is important to the turbine to operate under fixed conditions. Also, since a single turbine generator set was considered, the system response is pressure dependent only.

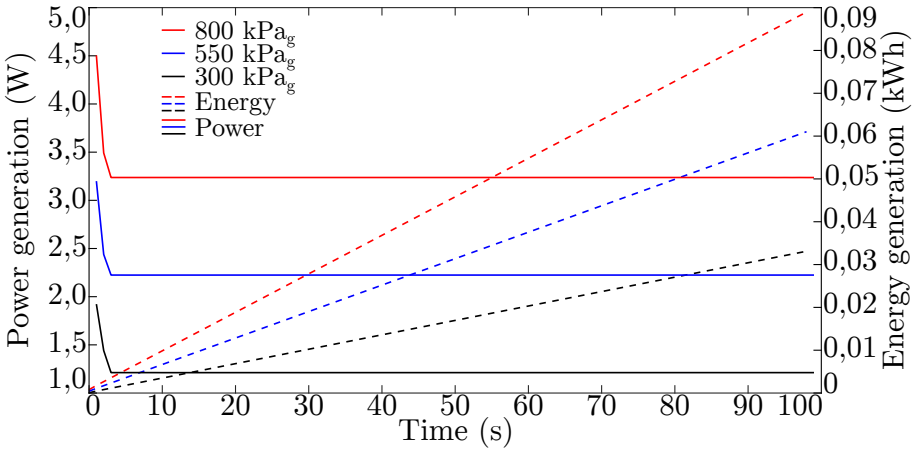

Figure 4.9 – Power (solid) and energy (dashed) generation for three operating pressures, 300 (black), 550 (blue) and 800 kPa_g (red).

Figure 4.9 presents the generator GEN-01 power output over the generation process. The initial pressure transient, observed in Figures 4.2 and 4.3, is seen in the initial power generation, starting at a higher level and quickly decreasing to its nominal figure. On average, this initial transient takes around three seconds. During the first few seconds, the water volumetric flow rates is also not constant, presenting a similar behaviour, starting at higher values and decreasing to the nominal 5 $\ell\ s^{-1}$. Even though this transient is brief, in real systems it must be accounted for to prevent damage downstream.

The generated energy increases linearly, apart from the initial transient, due to the constant power generation. Now, the PH-CAES system efficiencies will be discussed.

4.3.4 Efficiencies

The main evolution from the initial PH-CAES design is the efficiency. While the first prototype only reached around 1% round trip efficiency (E_{gen}/E_{cons}), the proposed improvements were able to greatly increase the efficiency. In this section, Energy η (First Law) and Exergy Ψ (Second Law) efficiencies will be discussed.

First, the charging energy efficiency, η_{char}, is defined as the ratio between the energy actually used to compress the air (W, defined in Eq. 3.6) by the pump power consumption (W_{M-02}, taken from manufacturer datasheet), over the entire charging process

$$\eta_{char} = \frac{\sum_0^t W}{\sum_0^t W_{M-02}}, \tag{4.1}$$

From Eqs. 3.6 and 4.1, the charging efficiency is dictated by the pump efficiency and frictional losses. The latter, is significantly reduced by the relatively large pipe diameter (largest available from commercial manufacturers), and its value accounts for around $\leqslant 5\%$ of the total losses during charging. So, the main source of inefficiency during the charging process is the pump. The chosen models are relatively small, so viscous effects are more significant when compared to larger models. Also, large pumps are constructed and assembled under stricter parameters, which also contributes to larger efficiency. So, it is reasonable to expect that for medium to large scale applications, the pump efficiency to be higher.

In Tab. 4.5 the charging energy efficiency values are presented. The peak efficiency was around 60%, found for higher operating pressures and pump #2 and #3.

Table 4.5 – Charging energy efficiency values, for all 66 operating pressures.

	Pump model					
Op. Pres. (kPa_g)	BT4-2040E15 #1	BT42030E12 #2	BT4-2020E10 #3	BT42010E5 #4	WME-5840 #5	WME-5630 #6
300	0,33	0,39	0,44	0,59	0,43	0,47
350	0,36	0,43	0,48	0,53	0,44	0,51
400	0,40	0,46	0,52	×	0,46	0,53
450	0,43	0,50	0,55	×	0,49	0,55
500	0,46	0,53	0,58	×	0,52	0,56
550	0,49	0,55	0,59	×	0,54	0,55
600	0,51	0,57	0,60	×	0,55	0,53
650	0,53	0,59	0,60	×	0,56	0,47
700	0,55	0,60	0,58	×	0,56	×
750	0,57	0,60	0,54	×	0,55	×
800	0,59	0,60	×	×	0,53	×

In Tab. 4.5 the major benefits adopting the pump as compression method are evident. Even with its reduced size, simple construction and general application, the charging efficiency reached 60%, whilst on conventional CAES systems, several compression

stages intercooled in between are necessary to achieve the same figures. As comparison, in (CAMARGOS et al., 2018), with an ATG3 compressor, the charging efficiency peaked at 10%. Moreover, the process of choosing a pump is application dependent. Even though pump #4 can only operate at the two smaller pressure settings, it produces the higher charging efficiency at these conditions. On the opposite end, pump #1 is the most powerful from the BT4 series, however, its not recommended for smaller pressures, resulting in poor efficiency figures. This behaviour is presented in Fig. 4.10, for the three pumps presented in the previous sections.

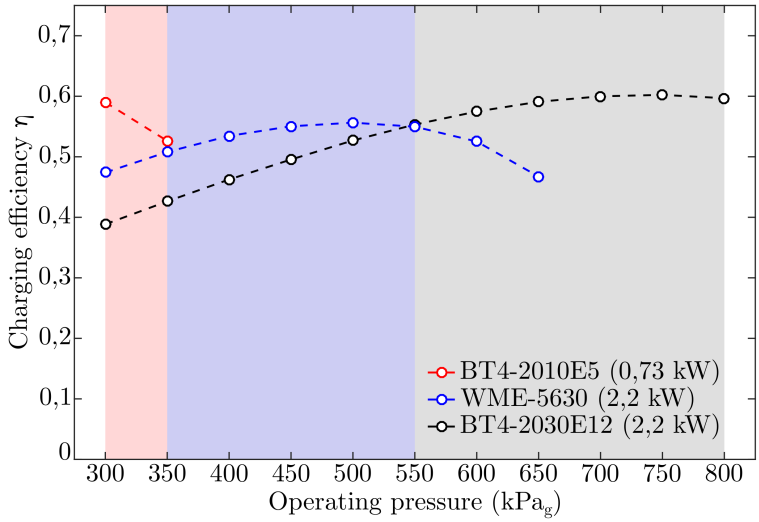

Figure 4.10 – Charging energy efficiency for three pumps, BT4-2010E5 (red), WME-5630 (blue) and (BT4-2030E12 (black). The highlighted shaded area color corresponds to the most efficient pump in each operating pressure. Note that only pump #2 is capable to operate in all scenarios.

The charging process efficiency is what defines the shape and overall system efficiency curve in the case study. This happens because, for reasons previously explained, the turbine and generator efficiency were considered constant and equal to $0,90$ each, for all cases. So, the highest charging efficiency will correspond to the peak Round-Trip Efficiency (RTE), which will now be addressed.

A high RTE is the main goal of the proposed system. In layman terms, it quantifies how much energy is not recovered over the entire operation. Conventional CAES systems cannot easily reach the same values of efficiency of its direct ESS competitors, namely PHES for bulk storage. Then, to get around this problem, several auxiliary components must be added to Compressed Air Energy Storage plants, which increases costs and reduces competitiveness. The energy η_{RTE} is simply defined as the ratio between energy generated by consumption.

$$\eta_{RTE} = \frac{E_{gen}}{\sum_0^t W_{M-02}} = \frac{E_{gen}}{E_{cons}} \tag{4.2}$$

The proposed system could reach relatively large efficiency figures, with a simple construction philosophy. The energy RTE figures, for all 66 operating points, are presented in Tab. 4.6

Table 4.6 – Energy Round-Trip Efficiency values, for all 66 operating pressures.

Op. Pres. (kPa_g)	Pump model					
	BT4-2040E15 #1	BT42030E12 #2	BT4-2020E10 #3	BT42010E5 #4	WME-5840 #5	WME-5630 #6
300	0,24	0,28	0,32	0,42	0,31	0,34
350	0,26	0,31	0,35	0,38	0,32	0,36
400	0,28	0,33	0,37	×	0,33	0,38
450	0,31	0,36	0,39	×	0,35	0,40
500	0,33	0,38	0,41	×	0,37	0,40
550	0,35	0,40	0,43	×	0,38	0,39
600	0,37	0,41	0,43	×	0,39	0,38
650	0,38	0,42	0,43	×	0,40	0,34
700	0,40	0,43	0,42	×	0,40	×
750	0,41	0,43	0,39	×	0,40	×
800	0,42	0,43	×	×	0,38	×

The Round-Trip Efficiency of the studied PH-CAES setup was considered promising. With a simple construction, a single pump system could reach approximately the same peak value of Huntorf's plant, $\eta_{RTE} \approx 43\%$ (BUDT et al., 2016). Later, in Sec 4.5, the system efficiency will be compared to other CAES alternatives. As expected, the RTE curves followed the same shape of the charging efficiency, offset by the losses in the turbine, generator and friction losses in the piping. The curves for the same three pumps are presented in Fig. 4.11.

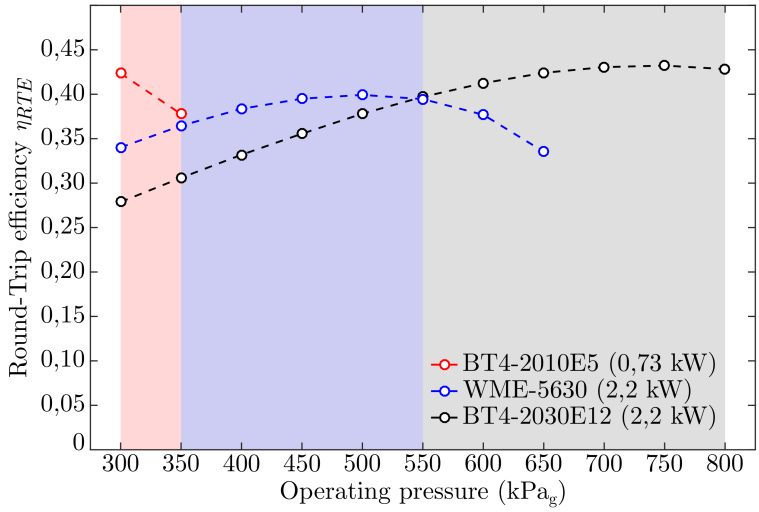

Figure 4.11 – Energy RTE for three pumps, BT4-2010E5 (red), WME-5630 (blue) and (BT4-2030E12 (black). Again, the highlighted shaded area color corresponds to the most efficient pump in each operating pressure.

Now the energy efficiencies are presented and assessed, a Second Law of Thermo-

dynamics efficiency analysis was performed. Three rational efficiencies are defined for (i) charging Ψ_{charg} (ii) generation Ψ_{gen} and (iii) round trip efficiency Ψ_{RTE}, being determined from Eqs. 4.3 to 4.5

$$\Psi_{char} = \frac{\left(\Delta X_{TK-01} + \Delta X_{TK-02}\right)_{char}}{E_{cons}}, \tag{4.3}$$

$$\Psi_{gen} = \frac{E_{gen}}{\left(\Delta X_{TK-01} + \Delta X_{TK-02}\right)_{gen}}, \tag{4.4}$$

$$\Psi_{RTE} = \Psi_{char} \cdot \Psi_{gen}. \tag{4.5}$$

Exergy variation in each tanks ΔX can be defined by Eq. 4.6 for tank TK-01 and Eq. 4.7 for tank TK-02 (ÇENGEL; BOLES, 2011)

$$\Delta X_{TK-01} = m_{air}\left[(u_2 - u_1) + P_0(\upsilon_2 - \upsilon_1) - T_0(s_2 - s_1)\right]_{air}, \tag{4.6}$$

$$\begin{aligned}\Delta X_{TK-02} = {} & m_{air}\left[(u_2 - u_1) + P_0(\upsilon_2 - \upsilon_1) - T_0(s_2 - s_1)\right]_{air} \\ & + m_{water}\left[(u_2 - u_1) + P_0(\upsilon_2 - \upsilon_1) - T_0(s_2 - s_1)\right]_{water}.\end{aligned} \tag{4.7}$$

Total exergy variation (ΔX) in the tanks during the generation process is (ÇENGEL; BOLES, 2011)

$$(\Delta X_{TK-01} + \Delta X_{TK-01})_{gen} = E_{gen} + Irr. \tag{4.8}$$

The near-isothermal nature of the PH-CAES results in heat performing a secondary role in the system operation. As heat is a major source of irreversibility, the entropy generation in the process is reduced. Also, from Figs. 4.2 and 4.4, it is possible to notice that in all simulated scenarios, for a given operating pressure each tank initial and final sates are nearly equal ($P_1, T_1, \upsilon_1 \approx P_2, T_2, \upsilon_2$). This brings as consequence

$$\Delta\chi_{char} = (\Delta X_{TK-01} + \Delta X_{TK-02})_{char}, \tag{4.9}$$

$$\Delta\chi_{gen} = (\Delta X_{TK-01} + \Delta X_{TK-02})_{gen}, \tag{4.10}$$

$$\Delta\chi_{char} \approx \Delta\chi_{gen}, \tag{4.11}$$

$$\Psi_{RTE} = \frac{\cancel{(\Delta\chi)_{char}}}{E_{cons}} \frac{E_{gen}}{\cancel{(\Delta\chi)_{gen}}} \approx \eta_{RTE}, \tag{4.12}$$

Then, rational efficiency is approximately equal to first law efficiency. This is yet another major benefit of the chosen compression method. By indirectly, slowly and acting upon the entire mass of air, exergy destruction is minimized. To confirm this statement, in Tab 4.7, the exergy RTE values for 66 pressure are presented.

Table 4.7 – Exergy Round-Trip Efficiency values, for all 66 operating pressures.

	Pump model					
Op. Pres. (kPa_g)	BT4-2040E15 #1	BT42030E12 #2	BT4-2020E10 #3	BT42010E5 #4	WME-5840 #5	WME-5630 #6
300	0,20	0,25	0,28	0,37	0,25	0,29
350	0,21	0,28	0,32	0,34	0,27	0,31
400	0,25	0,31	0,35	×	0,29	0,33
450	0,28	0,34	0,37	×	0,31	0,35
500	0,30	0,36	0,39	×	0,32	0,36
550	0,32	0,38	0,41	×	0,34	0,36
600	0,34	0,40	0,41	×	0,35	0,34
650	0,36	0,41	0,42	×	0,36	0,31
700	0,37	0,42	0,41	×	0,37	×
750	0,38	0,42	0,38	×	0,37	×
800	0,39	0,42	×	×	0,36	×

The values presented in Tabs. 4.6 and 4.7, especially for higher pressures, are virtually the same. In smaller pressure settings, the pumps are capable of performing the compression faster, and thus, bigger temperature variations are seen, which in turn, causes more heat to be exchanged, slightly decreasing the exergy efficiency. Even though, these values are considered promising.

Now that the main PH-CAES operating characteristics were presented and explained separately, it is convenient to present the results as a whole, to try and visualize the entire operation and performance simultaneously. So, for pump #2 (BT4-2030E12) and 750 kPa_g, in which the highest efficiency was achieved, firstly two doughnut chart are presented. These charts must be read inside out, red sections representing losses and green useful energy.

An interesting feature is that during the discharging, the higher water volumetric flow rate results in larger friction losses, as can be notice comparing Fig. 4.12a and 4.12b. For a laboratory scale project, the piping diameter is constrained by commercial dimensions. However, in a larger scale applications, the pipes diameter would be chosen to reduce these losses, similarly to penstocks in hydro power plants.

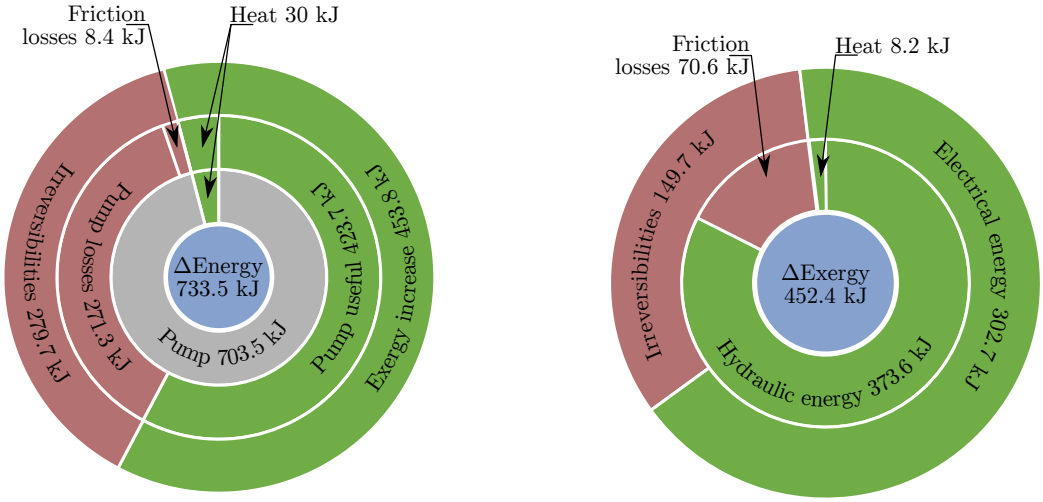

(a) Energy and exergy evolution during energy storage. The energy introduced in the system (ΔEnergy=733.5 kJ) results in an 455.3 kJ increase in stored exergy, *i.e.*, $\eta_{charg} = 0.62$ (see Fig. 4.10).

(b) Energy and exergy evolution during generation stage. The 452.4 kJ variation in the stored exergy results on 302.7 kJ of electrical energy generated, *i.e.*, $\Psi_{gen} = 0.67$.

Figure 4.12 – Energy and Exergy evolution during storage (**a**) and generation (**b**) stages, represented in a doughnut chart for operating pressure 750 kPa_g.

Lastly, in Fig. 4.13, a Sankey diagram depicts the complete operating cycle, broken down in its stages with their respective losses. It is clearly noticeable again that the main source of inefficiency is the pump, accounting for nearly 65% of all losses. Even though the pump is a major step up from the original compressor usually utilized, small equipments such as the chosen model are not able to deliver high efficiency levels. Considering a large scale system, in which the pump efficiency would figure at 85% and the frictional losses would be reduced to 5%, it is possible to expect the overall efficiency peaking as high as 75%, considering the same turbine and generator efficiencies, similarly to what has been reported in (MOZAYENI; WANG; NEGNEVITSKY, 2019).

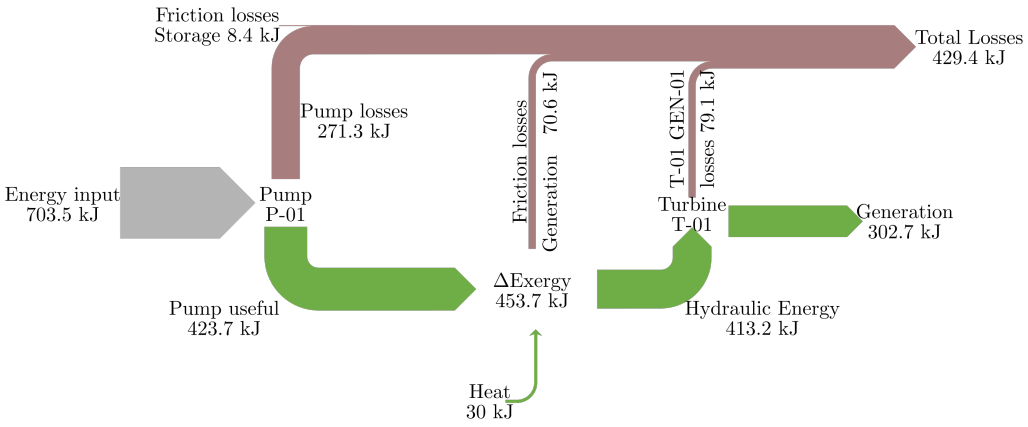

Figure 4.13 – Sankey diagram constructed for pump BT4-2030E12 and operating pressure 750 kPa_g, depicting the energy conversion and inefficiencies over the entirety of the operating cycle.

4.4 Dual pump operation

After presenting and explaining the system operation with a single pump, a simple but potentially effective improvement possible is to use two pumps instead of one. As seen in the previous sections, many operating points requirements were not attended by a single pump. By utilizing two pumps, it is expected a flexibility increase, allowing for operation over a wider range. Also, with two pumps, the increased output flow will reduce the charging time. In this proposed scenario, two equal pumps will be associated either in a series-parallel. These pumps will be the same model as strongly recommended by (MACINTYRE, 1987) to prevent reverse inflow between pumps. By associating pumps in parallel, it is possible to nearly double the water flow rate, while, if connected in series, each pump will provide half of the total pressure increase, reducing the demand in each pump. The proposed lay-out is presented in Fig. 4.14

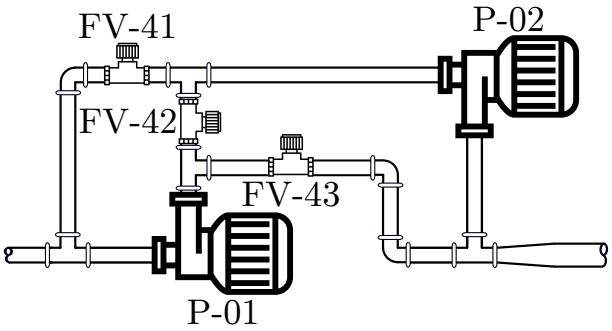

Figure 4.14 – Proposed layout for two pumps in series-parallel configuration.

The proposed series-parallel configuration presented in Fig. 4.14 is able to provide operation in both associations. In the beginning of the energy storage process, when TK-02 pressure is starting to increase, the pumps operate in parallel, increasing the total water flow and speeding the charging process up. Later, when the pressure increases, the pumps switch to a series setup, deceasing each pump pressure demand. Also, an objective of the dual-mode operation is to decrease the pressure range in each pump, maintaining each equipment closer to its optimal operation point. By using two pumps, all 66 operating points were covered. The two operation modes are depicted in Fig. 4.15.

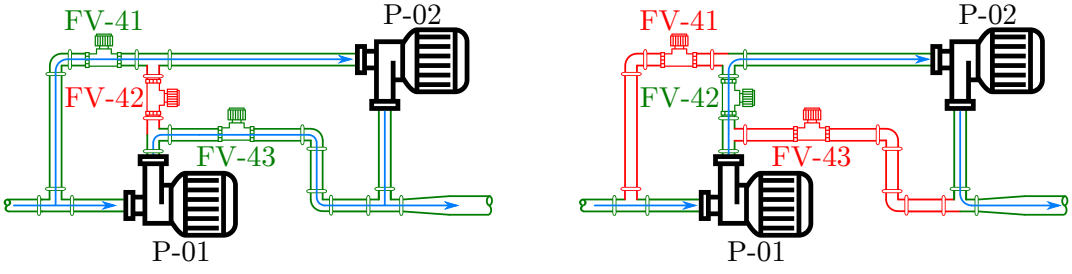

(a) Parallel pumps operation. (b) Series pumps operation

Figure 4.15 – Dual pump operation. In **(a)**, parallel layout and **(b)** series arrangement.

The algorithm to choose whether the system should operate in parallel or series arrangement based on the efficiency. Within a single time step $\langle i \Rightarrow i+1 \rangle$, the Matlab routine calculated the required power input and the compression work for both arrangements, and the option that returned the larges efficiency was chosen. To visually represent this fact, Fig. 4.16 presents the charging efficiency for two BT4-2020E10 (#3) and an operating pressure equal to 800 kPa_g.

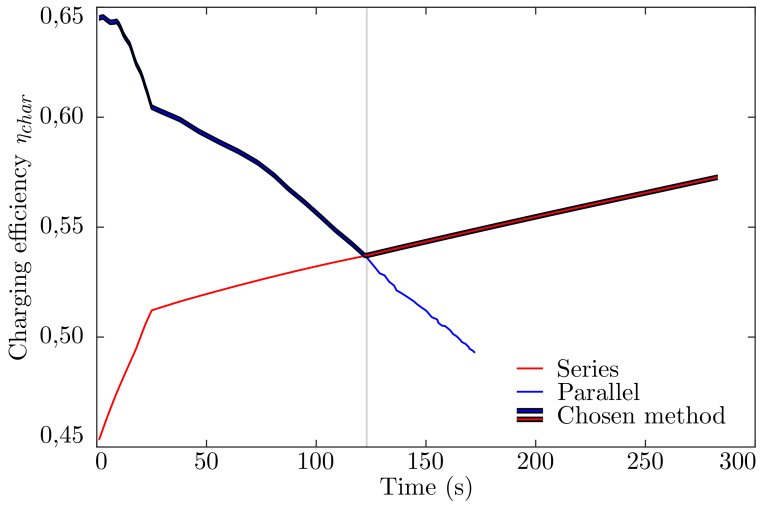

Figure 4.16 – Charging efficiency η_{charg} for two BT4-2020E10 pumps, in series-parallel arrangement, for an operating pressure equal to 800 kPa_g.

There are many interesting facts depicted in Fig. 4.16. Firstly, the two pumps association made it possible to operate in the designated pressure setting, while a single similar pump failed (see Tab. 4.4). The pumps switch operational mode at around 125 *sec*, indicated by the vertical line. Before this point, the setup was working with both pumps in parallel, but the increasing backpressure resulted in decreasing efficiency. From 125 *sec* onwards, it became more advantageous to switch to a series arrangement, with the net pressure increase equally divided by the two pumps. If the operating mode had not been altered, the pumps would not have been able to fully charge the PH-CAES system, stopping midway at 170 *sec*.

Another interesting point is the two curves stability difference. While the results for two pumps in series are extremely well behaved, the results for parallel setup fluctuate. This is the result of the extrapolation process, which provides a slightly unstable behaviour. This result, however, was still considered satisfactory enough to not be discarded and deemed unfit. Furthermore, the required time to fully charge the system decreased significantly. While for a single BT4-2030E12 pump, on the same pressure setting, it took almost 600 *s* (see Fig. 4.2), two smaller BT4-2020E10 pumps were able to perform it in around 275 *sec*. Lastly, the parallel operation mode would have failed at $\approx$ 170 *ses*. This is the nearly half elapsed time in which the single pump operation simulation would have stopped (see Fig. 4.8). This is due to the fact that when operating in parallel, the two pumps experience

the same pressure differential that a single pump would, but are able to provide nearly double the water flow rate. In Tab. 4.8, the operational arrangement for all 66 points are presented.

Table 4.8 – Dual pump operation arrangement, for all 66 operating pressures. **S** stands for series, **P** parallel only and **P/S** represents the scenarios in which the pumps switched modes during the charging procedure.

	Pump model					
Op. Pres. (kPa_g)	BT4-2040E15 #1	BT42030E12 #2	BT4-2020E10 #3	BT42010E5 #4	WME-5840 #5	WME-5630 #6
300	P	P	P	P	P	P
350	P	P	P	S/P	P	P
400	P	P	P	S/P	P	P
450	P	P	P	S/P	P	P
500	P	P	P	S/P	P	P
550	P	P	P	S	P	P
600	P	P	P	S	P	S/P
650	P	P	P	S	P	S/P
700	P	P	P	S	P	S/P
750	P	P	P/S	S	P	S/P
800	P	P	P/S	S	P	S/P

For a single pump, the influence of operating pressure and pump selection has already been thoroughly explained. With two pumps, the same analysis can be made, and for this reason, to avoid repetition and to narrow the analysis on the dual-pump setup, the comparisons will be made focusing on how the thermodynamic variables, power consumption and efficiency changed.

4.4.1 Pressure

Since the general behaviour of the pressure remains the same as when operating with a single pump, in this section, results for a single pump model will be presented. So, pump #3 was chosen because in lower pressure settings, it is able to operate only in parallel, but when the operating pressure increases, it needs to revert to operating in series. In Fig. 4.17, the results for pump BT4-2020E10, functioning in three pressure settings is shown. In this figure, only the charging process was presented.

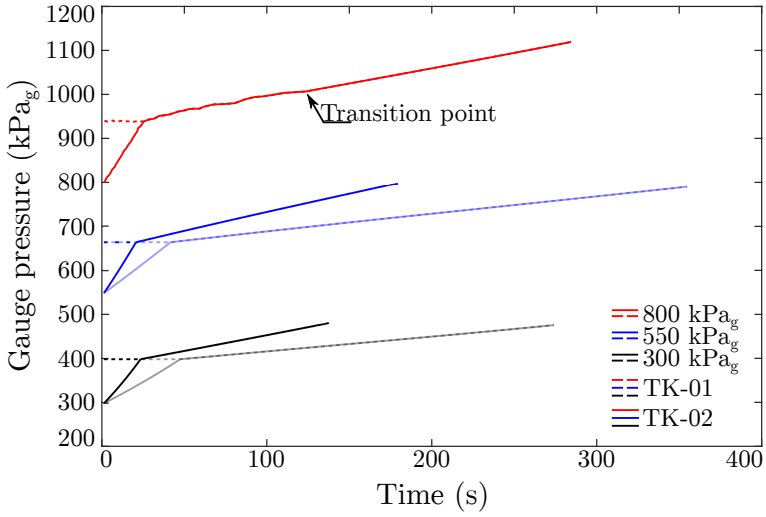

Figure 4.17 – Pressure evolution in tanks TK-01 (dashed line) and TK-02 (solid line) during charging stage, for pump #3 (BT4-2020E10), in three operating pressures: 300 (black); 550 (blue) and 800 kPa_g (red). For comparison wise, the faded lines represent the system operating with a single same model pump.

In Fig. 4.17, for operating pressures equal to 300 and 500 kPa_g the pumps were able to operate at all times in parallel configuration. At the highest pressure setting, however, it needed to switch modes at around 120 *sec*. As previously presented in Fig. 4.16, the extrapolation process caused instabilities in the data, as it can be seen for the highest pressure before switching modes. A major advantage noticeable is the decrease in the required time to fully charge the system, by comparing the results with the faded lines, representing the correspondent single pump operation. Also, it is possible to notice that for two pumps, the ending pressure is slightly above the single pump reference. This is due to the fact that the faster compression leading to higher temperatures, increasing thus, the pressure for a given fixed air mass.

4.4.2 Temperature

Once again, only the results for pump #3 will be presented, but this time, the 550 kPa_g data was also omitted. This is because not only the temperature graph is more complex and less intuitive than the pressure, but also the values sit closer together. This, added to the faded lines representing the singe pump operation for reference, made the presentation confuse. Also, since the omitted lines stands in between, with similar behaviours, no significant information is lost in the process.

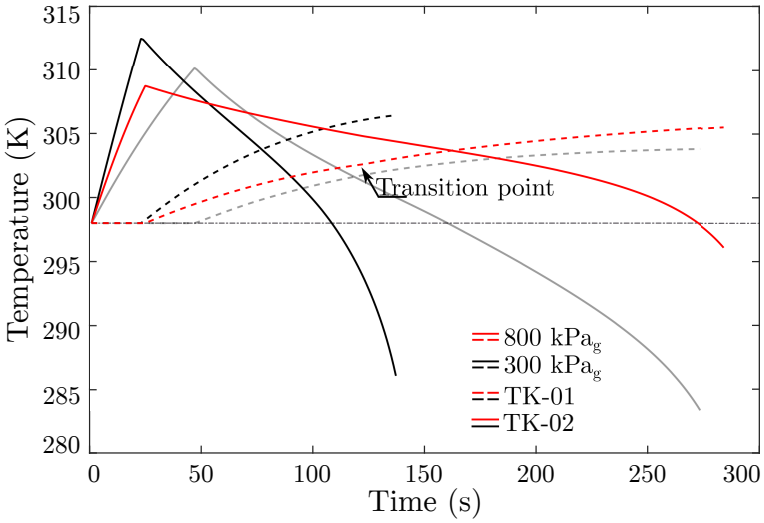

Figure 4.18 – Temperature evolution in tanks TK-01 (dashed line) and TK-02 (solid line) during charging stage, for pump #3 (BT4-2020E10), in two operating pressures: 300 (black) and 800 kPa_g (red). For comparison wise, the faded lines represent the system operating with a single pump.

In Fig. 4.18 it is possible to identify the temperature increase due to the faster compression rate. Nevertheless the effect is not significant, with tanks TK-01 and 02 peaking temperature less than 5 K higher than when operating with a single pump. Differently from the pressure behaviour, the 800 kPa_g temperature curve is smoother, especially before the switch over from parallel to series operation. The thermal inertia and heat transfer rates are capable of dampen the fluctuations resulted from the extrapolation process.

4.4.3 Power and energy

The main tradeoff proposed by operating with two pumps is to increase the efficiency. It is logical that two pumps will consume more power than just one, but for a shorter period of time, and possibly, in a more efficient manner. So being, now the power and energy consumption will be addressed. Beforehand to presenting any data, its expected that two pumps operating in parallel for the entire charging stage to be less efficient than just one. This is due to the fact that each pump efficiency is exclusively a function of the net head experienced, and two pumps in parallel are exposed to the same pressure differential than just one. In addition to this, two pumps will output nearly double the water flow rate than one, incurring in larger friction losses, decreasing thus, efficiency. The gains are expected when the assembly switches operating modes during the energy storage process.

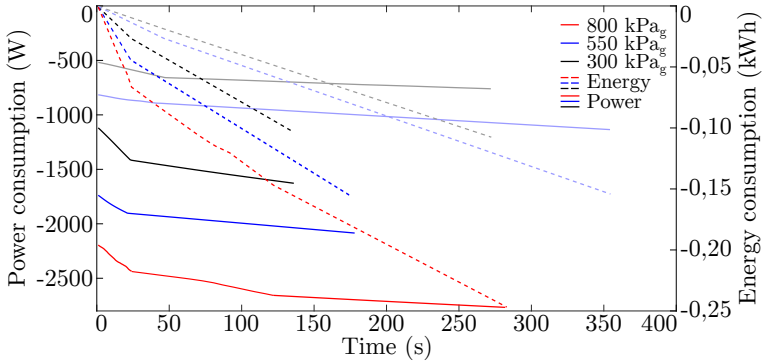

Figure 4.19 – Power (solid) and energy (dashed) consumption during charging, for pump #3 (BT4-2020E10). For clarity purposes, only three operating pressures were depicted: 300 (black); 550 (blue) and 800 kPa_g (red). For comparison wise, the faded lines represent the system operating with a single pump.

In Fig. 4.19, the power and energy consumption for two BT4-2020E10 pumps operating at 300, 550 and 800 kPa_g is presented. For the two first settings, in which the devices operated in parallel only, the total energy consumption is slightly higher than a single pump (faded lines, added for reference). So, energy wise only, it is not advantageous to operate with two pumps in parallel simultaneously, if the piping system is shared. The increased flow rate would intensify the friction losses. For the higher pressure setting, the pumps altered their operation mode during the charging process, enabling the system to run in a previously incapable level. For better comparison, the charging energy efficiency for all points are presented in Tab. 4.9.

Table 4.9 – Charging energy efficiency values, for all 66 operating pressures, in the dual pump scenario. The improvements are seen in the green shaded cells, in which the system operated first in parallel, then in series. The yellow shaded cells corresponds to cases in which the pump operated in series only.

	Pump model					
Op. Pres. (kPa_g)	BT4-2040E15 #1	BT42030E12 #2	BT4-2020E10 #3	BT42010E5 #4	WME-5840 #5	WME-5630 #6
300	0,31	0,38	0,43	0,56	0,41	0,45
350	0,35	0,42	0,47	0,57	0,42	0,47
400	0,39	0,45	0,51	0,57	0,43	0,50
450	0,42	0,49	0,53	0,59	0,46	0,52
500	0,45	0,51	0,56	0,61	0,50	0,54
550	0,49	0,53	0,57	0,61	0,52	0,53
600	0,51	0,56	0,58	0,62	0,54	0,56
650	0,52	0,57	0,58	0,61	0,54	0,57
700	0,53	0,58	0,59	0,59	0,55	0,58
750	0,56	0,59	0,61	0,56	0,54	0,59
800	0,60	0,58	0,63	0,46	0,51	0,58

From Tab. 4.9 the predicted behaviour was confirmed. For operations in parallel only, see Tab. 4.8, the charging efficiency was slightly smaller for two pumps than it is for one (also, see Tab. 4.5). However, when the two pumps started charging the system

in parallel, and later switched to running in series, an improvement was seen. The green shaded values returned higher values than its corresponding 1 pump solution, or even enabled operation altogether. These results show the importance of correctly understanding the system performance prior to choosing a pump. The application dictated the system setup and operation, and it is no simply a matter of installing additional or larger pumps. In some aspects, two pumps increase the efficiency, and always enable greater flexibility and agility in operation. However, if incorrectly applied, the increased flow rate intensify losses, temperature variation and can lead to smaller efficiency. The yellow shaded cells represent scenarios in which the system operated only in series. Since there is no correspondence to a single pump operation at these points, they cannot be compared to results presented in Sec.4.3. Lastly, in Tab. 4.10, the energy RTE values for two pump configuration are presented.

Table 4.10 – Energy RTE for all 66 operating point, in dual pump arrangement.

	Pump model					
Op. Pres. (kPa_g)	BT4-2040E15 #1	BT42030E12 #2	BT4-2020E10 #3	BT42010E5 #4	WME-5840 #5	WME-5630 #6
300	0,22	0,27	0,31	0,40	0,29	0,32
350	0,25	0,30	0,34	0,41	0,30	0,34
400	0,28	0,32	0,37	0,41	0,31	0,36
450	0,30	0,35	0,38	0,42	0,33	0,37
500	0,32	0,37	0,40	0,44	0,36	0,39
550	0,35	0,38	0,41	0,44	0,37	0,38
600	0,37	0,40	0,42	0,44	0,39	0,40
650	0,37	0,41	0,42	0,44	0,39	0,41
700	0,38	0,42	0,42	0,42	0,39	0,42
750	0,40	0,42	0,44	0,40	0,39	0,42
800	0,43	0,42	0,45	0,33	0,37	0,42

When comparing Tabs. 4.10 and 4.6, the peak efficiency increased from 43% to 45%. It is a small yet significative gain, considering the simplicity of the proposed improvement. Not only the value increased, it shifted pump model, from BT4-2030E12 in the single pump mode to two smaller BT4-2020E10 operating first in parallel, and later switching to series.

The two pump solution is one, simple and intuitive possible improvement proposed to the PH-CAES system. It is not this document goal or ambition to pinpoint a definitive solution, nor the author sees that a complex and relevant study subject such as the hereby discussed will ever reach an optimal and definite arrangement. However, by presenting the results for a laboratory scale version, the system outlines are defined, its features and faults exposed aiming to reach a technical and economical competitive Energy Storage Systems. Now, the results found in this section will be compared to CAES values found in the literature.

4.5 Comparison to other CAES systems

When considering that the simulated model consisted of a laboratory scale PH-CAES prototype, the efficiency figures can be seeing as promising. When compared to the work performed by Camargos *et al.* (CAMARGOS et al., 2018), for example, it is clear that the solution hereby proposed is a major improvement of initial concept, resulting in considerably higher efficiency and generation figures. Comparing to the results obtained by Maia *et al.* (MAIA et al., 2016), power levels are of the same order ($<10\ kW$), but the PH-CAES system presents to be more efficient. Wang *et. al.* (WANG et al., 2013) compares the cost of a similar PH-CAES solution to conventional CAES and PHES systems, finding cost 15% smaller for a 1 MW installation. In (DENHOLM; KULCINSKI, 2004), the authors found that over a 40-year operation cycle conventional CAES plant, 48% of its energy output would come from burning fuel prior to the expansion system, and even though, it would present a life cycle efficiency of 65%. A large scale PH-CAES, on the other hand, could figure at efficiency levels as high as the conventional CAES, without the major drawback of requiring fuel.

So, in Tab. 4.11 the PH-CAES system proposed is compared to a diversity of systems from the literature. In this table, it is possible to notice the proximity of the small scale PH-CAES efficiency to larger scale systems (inherently more efficient systems), despite of being considerably simpler and cheaper. More efficient systems usually have complex regenerative systems, intercoolers or depend on an external heat source to operate efficiently. The PH-CAES concept described in this article is competitive against these more complex systems, achieving similar efficiency levels.

Also, by scaling the PH-CAES system up, a significant increase in efficiency is to be expected. Larger hydraulic equipments are less sensitive to viscous effects, which in turn reduces the performance.

Table 4.11 – Comparison table, in which the hereby proposed system is compared to several literature references.

System type	Scale	Features	η_{RTE}	Power Output	Ref.
PH-CAES	Laboratory	-Uses pump and hydraulic turbine to replace conventional compressor and air turbine; -Near isothermal operation; -No external heat sources or combustion is required; -Constant generation due to backpressure maintenance.	$0,45$	$3\ kW$	
PH-CAES	Laboratory	-Experimental study performed to assess if the PH-CAES solution would be technically viable.	$0,01$	$110\ W$	[1]
PH-CAES	Medium/large	-Assumes constant turbine (90%) and pump (88%) efficiency.	$< 0,7$	-	[2]
PH-CAES	Medium/large	-Proposes a two-tank PH-CAES system, with a micro pump turbine; -A severe decrease in power output occurs as the pressure reduces over time.	$0,5 - 0,85$	$20 - 200\ kW$	[3]
PH-CAES	Large	-Similar system to the hereby proposed; -However, no constant pressure during generation.	$0,6 - 0,8$	-	[4]
D-CAES	Laboratory	-Integrates a scroll expander with a CAES system; -The experimental study consists of the generation stage only.	$0,55$	$600 - 980\ W$	[5]
D-CAES	Small	-Micro D-CAES system operating with an automotive turbocharger adapted as the turbine.	$0,45$	$3,5\ kW$	[6]
D-CAES	Small	-Focused on modelling the turbine; -Highly dependent on an external heat source; -Does not detail the compression stage and storage losses.	$0,59$	$2 - 3\ kW$	[7]
D-CAES	Medium/large	-Wind powered; -Requires external fuel supply.	$0,44(thermal)$	$2\ MW$	[8]
D-CAES	Medium/Large	-Integrated to a gas-steam combined plant; -Requires burning fuel as heat source; -Heat used to generate steam (to steam turbine) and mixed with cold stored compressed air from CAES system.	$0,6$	$5 - 10MW$	[9]
D-CAES	Large	-Huntorf Plant; -25% input energy spent in cooling system.	$0,42$	$321\ MW$	[10]
D-CAES	Large	-Mcintosh plant.	$0,54$	$110\ MW$	[10]
D-CAES	Large	-Huntorf plant modification.	$0,41$	$344\ MW$	[11]
D-CAES	Large	-Wind powered D-CAES; -Burns fuel prior to turbine; -Regenerator after turbine.	$0,54$	$75,5\ MW$	[12]
D-CAES	Large	-Uses operation curves for turbomachinery equipment to predict the system behaviour; -Uses data from Huntorf power plant.	$0,43$	$290\ MW$	[13]
A-CAES	Small	-Compression and storage stages only.	$< 0,4$ (charging only)	$200 - 300\ kW$	[14]
A-CAES	Medium/large	-Variable pressure ratio by using the compressor and turbines in series or parallel, depending on the output requirements.	$0,52$	$500\ kW$	[15]

(*table continues*)

Table 4.11 – Table 6: Comparison table, in which the hereby proposed system is compared to various literature references *(continued)*.

System type	Scale	Features	η_{RTE}	Power Output	Ref.
IA-CAES	Medium/large	-Variable volume storage vessel ensures isobaric operation.	$0,72$	$1\ MW$	[16]
A-CAES	Large	-Wind powered CAES system; -Cold and hot TES with molten salt and electrical heating system;	$< 0,6$	$185\ MW$	[17]
A-CAES	Large	-Utilizes an abandoned coal mine in China.	$0,50$	$8,76\ MW$	[18]
A-CAES	Large	-Lower temperature operating range for A-CAES systems.	$0,52 - 0,6$	$30\ MW$	[19]
IA-CAES	Large	-Hybrid IA-CAES concept, with water pumps and turbineas auxiliary components.	$0,55$	$100\ MW$	[20]
T-CAES	Small	-Theoretical and experimental study of Trigenerative CAES.	$0,16$	$0,45\ kW$	[21]
T-CAES	Small	-Theoretical trigenerative micro CAES	$0,30$	$18kW$	[22]
PSS-CAES	Small	-"Polygeneration Small-Scale Compressed Air Energy Storage"; -Multiple regeneration stages, may not be economically viable due to elevated cost and small power output.	$0,57$	$1,35\ kW$	[23]
HTH-CAES	Large	-High Temperature Hybrid CAES; -Allows high temperature air storage.	$0,53$	$100\ MW$	[24]
Hybrid	Small	-Studies integrating CAES system to a Diesel generator for rural areas.	$0,15 - 0,35$	$60 - 180\ kW$	[25]

Table 4.12 – Reference guide for Tab. 4.11

Reference guide		
[1] (CAMARGOS et al., 2018)	[10] (BUDT et al., 2016)	[19] (WOLF; BUDT, 2014)
[2] (YAO et al., 2015)	[11] (ZHANG et al., 2019)	[20] (MAZLOUM; SAYAH; NEMER, 2017)
[3] (YIN et al., 2014)	[12] (MENG et al., 2019)	[21] (CHEAYB et al., 2019)
[4] (MOZAYENI; WANG; NEGNEVITSKY, 2019)	[13] (BRIOLA et al., 2016)	[22] (FACCI et al., 2015)
[5] (SUN; LUO; WANG, 2015)	[14] (SALVINI; MARIOTTI; GIOVANNELLI, 2017)	[23] (JANNELLI et al., 2014)
[6] (MAIA et al., 2016)	[15] (HE et al., 2019)	[24] (HOUSSAINY et al., 2018)
[7] (JUBORI; JAWAD, 2019)	[16] (CHEN et al., 2018)	[25] (LI et al., 2016)
[8] (JIN; LIU; LI, 2019)	[17] (THOMASSON et al., 2017)	
[9] (SALVINI, 2017)	[18] (FAN et al., 2018)	

5 Conclusions

Given the world rising energy demand, with an inclination to boost renewable generation sources, Energy Storage Systems (ESS) are seen as an important step towards a sustainable future. In this scenario, the present research proposed a hybrid solution, in which positive features of Pumped Hydroelectric Energy Storage and Compressed Air Energy Storage have been merged. This new system is named Pumped Hydraulic Compressed Air Energy Storage (PH-CAES). The developed system utilizes hydraulic pump(s) to pump water intro a closed reservoir, compressing the air trapped above it. The pumps in the PH-CAES fulfill the same role as in PHES, driving the water from a smaller to higher pressure. While in PHES a physical height difference is necessary to generate this pressure differential, in the PH-CAES the compressed air resists the incoming water, to the same effect. The now compressed air stored the energy surplus as mechanical exergy. When this reserved energy is necessary, the air is allowed to expand, and it pressurizes the water towards a hydraulic turbine, which drives an electric generator. In summary, the charging and discharging process are taken from PHES, while the energy storage in itself origins in CAES.

By combining two of the most used bulk Energy Storage Systems methods currently applied worldwide, a number of advantages have been accomplished. By switching the conventionally used set of compressor and air turbines, a great deal of simplicity was added to the system, reducing not only installation costs, but operational and maintenance expenditures. In air compressors, a relatively small air mass is rapidly compressed in a confined volume, resulting in severe temperature increase and high specific power requirement. Dealing with hot air requires special materials, construction and imposes the necessity of intercoolers, and possibly Thermal Energy Storage systems. If, instead, the air is indirectly compressed by the moving water boundary, the process occurs over the entirety of the gaseous mass simultaneously, and most important, considerably slower. This results in a shorter temperature variation during the charging process. Also, as water is an incompressible fluid, pumping it requires significantly less energy than compressing the same air mass by an equal pressure ratio. Furthermore, in addition to having higher efficiency vales, pumps are cheaper than compressors.

During expansion, the compressed air pressurizes the water, resulting in a *virtual* head. For instance, air at 650 kPa_g is roughly similar to to a 65 m physical height difference. The pressurized water is driven towards a hydraulic turbine, which powers the electric generator. Once again, by utilizing water instead of air, a great deal of simplicity is achieved without having to sacrifice efficiency. While in conventional CAES systems, several turbines are connected in series, and air must be reheated in between, a single

hydraulic turbine is necessary. Air turbines are also more expensive, since they must deal with high temperature gases, and thus, special materials and manufacturing techniques are required. The hydraulic turbine is simpler in construction and operation. Equally important, the air heating process prior to entering the turbine can require burning fuels, or complex TES systems, which recovers heat generated during compression to return it when expanding. This leads to a large thermal inertia, meaning that conventional CAES may take a few minutes to reach full energy output. Yet another drawback surpassed by the proposed system is related to the variable inlet pressure at the turbine. In conventional CAES plants, the storage pressure is variable, leading to decrease in turbine performance. In the hereby solution, the stored air is divided into two separate tanks, and a pressure regulator ensures pressure stability, and ultimately, power quality.

The proposed Pumped Hydraulic Compressed Air Energy Storage system operation was fully described thermodynamically, under the scope of the First Law of Thermodynamics, assisted by Heat Transfer and Fluid Mechanics concepts, through a uniform transient model. Later, the Second Law of Thermodynamics was used to perform a exergy and irreversibility analysis, considering initial and final states. The mathematical models was then applied to a laboratory scale case study, in which the PH-CAES system was simulated on Matlab, aided by the CoolProp package.

The laboratory scale model simulated was conceived taking in account previous studies in the field, in which a prototype was built and tested. The constructed system had a number of faults that leaded to extremely low efficiency figures, but it served as proof of concept that such system was indeed plausible. These problems were addressed in the hereby proposed PH-CAES. To fully comprehend the system behaviour, eleven pressure levels and six different pump models were simulated. The simulation parameters took in account a preliminary layout, and data was taken from commercial data sheets, that while it increases the similarities between simulations and an eventually constructed system, results in technical constrains to match specific equipment requirements (*e.g.*, pipe diameter). The continuous nature of the operation was discretized into 1 *sec* time steps, in which all variables were calculated by iterative loops.

The simulations were conducted for a single pump scenario at first. The pressure evolution during operation was well behaved, and followed the predicted paths. Temperature wise, the proposed PH-CAES experiences considerably less variation than the conventional CAES. Also, the ΔT magnitude is mostly dependent on the pressure settings, not the chosen pump, with higher values being found for smaller operating pressures. When comparing the power consumption during charging, the studied model required less energy than both conventional CAES and the previous experimental study. It used approximately the same amount of energy than the constructed prototype, however, it compressed over 10 times more air, volume wise.

During generation, the system was quick to settle around its nominal production level, providing a stable power output throughout the entire discharging process. Thus, the energy charging efficiency was able to reach elevated figures, peaking at 60% for pump #2. A critical point observed in the simulation is that different pump models are more efficient at specific pressure requirements, and so, there is no single solution to correctly selecting a model. The energy RTE peaked at 43%, considered a promising and satisfactory result, being comparable to larger and more complex systems. From the Second Law of Thermodynamics point of view, the near isothermal nature of the system resulted in similar figures for energy and exergy efficiencies, as heat transfer performs a much secondary role. Due to the small equipment size, especially pump P-01, the RTE efficiencies were reduced. However, in larger applications, it can be easily expected to reach at least 70 to 75%.

Then, a simple potential improvement was proposed, substituting the single pump by two similar models, operating in parallel or series, depending on the requirements. The system general behaviour was the same, and a minor energy Round-Trip Efficiency improvement was achieved, from 43 to 45%. However small, the main objective of this layout change was to expose the system flexibility and adaptability. Lastly, its peak efficiency was compared to several literature sutdies on CAES, and the proposed Pumped Hydraulic Compressed Air Energy Storage system proved to be technically competitive, reaching an efficiency comparable to larger, more complex and expensive systems.

5.1 Future works suggestions

- Construct and test an actual PH-CAES system;
- Model and design a turbine fit for the PH-CAES application;
- Study the possibility of utilizing a pump as turbine;
- Apply the methodology hereby presented to large scale scenarios;
- Study replacing air and water by other fluids;
- Controlling flow rate during discharge first stage to mitigate transient effects;
- Study including speed control to M-02 during system charge;
- Propose an optimized layout, reducing losses;
- Investigate applying the proposed PH-CAES methodology to Huntorf CAES plant.

Bibliography

ABB. *EssPro Grid Battery energy storage systems*. [S.l.], 2017. Cited 2 times, in page(s): 5 and 6.

AGUADO, J.; TORRE, S. de la; TRIVIñO, A. Battery energy storage systems in transmission network expansion planning. *Electric Power Systems Research*, v. 145, p. 63 – 72, 2017. Cited on page(s): 13.

ALAMI, A. H. et al. Low pressure, modular compressed air energy storage (CAES) system for wind energy storage applications. *Renewable Energy*, v. 106, p. 201 – 211, 2017. Cited on page(s): 34.

ALDALUR, I. et al. Flowable polymer electrolytes for lithium metal batteries. *Journal of Power Sources*, v. 423, p. 218 – 226, 2019. Cited on page(s): 20.

ALVA, G.; LIN, Y.; FANG, G. An overview of thermal energy storage systems. *Energy*, v. 144, p. 341 – 378, 2018. Cited 2 times, in page(s): 4 and 28.

AMIRYAR, M.; PULLEN, K. A Review of Flywheel Energy Storage System Technologies and Their Applications. *Applied Sciences*, v. 7, p. 286, 03 2017. Cited 2 times, in page(s): 30 and 31.

BABACAN, O.; TORRE, W.; KLEISSL, J. Siting and sizing of distributed energy storage to mitigate voltage impact by solar PV in distribution systems. *Solar Energy*, v. 146, p. 199 – 208, 2017. Cited on page(s): 7.

BARDEEN, J.; COOPER, L. N.; SCHRIEFFER, J. R. Theory of Superconductivity. *Phys. Rev.*, American Physical Society, v. 108, p. 1175–1204, Dec 1957. Cited on page(s): 25.

BARTON, J.; INFIELD, D. Energy Storage and Its Use With Intermittent Renewable Energy. *IEEE Transactions on Energy Conversion*, Institute of Electrical and Electronics Engineers (IEEE), v. 19, n. 2, p. 441–448, jun. 2004. Cited on page(s): 3.

BATHURST, G.; STRBAC, G. Value of combining energy storage and wind in short-term energy and balancing markets. *Electric Power Systems Research*, v. 67, n. 1, p. 1 – 8, 2003. Cited on page(s): 1.

BEACONPOWER. *20 MW Flywheel Energy Storage Plant*. [S.l.], 2014. Cited 2 times, in page(s): v and 31.

BEACONPOWER. *Convergent energy + power acquires 40 MW of flywheel projects*. 2018. News report. Https://beaconpower.com/wp-content/uploads/2018/05/Convergent-Energy-Power-Acquires-40-MW-of-Flywheel-Projects-%E2%80%93-Convergent-Energy-Power.pdf. Cited on page(s): 31.

BHUNIA, U. et al. Design of a 4.5MJ/1MW sectored toroidal superconducting energy storage magnet. *Cryogenics*, v. 63, p. 186 – 198, 2014. Cited on page(s): 26.

BIASI, V. D. 110 MW McIntosh CAES plant over 90% availability and 95% reliability. *Gas Turbine World*, v. 28, p. 26–28, 1998. Cited 2 times, in page(s): 1 and 33.

BLACK, M.; STRBAC, G. Value of Bulk Energy Storage for Managing Wind Power Fluctuations. *IEEE Transactions on Energy Conversion*, v. 22, n. 1, p. 197–205, March 2007. Cited on page(s): 1.

BOGENRIEDER, W. *2.6. Pumped storage power plants: Datasheet from Landolt-Börnstein - Group VIII Advanced Materials and Technologies · Volume 3C: "Renewable Energy" in Springer Materials*. [S.l.]: Springer Verlag Berlin Heidelberg, 2006. Cited on page(s): 1.

BORGNAKKE, C.; SONNTAG, R. E. *Fundamentals of Thermodynamics*. Eighth ed. [S.l.]: Wiley, 2013. Cited on page(s): 48.

BRIOLA, S. et al. A novel mathematical model for the performance assessment of diabatic compressed air energy storage systems including the turbomachinery characteristic curves. *Applied Energy*, v. 178, n. Supplement C, p. 758 – 772, 2016. Cited 2 times, in page(s): 33 and 81.

BUDT, M. et al. A review on compressed air energy storage: Basic principles, past milestones and recent developments. *Applied Energy*, v. 170, n. Supplement C, p. 250 – 268, 2016. Cited 7 times, in page(s): 1, 33, 34, 36, 62, 68, and 81.

BUDYNAS, R. G.; NISBETT, J. K. *Shigley's Mechanical Engineering Design*. Ninth ed. [S.l.]: McGraw Hill, 2011. Cited on page(s): 30.

CAMARGOS, T. P. et al. Experimental study of a PH-CAES system: Proof of concept. *Energy*, Elsevier BV, v. 165, p. 630–638, dec 2018. Cited 7 times, in page(s): 38, 54, 63, 65, 67, 79, and 81.

CAMARGOS, T. P. L. *Estudo experimentao de um sistema de armazenamento de energia H-CAES operando com uma turbina hidráulica*. Dissertação (Mestrado) — Universidade Federal de Minas Gerais, Belo Horizonte, Brasil, 2018. Cited 2 times, in page(s): 54 and 65.

CAZZANIGA, R. et al. Compressed air energy storage integrated with floating photovoltaic plant. *Journal of Energy Storage*, v. 13, p. 48 – 57, 2017. Cited on page(s): 34.

ÇENGEL, Y.; BOLES, M. *Thermodynamics: An Engineering Approach*. Seventh ed. [S.l.]: McGraw-Hill, 2011. Cited 2 times, in page(s): 36 and 69.

CHAE, J. S. et al. Non-aqueous quasi-solid electrolyte for use in supercapacitors. *Journal of Industrial and Engineering Chemistry*, v. 59, p. 192 – 195, 2018. Cited on page(s): 25.

CHAZARRA, M. et al. Economic viability of pumped-storage power plants participating in the secondary regulation service. *Applied Energy*, v. 216, p. 224 – 233, 2018. Cited on page(s): 9.

CHEAYB, M. et al. Modelling and experimental validation of a small-scale trigenerative compressed air energy storage system. *Applied Energy*, Elsevier BV, v. 239, p. 1371–1384, abr. 2019. Cited on page(s): 81.

CHEN, H. et al. Progress in electrical energy storage system: A critical review. *Progress in Natural Science*, v. 19, n. 3, p. 291–312, 2009. Cited on page(s): 32.

CHEN, L. X. et al. A novel isobaric adiabatic compressed air energy storage (IA-CAES) system on the base of volatile fluid. *Applied Energy*, Elsevier BV, v. 210, p. 198–210, jan 2018. Cited on page(s): 81.

CHEUNG, B. C.; CARRIVEAU, R.; TING, D. S.-K. Parameters affecting scalable underwater compressed air energy storage. *Applied Energy*, v. 134, n. Supplement C, p. 239 – 247, 2014. Cited on page(s): 34.

CONWAY, B. E.; BOCKRIS, J. O.; AMMAR, I. A. The dielectric constant of the solution in the diffuse and Helmholtz double layers at a charged interface in aqueous solution. *Trans. Faraday Soc.*, The Royal Society of Chemistry, v. 47, p. 756–766, 1951. Cited on page(s): 25.

CORRAL-VEGA, P. J.; FERNÁNDEZ-RAMÍREZ, L. M.; GARCÍA-TRIVIÑO, P. Hybrid powertrain, energy management system and techno-economic assessment of rubber tyre gantry crane powered by diesel-electric generator and supercapacitor energy storage system. *Journal of Power Sources*, v. 412, p. 311 – 320, 2019. ISSN 0378-7753. Cited on page(s): 4.

CROTOGINO, F.; MOHMEYER, K.-U.; SCHARF, R. Huntorf CAES. More than 20 years of successful operation. In: SMRI SPRING MEETING. [S.l.], 2001. Cited 5 times, in page(s): 1, 28, 33, 34, and 36.

CRUISE, J. R.; GIBBENS, R. J.; ZACHARY, S. Optimal control of storage for arbitrage, with applications to energy systems. In: *2014 48th Annual Conference on Information Sciences and Systems (CISS)*. [S.l.: s.n.], 2014. p. 1–6. Cited on page(s): 1.

DAS, C. K. et al. Overview of energy storage systems in distribution networks: Placement, sizing, operation, and power quality. *Renewable and Sustainable Energy Reviews*, v. 91, p. 1205 – 1230, 2018. ISSN 1364-0321. Cited 9 times, in page(s): 3, 4, 7, 25, 28, 30, 31, 32, and 33.

DENHOLM, P.; KULCINSKI, G. L. Life cycle energy requirements and greenhouse gas emissions from large scale energy storage systems. *Energy Conversion and Management*, Elsevier BV, v. 45, n. 13-14, p. 2153–2172, aug 2004. Cited on page(s): 79.

DIVYA, K.; ØSTERGAARD, J. Battery energy storage technology for power systems—An overview. *Electric Power Systems Research*, v. 79, n. 4, p. 511 – 520, 2009. Cited 5 times, in page(s): 4, 17, 18, 22, and 23.

DöSOGLU, M. K.; ARSOY, A. B. Transient modeling and analysis of a DFIG based wind farm with supercapacitor energy storage. *International Journal of Electrical Power & Energy Systems*, v. 78, p. 414 – 421, 2016. ISSN 0142-0615. Cited on page(s): 4.

EDF-RE. *FAQ Energy storage solutions and peak shaving service*. 2019. Online. Availabe on May 23^{th}, 2019. Cited 2 times, in page(s): v and 6.

EIA. *Electricity prices reflect rising delivery costs, declining power production costs*. [S.l.], 2017. Available on : https://www.eia.gov/todayinenergy/detail.php?id=32812. Cited on page(s): 14.

ELECTREK. *World's largest battery:* 200 *MW/*800 *MWh vanadium flow battery – site work ongoing*. 2017. Online. Available on: https://electrek.co/2017/12/21/worlds-largest-battery-200mw-800mwh-vanadium-flow-battery-rongke-power/. Cited on page(s): 4.

ENERGIZER. *Produc Datasheet: CR2032*. [S.l.], 2018. Cited on page(s): 4.

ENNIL, A. B. *Optimization of small-scale axial turbine for distributed Compressed Air Energy Storage system*. Tese (Doutorado) — University of Birmingham, 2016. Cited on page(s): 35.

FACCI, A. L. et al. Trigenerative micro compressed air energy storage: Concept and thermodynamic assessment. *Applied Energy*, v. 158, n. Supplement C, p. 243 – 254, 2015. Cited on page(s): 81.

FAN, J. et al. Thermodynamic and applicability analysis of a hybrid CAES system using abandoned coal mine in china. *Energy*, Elsevier BV, v. 157, p. 31–44, aug 2018. Cited on page(s): 81.

FERC. *Licensed Pumped Storage Projects*. [S.l.], 2019. Federal Energy Regulatory Commision. Cited on page(s): 5.

FOLEY, A. et al. A long-term analysis of pumped hydro storage to firm wind power. *Applied Energy*, v. 137, p. 638 – 648, 2015. ISSN 0306-2619. Cited on page(s): 3.

FOLEY, A.; OLABI, A. G. Renewable energy technology developments, trends and policy implications that can underpin the drive for global climate change. *Renewable and Sustainable Energy Reviews*, v. 68, p. 1112 – 1114, 2017. ISSN 1364-0321. Cited on page(s): 3.

FOX, R.; MCDONALD, A. *Introduction to fluid mechanics*. [S.l.]: Wiley, 1985. Cited on page(s): 41.

GHORBANI, N.; MAKIAN, H.; BREYER, C. A GIS-based method to identify potential sites for pumped hydro energy storage - Case of Iran. *Energy*, v. 169, p. 854 – 867, 2019. Cited on page(s): 32.

GIRISHKUMAR, G. et al. Lithium-Air Battery: Promise and Challenges. *The journal of Physical Chemistry letters*, v. 1, n. 14, p. 2193–2203, 2010. Cited on page(s): 21.

GRAZZINI, G.; MILAZZO, A. Thermodynamic analysis of CAES/TES systems for renewable energy plants. *Renewable Energy*, v. 33, n. 9, p. 1998 – 2006, 2008. Cited 2 times, in page(s): 29 and 33.

GUANWEI, J. et al. Micron-sized water spray-cooled quasi-isothermal compression for compressed air energy storage. *Experimental Thermal and Fluid Science*, v. 96, p. 470 – 481, 2018. Cited on page(s): 34.

GUO, C. et al. Comparison of compressed air energy storage process in aquifers and caverns based on the Huntorf CAES plant. *Applied Energy*, v. 181, p. 342 – 356, 2016. Cited on page(s): 34.

GUO, C. et al. Numerical investigation of a joint approach to thermal energy storage and compressed air energy storage in aquifers. *Applied Energy*, v. 203, n. Supplement C, p. 948 – 958, 2017. Cited on page(s): 34.

GUO, H. et al. Off-design performance of CAES systems with low-temperature thermal storage under optimized operation strategy. *Journal of Energy Storage*, v. 24, p. 100787, 2019. Cited on page(s): 29.

HALLIDAY, D.; RESNICK, R.; WALKER, J. *Fundamentals of Physics*. [S.l.]: John Wiley & Sons Canada, Limited, 2010. (Halliday & Resnick Fundamentals of Physics, v. 2 - Electromagnetism). Cited 2 times, in page(s): 23 and 24.

HE, Q. et al. A compressed air energy storage system with variable pressure ratio and its operation control. *Energy*, Elsevier BV, v. 169, p. 881–894, feb 2019. Cited on page(s): 81.

HEIDARI, M.; MORTAZAVI, M.; RUFER, A. Design, modeling and experimental validation of a novel finned reciprocating compressor for Isothermal Compressed Air Energy Storage applications. *Energy*, v. 140, n. Part 1, p. 1252 – 1266, 2017. Cited on page(s): 33.

HEILBRON, J. *Electricity in the* 17^{th} *and* 18^{th} *Centuries: A Study of Early Modern Physics*. [S.l.]: University of California Press, 1979. Cited on page(s): 23.

HIGHVIEWPOWER. *LAES Power Plant*. 2019. Digital. URL: https://www.highviewpower.com/. Cited on page(s): 28.

HOUSSAINY, S. et al. Thermodynamic analysis of a high temperature hybrid compressed air energy storage (HTH-CAES) system. *Renewable Energy*, Elsevier BV, v. 115, p. 1043–1054, jan. 2018. Cited on page(s): 81.

HREINSSON, K.; VRAKOPOULOU, M.; ANDERSSON, G. Spinning and non-spinning reserve allocation for stochastic security constrained unit Commitment. In: *2014 Power Systems Computation Conference*. [S.l.: s.n.], 2014. p. 1–7. Cited on page(s): 10.

IEA. *World Energy Outlook 2017*. [S.l.], 2017. 763 p. Cited on page(s): 1.

IHA. *The world's water battery: Pumped hydropower storage and the clean energy transition*. International Hydropower Association, 2018. Cited 2 times, in page(s): 30 and 32.

INTERTECHNOLOGY, I. V. *Aluminum Electrolytic Capacitors*. [S.l.], 2015. Cited on page(s): 25.

JAIN, P.; DAS, A.; JAIN, T. Aggregated electric vehicle resource modelling for regulation services commitment in power grid. *Sustainable Cities and Society*, v. 45, p. 439 – 450, 2019. Cited on page(s): 9.

JANNELLI, E. et al. A small-scale CAES (compressed air energy storage) system for stand-alone renewable energy power plant for a radio base station: A sizing-design methodology. *Energy*, Elsevier BV, v. 78, p. 313–322, dez. 2014. Cited 2 times, in page(s): 37 and 81.

JIN, H.; LIU, P.; LI, Z. Dynamic modelling of a hybrid diabatic compressed air energy storage and wind turbine system. In: *27th European Symposium on Computer Aided Process Engineering*. [S.l.]: Elsevier, 2017, (Computer Aided Chemical Engineering, Supplement C). p. 2569 – 2574. Cited on page(s): 33.

JIN, H.; LIU, P.; LI, Z. Dynamic modeling and design of a hybrid compressed air energy storage and wind turbine system for wind power fluctuation reduction. *Computers & Chemical Engineering*, Elsevier BV, v. 122, p. 59–65, mar. 2019. Cited on page(s): 81.

JOHNSON, S. C. et al. Chapter Five - Selecting Favorable Energy Storage Technologies for Nuclear Power. In: BINDRA, H.; REVANKAR, S. (Ed.). *Storage and Hybridization of Nuclear Energy*. [S.l.]: Academic Press, 2019. p. 119 – 175. Cited on page(s): 27.

JUBORI, A. M. A.; JAWAD, Q. A. Investigation on performance improvement of small scale compressed-air energy storage system based on efficient radial-inflow expander configuration. *Energy Conversion and Management*, Elsevier BV, v. 182, p. 224–239, fev. 2019. Cited on page(s): 81.

KAMAL, R. et al. Strategic control and cost optimization of thermal energy storage in buildings using EnergyPlus. *Applied Energy*, v. 246, p. 77 – 90, 2019. Cited on page(s): 4.

KIEHNE, H. A. *Battery Technology handbook*. Second ed. [S.l.]: Marcel Dekker inc., 2003. ISBN: 0-8247-4249-4. Cited 6 times, in page(s): 16, 17, 18, 19, 21, and 23.

KIM, J.; CHANG, D. Pressurized cryogenic air energy storage for efficiency improvement of liquid air energy storage. *Energy Procedia*, v. 158, p. 5086 – 5091, 2019. Innovative Solutions for Energy Transitions. Cited 2 times, in page(s): 27 and 28.

KIM, Y.; SHIN, D.; FAVRAT, D. Operating characteristics of constant-pressure compressed air energy storage (CAES) system combined with pumped hydro storage based on energy and exergy analysis. *Energy*, v. 36, n. 10, p. 6220 – 6233, 2011. Cited on page(s): 36.

KUMAR, A.; KISHORE, V. Construction and operational experience of a 6000 m^2 solar pond at Kutch, India. *Solar Energy*, v. 65, n. 4, p. 237 – 249, 1999. Cited on page(s): 4.

LAM, L.; FURUKAWA, J. Secondary B - Lead - acid systems | Supercap Hybrid (UltraBattery). In: GARCHE, J. (Ed.). *Encyclopedia of Electrochemical Power Sources*. Amsterdam: Elsevier, 2009. p. 755 – 763. Cited on page(s): 18.

LEE, J.-S. et al. Metal–Air Batteries with High Energy Density: Li–Air versus Zn–Air. *Advanced Energy Materials*, v. 1, n. 1, p. 34–50, 2011. Cited on page(s): 21.

LEE, S. et al. Coordinated Control Algorithm for Distributed Battery Energy Storage Systems for Mitigating Voltage and Frequency Deviations. *IEEE Transactions on Smart Grid*, v. 7, n. 3, p. 1713–1722, May 2016. Cited on page(s): 7.

LESIEUTURE, B. C.; ETO, J. H. *Electricity Transmission Congestion Costs: A Review of Recent Reports*. [S.l.], 2003. Cited on page(s): 14.

LEUNG, P. et al. Ce(III)/Ce(IV) in methanesulfonic acid as the positive half cell of a redox flow battery. *Electrochimica Acta*, v. 56, n. 5, p. 2145 – 2153, 2011. Cited 2 times, in page(s): 22 and 23.

LEUNG, P. et al. Characterization of a zinc–cerium flow battery. *Journal of Power Sources*, v. 196, n. 11, p. 5174 – 5185, 2011. Cited 2 times, in page(s): 22 and 23.

LI, B.; DECAROLIS, J. F. A techno-economic assessment of offshore wind coupled to offshore compressed air energy storage. *Applied Energy*, v. 155, n. Supplement C, p. 315 – 322, 2015. Cited on page(s): 34.

LI, L. et al. A rapid cell voltage balancing scheme for supercapacitor based energy storage systems for urban rail vehicles. *Electric Power Systems Research*, v. 142, p. 329 – 340, 2017. ISSN 0378-7796. Cited on page(s): 4.

LI, Y.; LU, J. Metal-Air Batteries: Future Electrochemical Energy Storage of Choise? *U.S. Department of Energy Office of Scientific and Technical Information*, p. 23, May 2017. Cited 2 times, in page(s): 20 and 21.

LI, Y. et al. Integrating compressed air energy storage with a diesel engine for electricity generation in isolated areas. *Applied Energy*, v. 171, n. Supplement C, p. 26 – 36, 2016. Cited on page(s): 81.

LIANG, X. et al. Comparison of building performance between Conventional House and Passive House in the UK. *Energy Procedia*, v. 142, p. 1823 – 1828, 2017. Proceedings of the 9th International Conference on Applied Energy. Cited on page(s): 29.

LIU, M.; SAMAN, W.; BRUNO, F. Review on storage materials and thermal performance enhancement techniques for high temperature phase change thermal storage systems. *Renewable and Sustainable Energy Reviews*, v. 16, n. 4, p. 2118 – 2132, 2012. Cited on page(s): 4.

LU, B. et al. Geographic information system algorithms to locate prospective sites for pumped hydro energy storage. *Applied Energy*, v. 222, p. 300 – 312, 2018. Cited on page(s): 32.

LUO, X. et al. Overview of current development in electrical energy storage technologies and the application potential in power system operation. *Applied Energy*, v. 137, p. 511–536, 2015. Cited 4 times, in page(s): v, 31, 32, and 33.

MACINTYRE, A. J. *Bombas e Instalações de Bombeamento*. Second ed. [S.l.]: Editora Guanabara, 1987. Cited on page(s): 72.

MAIA, T. A. et al. Experimental performance of a low cost micro-CAES generation system. *Applied Energy*, v. 182, n. Supplement C, p. 358 – 364, 2016. Cited 4 times, in page(s): 34, 35, 79, and 81.

MAYTAL, B.-Z. Maximizing production rates of the Linde–Hampson machine. *Cryogenics*, v. 46, n. 1, p. 49 – 54, 2006. Cited on page(s): 27.

MAZLOUM, Y.; SAYAH, H.; NEMER, M. Exergy analysis and exergoeconomic optimization of a constant-pressure adiabatic compressed air energy storage system. *Journal of Energy Storage*, Elsevier BV, v. 14, p. 192–202, dec 2017. Cited on page(s): 81.

MCBRIDE, T.; BELL, A.; KEPSHIRE, D. ICAES *innovation: foam-based heat exchange*. USA: Seabrook: [s.n.], 2013. Cited on page(s): 34.

MENG, H. et al. Process design, operation and economic evaluation of compressed air energy storage (CAES) for wind power through modelling and simulation. *Renewable Energy*, Elsevier BV, v. 136, p. 923–936, jun 2019. Cited on page(s): 81.

MOUSER. *SCC LE Series SuperCapacitors*. https://www.mouser.com/datasheet/2/40/AVX-SCC-LE-1222679.pdf, 2017. Cited on page(s): 25.

MOZAYENI, H.; WANG, X.; NEGNEVITSKY, M. Thermodynamic and exergy analysis of a combined pumped hydro and compressed air energy storage system. *Sustainable Cities and Society*, Elsevier BV, v. 48, p. 101527, jul. 2019. Cited 2 times, in page(s): 71 and 81.

MUKHERJEE, P.; RAO, V. Design and development of high temperature superconducting magnetic energy storage for power applications - A review. *Physica C: Superconductivity and its Applications*, v. 563, p. 67 – 73, 2019. Cited on page(s): 27.

NICK, M.; CHERKAOUI, R.; PAOLONE, M. Optimal Planning of Distributed Energy Storage Systems in Active Distribution Networks Embedding Grid Reconfiguration. *IEEE Transactions on Power Systems*, v. 33, n. 2, p. 1577–1590, March 2018. Cited on page(s): 7.

NIKIFORIDIS, G. et al. Impact of electrolyte composition on the performance of the zinc–cerium redox flow battery system. *Journal of Power Sources*, v. 243, p. 691 – 698, 2013. Cited 2 times, in page(s): 22 and 23.

NIU, J. et al. Flexible dispatch of a building energy system using building thermal storage and battery energy storage. *Applied Energy*, v. 243, p. 274 – 287, 2019. Cited on page(s): 29.

NZOTCHA, U.; KENFACK, J.; MANJIA, M. B. Integrated multi-criteria decision making methodology for pumped hydro-energy storage plant site selection from a sustainable development perspective with an application. *Renewable and Sustainable Energy Reviews*, v. 112, p. 930 – 947, 2019. Cited on page(s): 32.

ORTEGA-VAZQUEZ, M. A.; KIRSCHEN, D. S. Estimating the Spinning Reserve Requirements in Systems With Significant Wind Power Generation Penetration. *IEEE Transactions on Power Systems*, v. 24, n. 1, p. 114–124, Feb 2009. Cited on page(s): 10.

OUALI, A. E. et al. Heat transfer within mortar containing micro-encapsulated PCM: Numerical approach. *Construction and Building Materials*, v. 210, p. 422 – 433, 2019. Cited on page(s): 29.

PARK, M.-S. et al. Porous nanoarchitectures of spinel-type transition metal oxides for electrochemical energy storage systems. *Physical chemistry chemical physics : PCCP*, v. 17, 11 2015. Cited on page(s): 21.

PENG, H. et al. A flexible and self-healing hydrogel electrolyte for smart supercapacitor. *Journal of Power Sources*, v. 431, p. 210 – 219, 2019. Cited on page(s): 25.

PENG, H. et al. Thermodynamic analysis of an improved adiabatic compressed air energy storage system. *Applied Energy*, v. 183, n. Supplement C, p. 1361 – 1373, 2016. Cited on page(s): 33.

PENG, X. et al. Liquid Air Energy Storage with LNG cold recovery for air liquefaction improvement. *Energy Procedia*, v. 158, p. 4759 – 4764, 2019. Innovative Solutions for Energy Transitions. Cited 2 times, in page(s): 27 and 28.

PERERA, K. S. et al. Application of polyacrylonitrile-based polymer electrolytes in rechargeable lithium batteries. *Journal of Solid State Electrochemistry*, v. 12, n. 7, p. 873–877, Aug 2008. Cited on page(s): 20.

PERSSON, U.; WENER, A. *Quantifying the Heating and Cooling Demand in Europe*. [S.l.], 2008. Cited on page(s): 29.

PINNANGUDI, B.; KUYKENDAL, M.; BHADRA, S. 4 - Smart Grid Energy Storage. In: D'ANDRADE, B. W. (Ed.). *The Power Grid*. [S.l.]: Academic Press, 2017. p. 93 – 135. Cited 3 times, in page(s): 17, 18, and 19.

POLLAK, R. *History of first U.S. Compressed Air Energy Storage* (CAES) *plant (110MW 26h): volume 2: Construction*. Palo Alto: [s.n.], 1994. Cited 3 times, in page(s): 1, 33, and 34.

PUNYS, P. et al. Assessment of renewable electricity generation by pumped storage power plants in EU Member States. *Renewable and Sustainable Energy Reviews*, v. 26, p. 190 – 200, 2013. Cited on page(s): 1.

QIAO, H.; WEI, Q. 10 - Functional nanofibers in lithium-ion batteries. In: WEI, Q. (Ed.). *Functional Nanofibers and their Applications*. [S.l.]: Woodhead Publishing, 2012, (Woodhead Publishing Series in Textiles). p. 197 – 208. Cited on page(s): 19.

REHMAN, S.; AL-HADHRAMI, L. M.; ALAM, M. M. Pumped hydro energy storage system: A technological review. *Renewable and Sustainable Energy Reviews*, Elsevier BV, v. 44, p. 586–598, apr 2015. Cited 2 times, in page(s): 1 and 32.

REN21. *Renewables 2017 Global Status Report*. [S.l.], 2017. 302 p. Cited 5 times, in page(s): 1, 3, 5, 32, and 33.

SALVINI, C. Performance assessment of a CAES system integrated into a gas-steam combined plant. *Energy Procedia*, Elsevier BV, v. 136, p. 264–269, out. 2017. Cited on page(s): 81.

SALVINI, C.; MARIOTTI, P.; GIOVANNELLI, A. Compression and Air Storage Systems for Small Size CAES Plants: Design and Off-design Analysis. *Energy Procedia*, v. 107, p. 369 – 376, 2017. 3rd International Conference on Energy and Environment Research, ICEER 2016, 7-11 September 2016, Barcelona, Spain. Cited 2 times, in page(s): 34 and 81.

SCHMIDT, T.; MANGOLD, D.; MüLLER-STEINHAGEN, H. Central solar heating plants with seasonal storage in Germany. *Solar Energy*, v. 76, n. 1, p. 165 – 174, 2004. Solar World Congress 2001. Cited on page(s): 4.

SCHNEIDER. *Curvas das bombas WME*. [S.l.], 2013. Available on: https://schneidermotobombas.blob.core.windows.net/media/203638/Curvas-VME.pdf. Cited 2 times, in page(s): viii and 113.

SCHNEIDER. *Curvas das bombas BT4*. [S.l.], 2017. Available on: https://schneidermotobombas.blob.core.windows.net/media/205139/curvas-bt4-04-2017.pdf. Cited 2 times, in page(s): viii and 112.

SCIACOVELLI, A. et al. Dynamic simulation of Adiabatic Compressed Air Energy Storage (A-CAES) plant with integrated thermal storage – Link between components performance and plant performance. *Applied Energy*, v. 185, n. Part 1, p. 16 – 28, 2017. Cited on page(s): 33.

SCIACOVELLIA, A.; LIA, Y.; DINGA, Y. Adiabatic compressed air energy storage – a study on dynamic performance with thermal energy storage. In: PROCEEDINGS OF ECOS 2016. *The 29 th international conference on efficiency, cost, optimization, simulation and environmental impact of energy systems*. Slovenia: ECOS, 2016. p. 12. Cited on page(s): 36.

SEDGHI, M.; AHMADIAN, A.; ALIAKBAR-GOLKAR, M. Optimal Storage Planning in Active Distribution Network Considering Uncertainty of Wind Power Distributed Generation. *IEEE Transactions on Power Systems*, v. 31, n. 1, p. 304–316, Jan 2016. Cited on page(s): 7.

SHI, J. et al. Integrated design method for superconducting magnetic energy storage considering the high frequency pulse width modulation pulse voltage on magnet. *Applied Energy*, v. 248, p. 1 – 17, 2019. Cited on page(s): 26.

SHIMADA, R.; MUKAI, K. Load-leveling and electric energy storage. *IEEJ Transactions on Electrical and Electronic Engineering*, Wiley, v. 2, n. 1, p. 33–38, 2006. Cited 3 times, in page(s): v, 5, and 6.

SKYLLAS-KAZACOS, M. 10 - Electro-chemical energy storage technologies for wind energy systems. In: KALDELLIS, J. (Ed.). *Stand-Alone and Hybrid Wind Energy Systems*. [S.l.]: Woodhead Publishing, 2010, (Woodhead Publishing Series in Energy). p. 323 – 365. Cited 6 times, in page(s): 17, 18, 19, 20, 21, and 23.

SNL. *Electric Utility Transmission and Distribution Upgrade Deferral Benefits from Modular Electricity Storage*. [S.l.], 2009. Available on : https://prod-ng.sandia.gov/techlib-noauth/access-control.cgi/2009/094070.pdf. Cited on page(s): 15.

SNL. *DOE/EPRI Electricity Storage Handbook in Collaboration with NRECA*. [S.l.]: Sandia National Laboratories, 2016. Cited 14 times, in page(s): 1, 3, 5, 7, 8, 9, 10, 11, 12, 14, 15, 16, 33, and 36.

SUN, H.; LUO, X.; WANG, J. Feasibility study of a hybrid wind turbine system – Integration with compressed air energy storage. *Applied Energy*, v. 137, n. Supplement C, p. 617 – 628, 2015. Cited on page(s): 81.

TESLA. *Powerwall Datasheet*. [S.l.], 2019. Cited on page(s): 20.

THOMASSON, T. et al. Dynamic analysis of adiabatic CAES with electric resistance heating. *Energy Procedia*, Elsevier BV, v. 135, p. 464–471, oct 2017. Cited on page(s): 81.

TOKIN. *SuperCapacitor*. https://www.tokin.com/english/product/pdf-dl/supercapacitors.pdf, 2017. Cited on page(s): 25.

TOLA, V. et al. Performance assessment of Adiabatic Compressed Air Energy Storage (A-CAES) power plants integrated with packed-bed thermocline storage systems. *Energy Conversion and Management*, v. 151, p. 343 – 356, 2017. Cited on page(s): 33.

USDE. Electric market and utility operation terminology. In: ENERGY, U. D. of (Ed.). *Solar Energy Technologies Program*. DOE/GO-102011-3207, 2011. (Energy Efficiency & Renewable Energy). Cited 2 times, in page(s): 10 and 11.

USDE. *Grid Energy Storage*. https://www.energy.gov/oe/downloads/grid-energy-storage-december-2013, 2013. Cited 2 times, in page(s): 25 and 27.

VELKESS. *Velkess L Datasheet*. [S.l.], 2013. Cited on page(s): 30.

VEN, J. D. V. de; LI, P. Y. Liquid piston gas compression. *Applied Energy*, v. 86, n. 10, p. 2183 – 2191, 2009. Cited on page(s): 33.

VERMA, U. K. et al. Black start in power system — A case study in Western Region, India. *Proceedings - 2011 International Conference on Energy, Automation and Signal, ICEAS - 2011*, 12 2011. Cited on page(s): 11.

VOLLARO, R. D. L. et al. Energy and Thermodynamical Study of a Small Innovative Compressed Air Energy Storage System (micro-CAES). *Energy Procedia*, v. 82, p. 645 – 651, 2015. 70th Conference of the Italian Thermal Machines Engineering Association, ATI2015. Cited on page(s): 34.

WANG, C.; STRAUSS, V.; KANER, R. B. Carbon Nanodots for Capacitor Electrodes. *Trends in Chemistry*, p. 1–11, jul 2019. (In press). Cited on page(s): 25.

WANG, H. et al. A Novel Pumped Hydro Combined with Compressed Air Energy Storage System. *Energies*, v. 6, p. 1554 – 1567, 2013. Cited on page(s): 79.

WANG, Z. et al. Conventional and advanced exergy analyses of an underwater compressed air energy storage system. *Applied Energy*, v. 180, n. Supplement C, p. 810 – 822, 2016. Cited on page(s): 34.

WOLF, D.; BUDT, M. LTA-CAES – A low-temperature approach to Adiabatic Compressed Air Energy Storage. *Applied Energy*, v. 125, n. Supplement C, p. 158 – 164, 2014. Cited 3 times, in page(s): 29, 33, and 81.

XIAO, Q. et al. A novel sandwiched membrane as polymer electrolyte for application in lithium-ion battery. *Journal of Membrane Science*, v. 326, n. 2, p. 260 – 264, 2009. Cited on page(s): 20.

YAN, T. et al. Dynamic simplified PCM models for the pipe-encapsulated PCM wall system for self-activated heat removal. *International Journal of Thermal Sciences*, v. 144, p. 27 – 41, 2019. Cited on page(s): 29.

YANG, H. et al. Biopolymer-based carboxylated chitosan hydrogel film crosslinked by HCl as gel polymer electrolyte for all-solid-sate supercapacitors. *Journal of Power Sources*, v. 426, p. 47 – 54, 2019. Cited on page(s): 25.

YANG, J.; LIU, W.; LIU, P. Application of SMES Unit in Black Start. *Physics Procedia*, v. 58, p. 277 – 281, 2014. Proceedings of the 26th International Symposium on Superconductivity (ISS 2013). Cited on page(s): 11.

YAO, E. et al. A Novel Constant-Pressure Pumped Hydro Combined with Compressed Air Energy Storage System. *Energies*, v. 8, p. 154 – 171, 2015. Cited on page(s): 81.

YAO, W. et al. Epoxy containing solid polymer electrolyte for lithium ion battery. *Electrochimica Acta*, v. 318, p. 302 – 313, 2019. Cited on page(s): 20.

YIN, J. lian et al. A hybrid energy storage system using pump compressed air and micro-hydro turbine. *Renewable Energy*, v. 65, n. Supplement C, p. 117 – 122, 2014. Cited on page(s): 81.

ZHANG, J. et al. Performance analysis of diabatic compressed air energy storage (d-CAES) system. *Energy Procedia*, Elsevier BV, v. 158, p. 4369–4374, feb 2019. Cited 2 times, in page(s): 36 and 81.

ZHANG, L. L.; ZHAO, X. S. Carbon-based materials as supercapacitor electrodes. *Chem. Soc. Rev.*, The Royal Society of Chemistry, v. 38, p. 2520–2531, 2009. Cited on page(s): 25.

ZHANG, N. et al. Preparation and characterization of lauric–myristic–palmitic acid ternary eutectic mixtures/expanded graphite composite phase change material for thermal energy storage. *Chemical Engineering Journal*, v. 231, p. 214 – 219, 2013. ISSN 1385-8947. Cited on page(s): 29.

ZHANG, X. et al. A near-isothermal expander for isothermal compressed air energy storage system. *Applied Energy*, v. 225, p. 955 – 964, 2018. Cited on page(s): 34.

ZHU, J. et al. Recent progress in polymer materials for advanced lithium-sulfur batteries. *Progress in Polymer Science*, v. 90, p. 118 – 163, 2019. Cited on page(s): 20.

ÖZRAHAT, E.; ÜNALAN, S. Thermal performance of a concrete column as a sensible thermal energy storage medium and a heater. *Renewable Energy*, v. 111, p. 561 – 579, 2017. ISSN 0960-1481. Cited on page(s): 29.

ČEPIN, M. Evaluation of the power system reliability if a nuclear power plant is replaced with wind power plants. *Reliability Engineering & System Safety*, v. 185, p. 455 – 464, 2019. Cited on page(s): 8.

Appendix

APPENDIX A – Complementary results

A.1 Single pump operation

A.1.1 Pressures

Following, the gauge pressures in points **A** → **D** for all 66 operating points are presented.

Table A.1 – Gauge pressures for pump #1, BT4-2040E15 in all operating points.

	A	B	C	D	
Op. Pres. (kPa_g)	TK-01=TK-02	TK-01=TK-02	TK-02	TK-01	TK-02
300	399	476	300	381	300
350	449	536	350	428	350
400	499	596	400	477	400
450	551	659	450	530	450
500	609	727	500	585	500
550	664	792	550	637	550
600	719	857	600	688	600
650	774	922	650	740	650
700	829	988	700	793	700
750	884	1052	750	847	750
800	939	1117	800	903	800

Table A.2 – Gauge pressures for pump #2, BT4-2030E12 in all operating points.

	A	B	C	D	
Op. Pres. (kPa_g)	TK-01=TK-02	TK-01=TK-02	TK-02	TK-01	TK-02
300	399	475	300	381	300
350	449	535	350	428	350
400	499	596	400	477	400
450	551	658	450	529	450
500	609	726	500	584	500
550	664	791	550	636	550
600	719	855	600	688	600
650	774	920	650	740	650
700	829	984	700	792	700
750	884	1049	750	846	750
800	939	1113	800	902	800

Table A.3 – Gauge pressures for pump #3, BT4-2020E10 in all operating points.

	A	B	C	D	
Op. Pres. (kPa_g)	TK-01=TK-02	TK-01=TK-02	TK-02	TK-01	TK-02
300	399	475	300	381	300
350	449	535	350	427	350
400	499	595	400	477	400
450	551	657	450	529	450
500	609	725	500	584	500
550	664	789	550	636	550
600	719	854	600	688	600
650	774	918	650	739	650
700	829	982	700	791	700
750	884	1044	750	844	750
800	×	×	×	×	×

Table A.4 – Gauge pressures for pump #4, BT4-2010E5 in all operating points.

	A	B	C	D	
Op. Pres. (kPa_g)	TK-01=TK-02	TK-01=TK-02	TK-02	TK-01	TK-02
300	399	473	300	380	300
350	449	530	350	426	350
400	×	×	×	×	×
450	×	×	×	×	×
500	×	×	×	×	×
550	×	×	×	×	×
600	×	×	×	×	×
650	×	×	×	×	×
700	×	×	×	×	×
750	×	×	×	×	×
800	×	×	×	×	×

Table A.5 – Gauge pressures for pump #5, WME-5840 in all operating points.

	A	B	C	D	
Op. Pres. (kPa_g)	TK-01=TK-02	TK-01=TK-02	TK-02	TK-01	TK-02
300	399	489	300	387	300
350	449	544	350	431	350
400	499	601	400	479	400
450	551	663	450	531	450
500	609	731	500	586	500
550	664	796	550	638	550
600	719	861	600	689	600
650	774	926	650	742	650
700	829	989	700	794	700
750	884	1053	750	847	750
800	939	1116	800	903	800

Table A.6 – Gauge pressures for pump #6, WME-5630 in all operating points.

	A	B	C	D	
Op. Pres. (kPa_g)	TK-01=TK-02	TK-01=TK-02	TK-02	TK-01	TK-02
300	399	479	300	382	300
350	449	538	350	429	350
400	499	599	400	478	400
450	551	661	450	530	450
500	609	728	500	585	500
550	664	791	550	636	550
600	719	854	600	688	600
650	774	915	650	739	650
700	×	×	×	×	×
750	×	×	×	×	×
800	×	×	×	×	×

A.1.2 Temperatures

Following, temperatures in points **A** → **D** for all 66 operating points are presented.

Table A.7 – Temperatures for pump #1, BT4-2040E15 in all operating points.

	A		B		C	D	
Op. Pres. (kPa_g)	TK-01	TK-02	TK-01	TK-02	TK-02	TK-01	TK-02
300	298	311	304	286	257	289	294
350	298	310	304	287	260	288	294
400	298	310	305	288	262	289	294
450	298	309	305	289	264	290	295
500	298	309	305	290	265	289	295
550	298	309	305	290	266	289	294
600	298	309	305	291	267	289	294
650	298	309	305	292	268	288	294
700	298	308	305	293	269	288	295
750	298	308	305	294	270	289	295
800	298	308	305	294	270	290	295

Table A.8 – Temperatures for pump #2, BT4-2030E12 in all operating points.

	A		B		C	D	
Op. Pres. (kPa_g)	TK-01	TK-02	TK-01	TK-02	TK-02	TK-01	TK-02
300	298	310	304	282	255	289	294
350	298	310	304	283	257	288	294
400	298	309	304	284	259	289	294
450	298	309	304	285	261	290	294
500	298	309	304	286	262	289	294
550	298	308	304	287	264	289	294
600	298	308	304	289	265	289	294
650	298	308	304	289	265	288	294
700	298	308	304	289	266	288	294
750	298	308	304	290	267	288	294
800	298	308	304	291	268	289	294

Table A.9 – Temperatures for pump #3, BT4-2020E10 in all operating points.

	A		B		C	D	
Op. Pres. (kPa_g)	TK-01	TK-02	TK-01	TK-02	TK-02	TK-01	TK-02
300	298	310	304	283	255	289	294
350	298	309	304	285	258	288	294
400	298	309	304	286	260	289	294
450	298	309	304	286	262	290	294
500	298	309	304	287	263	289	294
550	298	308	304	288	264	289	294
600	298	308	304	289	265	288	294
650	298	308	304	291	267	288	294
700	298	308	303	291	268	288	294
750	298	308	303	292	269	288	294
800	×	×	×	×	×	×	×

Table A.10 – Temperatures for pump #4, BT4-2010E5 in all operating points.

	A		B		C	D	
Op. Pres. (kPa_g)	TK-01	TK-02	TK-01	TK-02	TK-02	TK-01	TK-02
300	298	309	302	289	260	289	293
350	298	308	302	292	265	288	293
400	×	×	×	×	×	×	×
450	×	×	×	×	×	×	×
500	×	×	×	×	×	×	×
550	×	×	×	×	×	×	×
600	×	×	×	×	×	×	×
650	×	×	×	×	×	×	×
700	×	×	×	×	×	×	×
750	×	×	×	×	×	×	×
800	×	×	×	×	×	×	×

Table A.11 – Temperatures for pump #5, WME-5840 in all operating points.

	A		B		C	D	
Op. Pres. (kPa_g)	TK-01	TK-02	TK-01	TK-02	TK-02	TK-01	TK-02
300	298	310	310	285	258	291	294
350	298	311	308	286	259	290	295
400	298	310	307	288	262	290	295
450	298	310	306	290	264	290	295
500	298	310	306	293	265	290	295
550	298	310	306	293	268	289	295
600	298	309	306	293	268	289	295
650	298	309	306	293	269	289	295
700	298	309	306	294	270	288	295
750	298	309	305	294	270	289	295
800	298	309	305	294	271	290	295

Table A.12 – Temperatures for pump #6, WME-5630 in all operating points.

	A		B		C	D	
Op. Pres. (kPa_g)	TK-01	TK-02	TK-01	TK-02	TK-02	TK-01	TK-02
300	298	312	306	286	260	289	295
350	298	311	305	289	261	289	295
400	298	310	305	289	263	289	295
450	298	310	305	290	265	290	295
500	298	310	305	291	266	290	295
550	298	309	305	292	267	289	294
600	298	309	304	293	268	289	294
650	298	309	303	294	270	288	294
700	×	×	×	×	×	×	×
750	×	×	×	×	×	×	×
800	×	×	×	×	×	×	×

A.2 Dual Pump operation

Following, the gauge pressures in points **A** → **D** for all 66 operating points in dual pump arrangement are presented.

Table A.13 – Gauge pressures for two pumps #1, BT4-2040E15 in all operating points.

	A	B	C	D	
Op. Pres. (kPa_g)	TK-01=TK-02	TK-01=TK-02	TK-02	TK-01	TK-02
300	399	481	300	382	300
350	449	542	350	429	350
400	499	603	400	479	400
450	551	666	450	531	450
500	609	734	500	587	500
550	664	800	550	639	550
600	719	866	600	691	600
650	774	932	650	743	650
700	829	997	700	795	700
750	884	1063	750	850	750
800	939	1128	800	907	800

Table A.14 – Gauge pressures for two pumps #2, BT4-2030E12 in all operating points.

	A	B	C	D	
Op. Pres. (kPa_g)	TK-01=TK-02	TK-01=TK-02	TK-02	TK-01	TK-02
300	399	481	300	382	300
350	449	542	350	429	350
400	499	602	400	479	400
450	551	665	450	531	450
500	609	733	500	586	500
550	664	799	550	638	550
600	719	864	600	690	600
650	774	930	650	743	650
700	829	995	700	795	700
750	884	1060	750	849	750
800	939	1123	800	905	800

Table A.15 – Gauge pressures for two pumps #3, BT4-2020E10 in all operating points.

	A	B	C	D	
Op. Pres. (kPa_g)	TK-01=TK-02	TK-01=TK-02	TK-02	TK-01	TK-02
300	399	481	300	382	300
350	449	542	350	429	350
400	499	602	400	479	400
450	551	665	450	531	450
500	609	733	500	586	500
550	664	799	550	638	550
600	719	864	600	690	600
650	774	930	650	743	650
700	829	995	700	795	700
750	884	1060	750	849	750
800	939	1123	800	905	800

Table A.16 – Gauge pressures for two pumps #4, BT4-2010E5 in all operating points.

	A	B	C	D	
Op. Pres. (kPa_g)	TK-01=TK-02	TK-01=TK-02	TK-02	TK-01	TK-02
300	399	481	300	382	300
350	449	542	350	429	350
400	499	602	400	479	400
450	551	665	450	531	450
500	609	733	500	586	500
550	664	799	550	638	550
600	719	864	600	690	600
650	774	930	650	743	650
700	829	995	700	795	700
750	884	1060	750	849	750
800	939	1123	800	905	800

Table A.17 – Gauge pressures for two pumps #5, WME-5840 in all operating points.

	A	B	C	D	
Op. Pres. (kPa_g)	TK-01=TK-02	TK-01=TK-02	TK-02	TK-01	TK-02
300	399	484	300	383	300
350	449	546	350	430	350
400	499	606	400	480	400
450	551	670	450	532	450
500	609	739	500	588	500
550	664	804	550	640	550
600	719	870	600	692	600
650	774	936	650	745	650
700	829	1000	700	796	700
750	884	1064	750	850	750
800	939	1128	800	907	800

Table A.18 – Gauge pressures for two pumps #6, WME-5630 in all operating points.

	A	B	C	D	
Op. Pres. (kPa_g)	TK-01=TK-02	TK-01=TK-02	TK-02	TK-01	TK-02
300	399	484	300	383	300
350	399	483	300	383	300
400	449	544	350	430	350
450	499	605	400	479	400
500	551	667	450	532	450
550	609	735	500	587	500
600	664	799	550	638	550
650	719	862	600	690	600
700	774	929	650	742	650
750	829	995	700	795	700
800	884	1061	750	849	750

A.2.1 Temperatures

Following, temperatures in points **A** → **D** for all 66 operating points in dual pump arrangement are presented.

Table A.19 – Temperatures for two pumps #1, BT4-2040E15 in all operating points.

	A		B		C	D	
Op. Pres. (kPa_g)	TK-01	TK-02	TK-01	TK-02	TK-02	TK-01	TK-02
300	298	313	307	286	256	290	294
350	298	312	307	287	259	289	295
400	298	311	307	289	262	290	295
450	298	310	307	291	265	290	295
500	298	310	307	292	266	290	295
550	298	310	308	293	267	290	295
600	298	310	308	294	269	289	295
650	298	310	308	295	270	289	295
700	298	309	308	296	271	289	296
750	298	309	308	297	272	289	296
800	298	309	308	297	272	290	296

Table A.20 – Temperatures for two pumps #2, BT4-2030E12 in all operating points.

	A		B		C	D	
Op. Pres. (kPa_g)	TK-01	TK-02	TK-01	TK-02	TK-02	TK-01	TK-02
300	298	313	307	285	256	290	295
350	298	312	307	287	260	289	295
400	298	311	307	289	262	290	295
450	298	310	307	290	265	290	295
500	298	310	307	292	266	290	295
550	298	310	307	293	267	290	295
600	298	310	307	294	269	289	295
650	298	309	307	295	270	289	295
700	298	309	307	295	271	289	295
750	298	309	307	296	272	289	296
800	298	309	306	297	272	290	296

Table A.21 – Temperatures for two pumps #3, BT4-2020E10 in all operating points.

	A		B		C	D	
Op. Pres. (kPa_g)	TK-01	TK-02	TK-01	TK-02	TK-02	TK-01	TK-02
300	298	312	306	286	256	290	294
350	298	311	307	288	260	289	295
400	298	311	307	289	263	289	295
450	298	310	307	291	265	290	295
500	298	310	307	292	266	290	295
550	298	310	306	293	267	290	295
600	298	310	306	294	269	289	295
650	298	309	306	295	270	289	295
700	298	309	306	295	271	289	295
750	298	309	305	295	271	289	295
800	298	309	306	296	272	290	295

Table A.22 – Temperatures for two pumps #4, BT4-2010E5 in all operating points.

	A		B		C	D	
Op. Pres. (kPa_g)	TK-01	TK-02	TK-01	TK-02	TK-02	TK-01	TK-02
300	298	312	304	288	258	289	294
350	298	311	304	289	261	288	294
400	298	310	304	290	264	289	294
450	298	309	304	291	266	290	294
500	298	309	304	292	267	289	294
550	298	309	304	293	268	289	294
600	298	309	304	294	269	289	294
650	298	308	304	294	270	288	294
700	298	308	303	295	271	288	294
750	298	308	303	296	272	288	294
800	298	308	302	297	273	289	294

Table A.23 – Temperatures for two pumps #5, WME-5840 in all operating points.

	A		B		C	D	
Op. Pres. (kPa_g)	TK-01	TK-02	TK-01	TK-02	TK-02	TK-01	TK-02
300	298	313	308	286	256	290	295
350	298	312	309	287	260	289	295
400	298	311	309	290	262	290	296
450	298	310	309	291	265	291	296
500	298	310	309	292	267	290	296
550	298	310	309	294	268	290	296
600	298	310	309	295	269	290	296
650	298	310	309	296	271	289	296
700	298	310	308	297	271	289	296
750	298	309	308	297	272	289	296
800	298	309	307	297	273	290	296

Table A.24 – Temperatures for two pumps #6, WME-5630 in all operating points.

	A		B		C	D	
Op. Pres. (kPa_g)	TK-01	TK-02	TK-01	TK-02	TK-02	TK-01	TK-02
300	298	313	308	285	256	290	295
350	298	312	308	288	259	289	295
400	298	311	308	290	262	290	295
450	298	310	308	291	265	291	296
500	298	310	308	292	266	290	296
550	298	310	307	294	268	290	295
600	298	310	306	294	269	289	295
650	298	310	307	295	270	289	295
700	298	309	307	296	271	289	295
750	298	309	307	296	272	289	296
800	298	309	307	297	272	290	296

APPENDIX B – Publications

B.1 Published papers

- Tomás P.L. Camargos, Daniel L.F. Pottie, Rafael A.M. Ferreira, Thales A.C. Maia, Matheus P. Porto,. *Experimental study of a PH-CAES system: Proof of concept*, Energy, Volume 165, Part A, 2018, Pages 630-638;
- Rafael A. M. Ferreira, Daniel L.F. Pottie, Leonardo H. C. Dias, Braz J. Cardoso Filho, Matheus P. Porto,. *A directional-spectral approach to estimate temperature of outdoor PV panel*s, Solar Energy, Volume 183, 2019, Pages 782-790.

B.2 Submitted papers

- Daniel L.F. Pottie, Gabriel A. Mendonça, Osvane A. Faria, Marco Túlio C. Faria, Thales A. C. Maia,. *Some aspects of the electromechanical design of High-Speed microturbines for power generation*, Applied Energy *(under review)*;
- Daniel L.F. Pottie, Rafael A.M. Ferreira, Thales A.C. Maia, Matheus P. Porto,. *An alternative sequence of operation for Pumped-Hydro Compressed Air Energy Storage (PH-CAES) systems*, Energy *(under review)*.

Annex

ANNEX A – Pump Charts

A.1 BT4 series

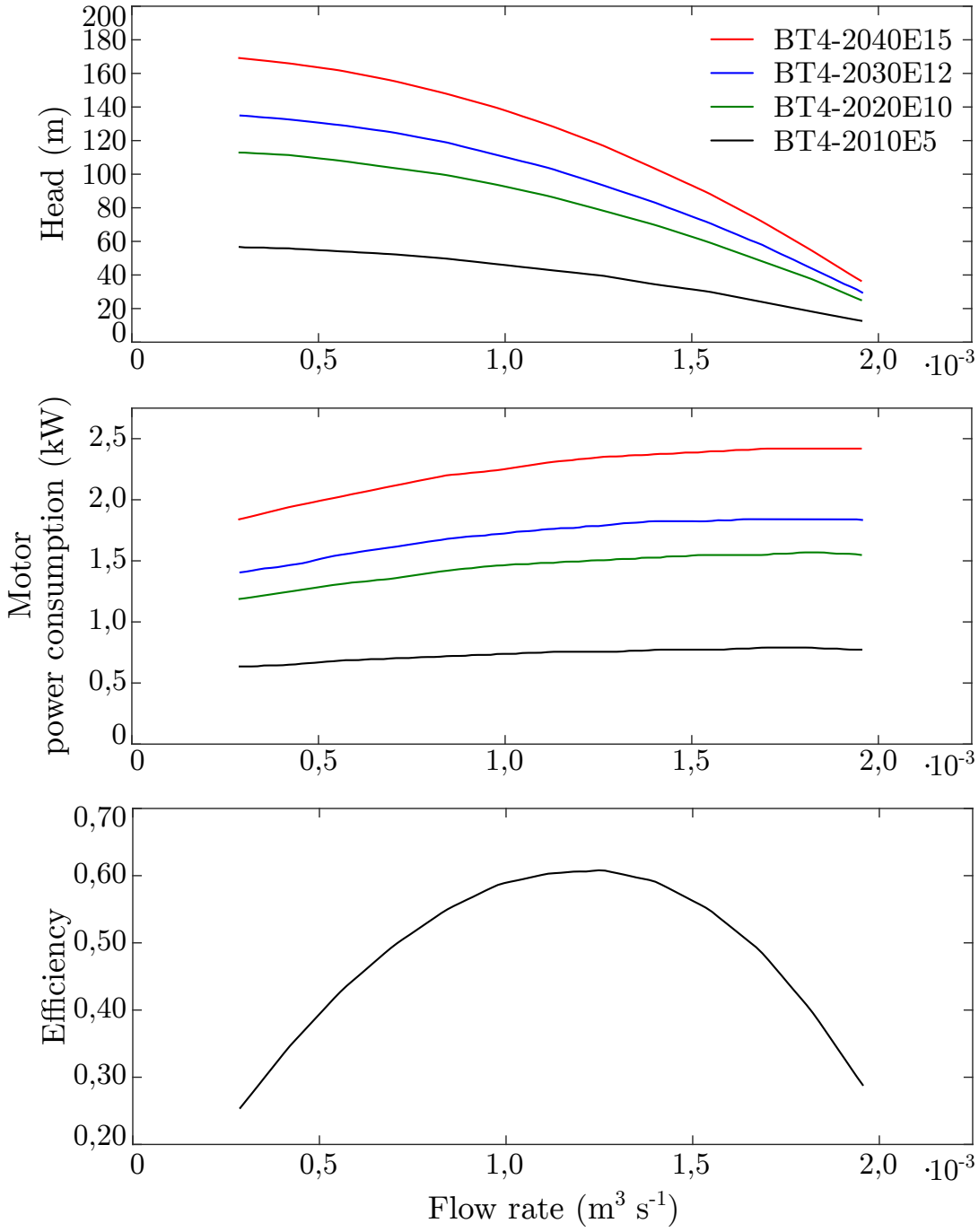

Figure A.1 – BT4 series pump chart, at 3600 *rpm*. Adapted from (SCHNEIDER, 2017).

A.2 WME series

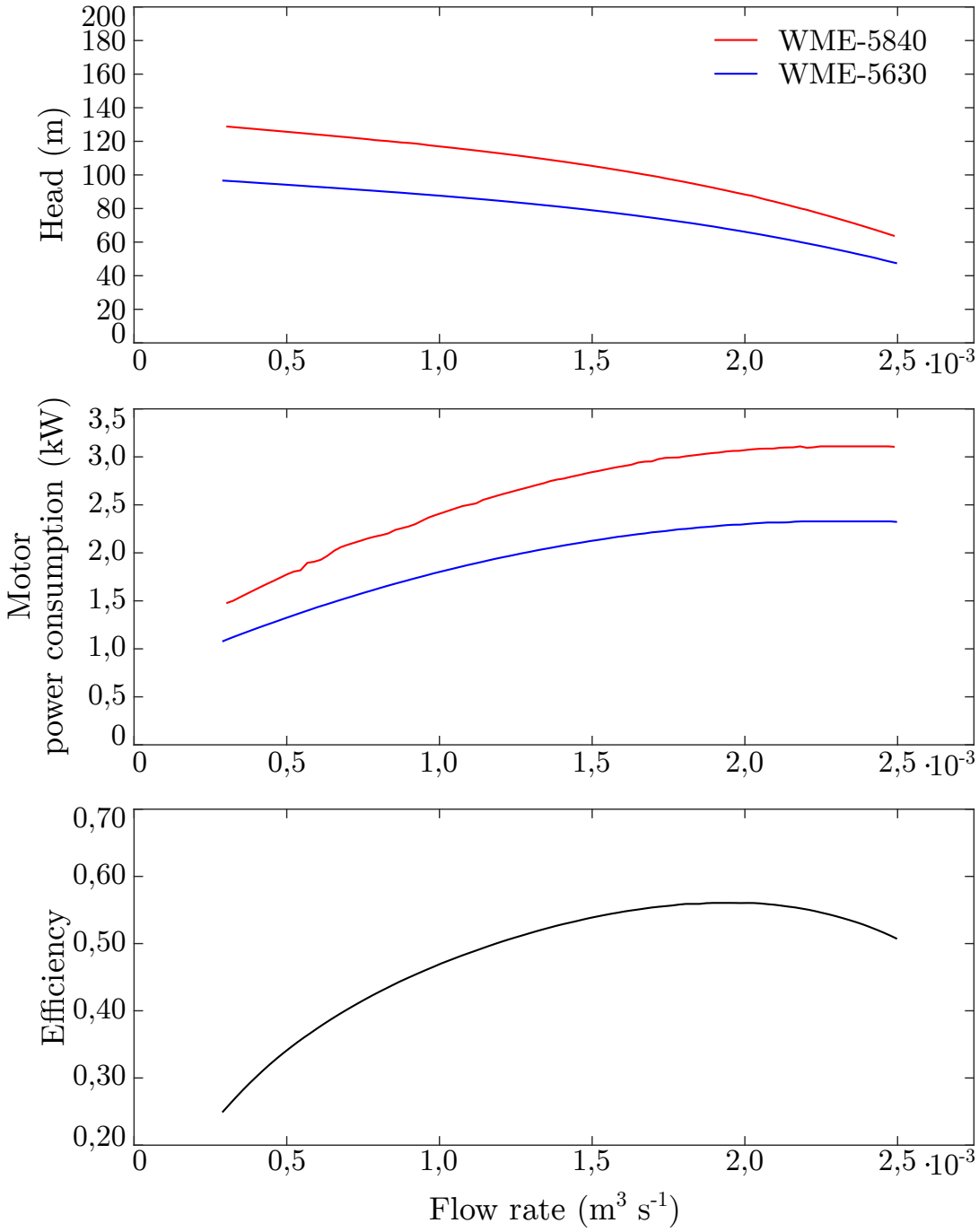

Figure A.2 – WME series pump chart, at 3600 *rpm*. Adapted from (SCHNEIDER, 2013).